科技部補助

大專學生研究計畫研究成果報告

計畫名稱：	二氫嘧啶水解酵素活性區的轉譯後羧化修飾與雙金屬結合機制之研究

執行計畫學生：鄭人豪
學生計畫編號：MOST 107-2813-C-040-031-B
研究期間：107年07月01日至108年02月28日止，計8個月
指導教授：黃晟洋

處理方式：本計畫涉及專利或其他智慧財產權，2年後可公開查詢

執行單位：中山醫學大學生物醫學科學學系（所）

中華民國　108年03月30日

目錄

摘要

二氫嘧啶水解酶 (dihydropyrimidinase; DHPase) 在嘧啶代謝過程中扮演最關鍵的速率決定步驟，其酵素活性是催化 5,6-dihydrouracil、5,6-dihydrothymine 的開環水解。由於 DHPase 在工業上製造抗生素前驅物常使用 hydantoin 作為受質，因此 DHPase 又常被稱為 hydantoinase。為了在工業應用以及學術上更了解其催化活性區，在此科技部大專生研究計畫 "**二氫嘧啶水解酵素活性區的轉譯後羧化修飾與雙金屬結合機制之研究**(107-2813-C-040-031-B)" 的執行，我們欲解出此酵素結構以及探討其活性中心，研究過程並伺機研究 DHPase 所屬的其他 cyclic amidohydrolase 家族酵素，如尿囊素水解酶 (allantoinase; ALLase)與二氫乳清酸水解酶 (dihydroorotase; DHOase) 以便比較。在之前的研究顯示綠膿桿菌的 DHPase (PaDHPase) 為一雙套體，其活性區含有一個雙金屬中心以及在原核生物中極為罕見的賴氨酸羧化 (lysine carboxylation)的轉譯後修飾 (post-translational modification)。為了探討結構上金屬與此賴氨酸的羧化 (COO^-) 後修飾關聯性，以及整體結構多聚體其他可能性，我們首先大量表現與純化出天然雙金屬 PaDHPase，接著想辦法製備去金屬的 DHPase。藉由純化出雙金屬的 DHPase 後，我們發現在特定螯合劑條件可分別抓出蛋白質活性區內的單(β)金屬或兩個金屬(α+β)。之後我們透過篩選各

種條件來晶體成長並得到蛋白質晶體、利用 X 光繞射結果與傅立葉轉換解出分子結構，並藉由結晶結構了解各項分子層次如金屬結合位、單金屬結合位與賴氨酸羧化成因的資訊。由於此類酵素家族其真核與原核生物的酵素特性明顯不同，因此我們也用昆蟲細胞來嘗試生產人類與斑馬魚的 DHPase, DHOase 與 ALLase。雖然在想像上，賴氨酸羧化提供了兩個負電氧原子使得正電賴氨酸轉為新的負電荷胺基酸用以結合兩個金屬，但結構的研究結果卻顯示賴氨酸羧化並不與全雙金屬中心有關連，而是僅影響 β 金屬的結合。我們亦解出人類 DHOase 的此賴氨酸突變的結晶結構，亦發現仍有 α 金屬，顯示長期以來對於此賴氨酸羧化在演化上是為了產生一個新的氨基酸以供雙金屬中心的學說是有問題的。目前此計畫執行結果已獲 2 篇 SCI 科學期刊接受刊登，本人皆為第一作者 [(1) Cheng JH (鄭人豪), Huang CC, Huang YH, Huang CY (2018) Structural basis for pH-dependent oligomerization of dihydropyrimidinase from *Pseudomonas aeruginosa* PAO1. ***Bioinorg. Chem. Appl.***, 2018, 9564391. (2) Cheng JH (鄭人豪), Huang YH, Lin JJ, Huang CY (2018) Crystal structures of monometallic dihydropyrimidinase and the human dihydroorotase domain K1556A mutant reveal no lysine carbamylation within the active site. ***Biochem. Biophys. Res. Commun.***, 505, 439-444.]。其他已經完成、仍待發表之結果包括不同的突變株的結構、活性、金屬含量分析與質譜法偵測分

子量有無後修飾之變化。此計畫的執行結果已明確的說明活性中心與賴氨酸羧化後修飾是息息相關，且亦揭露此罕見的賴氨酸羧化並非全然是為了雙金屬中心的自我聚集(assembly of the binuclear metal center)。下一階段的研究開啟將可能包括真核來源酵素的比較以及活性區胺基酸的改變，以便在工業應用上利用這些催化機制與結構上的知識來加大此酵素的活性，施以以結構為基礎的蛋白質工程。

第一章:緒論

1.1 DHPase 功能與活性

二氫嘧啶水解酶 (dihydropyrimidinase; DHPase) 廣泛存在於生物中，其在嘧啶鹼基代謝三步驟(去氫、開環與降解)中負責第二步驟幫助催化 5,6-dihydrouracil 與 5,6-dihydrothymine 的水解 [1]。此 DHPase 反應催化二氫嘧啶開環並產生溶解度高的產物 [2, 3]，為 DNA 鹼基生合成中扮演速率決定步驟的關鍵的酵素 [4]。另外，DHPase 屬於 cyclic amidohydrolase 家族 [5]，其家族成員還包括尿囊素水解酶 (allantoinase; ALLase) [6, 7]、二氫乳清酸水解酶 (dihydroorotase; DHOase) [6-10]、海因酶 (hydantoinase) [11, 12]、醯亞胺酶 (imidase) [13-15]，其活性區內同時含有 2 個金屬鋅 ，並且活性區重要的氨基酸均為四個 histidine、一個 aspartatate 和一個 post-carboxylated lysine [16]。DHPase 與二氫乳清酸水解酶以及尿囊素水解酶，其催化的機制亦相當類似，主要是在活性區產生極化的水分子對含氮鹼基的 cyclic imide bond 進行親核攻擊 [16]。由於 DHPase 在工業應用上被用來製造抗生素前驅物，使用 hydantoin 作為受質，因此 DHPase 又常被稱為 hydantoinase [2, 3]。目前已經有數百種抗生素製程專利運用 hydantoinase，同時並且希望獲得更多能在製程溫度

高時能耐熱的 hydantoinase [17, 18]。

雖然 cyclic amidohydrolase 家族其催化中心皆含有四個 histidine，一個 aspartatate，一個轉譯後 COO 修飾的 post-carboxylated lysine，以及兩個金屬離子(通常為鋅)，然而這些酵素卻擁有絕對不同的受質專一性，例如從 *Agrobacterium* species 純化出的 hydantoinase 沒有 5,6-dihydropyrimidine amidohydrolase 的活性 [19]；從 *Saccharomyces kluyveri* 和 *Dictyostelium discoideum* 純化出的 DHPase 也無法水解 hydantoin [20]。另外雖然所有的 DHPase 皆已知為四套體，但從 *Pseudomonas putida* YZ-26 來源的 hydantoinase 卻為二套體 [21, 22]。

1.2 研究動機與背景

DHPase 是一個雙金屬酵素，通常為四套體。在不同 pH 情況除活性明顯有差異外 [23]，*P. putida* hydantoinase [21, 22] 可發現雙套體構型。我們實驗室之前亦發現 *P. aeruginosa* DHPase (PaDHPase) [24] 為二套體。由於在演化上 [25, 26]，許多蛋白質都不是單套體，必須自我聚集成為多套體，不同機制的自我聚集而成的多套體通常與活性與穩定性以及其他蛋白質-蛋白質交互作用有關 [25]，DHPase 為何可以有不同種類的多套體以及不同套體與活性、耐熱性的關聯必須在結構上加以釐清。也因此，在此計畫的執行過程中我們發現了雙套體與

四套體的成因與不同 pH 有關，並解出了四套體的 PaDHPase 結構並比較其與雙套體的作用網絡 [27]。

DHPase 內含一罕見的賴氨酸羧化後修飾 [28, 29]，此修飾使用帶有正電的賴氨酸轉為負電而形成嶄新的胺基酸 (novel amino acid) 並因此可結合活性區中的雙金屬；而蛋白質的賴氨酸後修飾如最常見的甲基化通常是由轉甲基酶所催化 [30]。雖然這個羧化後修飾在 DHPase 的活性區賴氨酸上目前已知並不是由別的酵素催化，但是是如何自發性的自我形成，目前其機制仍然未知。若突變株如 K 突變成 A 的話，加入羧基如甲酸、乙酸、丙酸等可稍微回復此突變株之活性 [7, 11]。

過去實驗中發現 DHPase 若不經金屬結合與賴氨酸羧化後修飾並無活性 [23]，因此我們透過純化綠膿桿菌的 DHPase (PaDHPase)，包括製備單金屬與去金屬的各種 DHPases，希望得到各種結晶結構來了解此酵素的活性區是如何自我組裝 (self-assembly) 與自我活化 (self-activation)。同時，我們也嘗試將活性區中的幾個特定胺基酸分別進行點突變，希望進一部探討在演化過程中活性區內的氨基酸和雙金屬之間的關係是如何?是否有其他相類似的氨基酸能取代? 希望能對於 PaDHPase 有更多的了解。也因此，在此計畫的執行過程中，我們發現了賴氨酸羧化並不與全雙金屬中心有關連，而是僅影響 β 金屬

的結合 [31]。

由於此酵素是嘧啶鹼基代謝三步驟(去氫、開環與降解)中負責第二步驟幫助催化 5,6-dihydrouracil 與 5,6-dihydrothymine 的水解的最關鍵性的速率決定步驟，因此相關抑制劑亦可能用以研發新型抗菌劑與抗癌劑，例如 5-FU 是利用此途徑所開發的臨床藥物之一 [32]。為有機會研發新的抑制劑，達到抑制綠膿桿菌甚或其他超級細菌的嘧啶代謝，進一步影響其生長，希望此研究亦能提供藥物設計，解決目前超級細菌無藥可醫的一個新方向 [33, 34]。

第二章:材料與方法

2.1 細菌蛋白質相關操作

2.1.1 質體製備

(1.) 將菌液離心 12000 rpm、1 min，倒掉上清液只留 pellet。

(2.) 加 solution I (要冰) 200 µl pipetting (on ice 1 min)。

(3.) 加 solution II 200 µl (輕輕 pipetting)，反應 1 min。

(4.) 加 solution III 200 µl pipetting，反應 1 min。

(5.) 離心 12000 rpm、10 min。

(6.) 取上清(若吸到沉澱蛋白可取到新 eppendorf，稍微回至室溫在離心一次)，加進 spin column，離心 12000 rpm、1 min。

(7.) 加 wash buffer 700 µl，離心 12000 rpm、1 min (重複兩次)。

(8.) 再次離心 12000 rpm、2 min。

(9.) 將 spin column 放到新 eppendorf。

(10.) 加 50 µl ddH_2O，放 37°C 反應 2 min。

(11.) 離心 12000 rpm、1 min。

(12.) 放-20°C 保存。

2.1.2 膠體電泳

(1.) 配置 1 % agarose 的 DNA 膠，並用 0.5 倍 TAE 來溶解。

(2.) 利用微波爐加熱，勿沸騰使濃度不準，並且要時常搖晃確定混合均勻。

(3.) 稍微冷卻後倒入製膠架內，不要有氣泡(若有氣泡可用 tip 輕戳排除)。

(4.) Sample (DNA : dye = 2 μl : 1 μl 混合均勻)、marker 2 μl，依序加入。

(5.) 以 110V 跑 23 分鐘左右，並觀察之。

(6.) 戴上手套將膠拿到 EtBr 盒，外染 15 min。

(7.) 利用紫外光觀察顯影位置是否正確。

2.1.3 Transformation

(1.) 加入 10 μl 勝任細胞(Ecos 21) + 10 μl DNA，並在冰上靜置 5 min。

(2.) 放到 42°C 加熱 45 秒(離開冰上開始計時，時間到後馬上放回冰上 2 min)。

(3.) 將玻璃棒過火 3 次，確認降溫後塗盤。

(4.) 放 37°C 培養箱培養。

2.1.4 蛋白質表現:

(1.) 將先前 transformation 塗盤培養的菌落，利用 tip 輕挑（盡量選分散在不同區的單一菌落）分別排入 4 c.c.小管 LB 內培養到 OD 大於 1。

(2.) 取 1 c.c.到新的小管 LB 培養。

(3.) 剩下 3 c.c.取 200 μl 離心(12000 rpm、1min)，抽掉 180 μl 回溶，之後以 98°C 煮 20 min(此為不加 IPTG 之 sample)。

(4.) 之後將剩餘 LB 管加入 4 μl IPTG，以 37°C 培養 2 hr。

(5.) 之後同樣取 200 μl 離心 (12000 rpm、1min)，抽掉 180 μl 回溶，以 98°C 煮 20 min (此為加 IPTG 之 sample)。

(6.) 之後跑 SDS-PAGE 觀察表現前後蛋白量是否有明顯變化。

2.1.5 細菌放大培養

(1.) 拿小管LB液加入 1 M ampicillin 4 μl 再加 15 μl 的菌 (LB管在開和關都要過火) 放到培養箱以 37°C、200 rpm、4 hr培養。

(2.) 裝500 c.c. ddH_2O，加入12.5 g LB broth，然後瓶口蓋上鋁箔紙 (霧面朝外)並貼滅菌膠帶。

(3.) 放入滅菌釜 (須加水過底盤) 採用濕滅 15 min，等壓力降到和外在環境一樣時再打開蓋子。

(4.) 取出後放冷到室溫 (可用冰浴降溫)。

(5.) 先測量小管LB的O.D值 (要在1左右) ，不同的菌生長速度會不同，有些可能會多於或少於4hr。

(6.) 將大瓶加入1 M ampicillin 200 µl，再將小管加入大瓶 (一樣要過火)。

(7.) 放入培養箱約 7-8 hr 後 (測O.D值1-1.4) 加入1 M IPTG 125 µl，再放回培養箱以 25°C 12 hr 培養。

(8.) 取300 g到離心瓶 (含瓶子跟蓋子且要精確到小數點兩位)。

(9.) 使用高速離心機離心 (20 mins, 12000 rpm, 4°C)，完成後倒掉上清液。

2.1.6 高速離心機操作

(1.) 確認離心機使用之 rotor 型號、樣品容忍體積及最高轉速。

(2.) 確認 rotor 內及離心機轉軸周圍是否有多餘水分，若有則需擦乾。

(3.) 樣本秤重需精確到小數點第二位，並且樣品不可至全滿，以免離心管變形或溢出。

(4.) 確認樣品平衡對稱放入、確認rotor是否有和轉軸卡榫緊密嵌合，並且確認rotor上蓋是否有拴緊，檢查無誤後關上離心機蓋子。

(5.) 設定 rotor 號碼、轉速、時間、溫度以及起降的速度後，開始離

心。

(6.) 結束後取出樣本，維持儀器門蓋打開保持離心機乾燥，關閉電源。

2.1.7 蛋白質純化

(1.) 取 40 ml 的 5 mM imidazole 加入離心瓶回溶 pellet，回溶後再倒回 tube。

(2.) 拿冰桶裝冰，然後插入 tube 放至超音波震菌機震菌(震破細菌的細胞壁，使它的蛋白質跑出來) 機器的設定為 (震菌5秒，休息5秒，50個 cycle)震3-5次且勿超過 200w (不同的菌震的次數也不同，可觀察菌液顏色由米黃轉為灰黑即可)，如果只有1管則震完需放冰上等待10 mins (因震菌會產生熱，故我們要在冰上操作且冷卻避免蛋白質變性)。

(3.) 待震菌快完成前，先開啟離心機使其降溫至 4°C。

(4.) 將震好的菌拿去離心 (20 mins、12000 rpm、4°C)。

(5.) 離心結束後，將上清液倒至另一個乾淨 tube 並且插冰上。

(6.) 在快震好菌時可先清洗His Trap^{TM} HP column，將幫浦以上低下吸的方向按ddH_2O、$NiSO_4$ ddH_2O、5 mM imidazole的順序用5 ml/min的速度清洗10 min。

(7.) 取20 μl滅過菌的ddH_2O放入eppendorf並用tip輕點倒掉上清後的pellet使其溶於裝有滅過菌ddH_2O的eppendorf。

(8.) 取離心過後的上清液過濾到tube (事先取20 μl的上清液放入eppendorf)。

(9.) 將上清通完後的過濾液收集起來(一樣取 20 μl 放入eppendorf)。

(10.) 接著依序用含有500 mM NaCl pH 7.4的不同濃度imidazole (5、60、100、200、500 mM) 通入column，並收集洗出之蛋白溶液(5、60 mM部分收取50 ml其餘收取30 ml)。

(11.) 一樣將這5管分別取20 μl放入eppendorf

(12.) 將上述 9 個 eppendorf (IPTG 前、後、上、過、5、60、100、200、500 mM) 加入 10 μl 的 dye 並用 98°C 加熱 20 min，而沉澱管的 eppendorf 則是加 10 μl 的 dye 並用 98°C 加熱 30 min。

(13.) 依序用 EDTA、ddH_2O、EtOH 以 5 的速度各 10 min 來清洗 column，洗完後要將 column 的蓋子鎖緊再放回冰箱。

2.1.8 製作 SDS-PAGE 膠片與電泳

(1.) 製作下膠: 依序加入 ddH_2O、30% acrylamide、Tris-pH=8.8、SDS、APS、TEMED 混合均勻後加到製膠片上，並用 70% 酒精補滿液面將液面壓平。

(2.) 等出現明顯線條時，倒掉酒精開始做上膠。

(3.) 製作下膠 (依據不同蛋白配置的下膠濃度也會不同，濃度高的網狀較小適合小分子量): 本次實驗適用 15% 濃度較高的膠，依序加入 ddH_2O、30% acrylamide、Tris-pH=6.8、SDS、APS、TEMED 混合均勻後加到製膠片上並將尺梳插上。

(4.) 將煮過的 sample 取 10 µl loading 到格子內中一格加 2 µl 的 marker (順序是上、沉、過、5 mM imidazole、60 mM、100 mM、marker、200 mM、500 mM)，內外加入 running buffer 後以 70V 120 min 跑膠。

(5.) 之後放入 coomassie blue 中染 30 min (依染劑的新舊時間會不太一樣)。

(6.) 接著放入退染液中退染大約 4 hr 或是放入水中退染 (時間較久)。

(7.) 當膠的背景變得略淡或透明且 band 能清楚看見時就能封膠。

2.1.9 測 OD 值

(1.) 觀察跑膠後結果發現100 mM imidazole和200 mM imidazole的band質純且明顯單一。

(2.) 取 800 µl 滅過菌的ddH_2O + 200 µl Protein Assay Dye到cuvette搖

晃均勻後blank

(3.) 接著再加 2 µl 從100 和200 mM imidazole收集到的蛋白質液體。

(4.) 利用吸光值的不同來看蛋白質的濃淡。

2.1.10 保存純化的蛋白質

(1.) 將收集的目標蛋白加入 10%甘油，均勻混合後放入-80°C 的冰箱保存。

(2.) 以便之後能濃縮和降鹽

2.1.11 蛋白質濃縮

(1.) 使用Millipore Amicon ultra-10K 濃縮管來濃縮。

(2.) 取出濃縮管後，以酒精和ddH_2O小心清洗 (避免將過濾膜給弄壞)。

(3.) 加入10 ml ddH_2O至濃縮管，以3000 rpm、4°C、10 min來離心，觀察漏出水量是否正常以檢視膜的狀態。

(4.) 清洗和檢測完畢後，加入10 ml蛋白質溶液，以3000 rpm、10°C、15 min來離心，觀察蛋白質狀態是否有聚集沉澱，若有則調整溫度再重複上述條件離心，直到找到蛋白質適合溫度才可增加離心時間。

(5.) 使用完畢後以 ddH_2O 和酒精清洗，最後保存在 20% 酒精中。

2.1.12 蛋白質降鹽

(1.) 為了後續的實驗需求我們會將濃縮後的蛋白質依序以含有400 mM、300 mM、200 mM、100 mM鹽濃度的Tris或HEPES，來將原蛋白液降鹽。

(2.) 將濃縮後的蛋白質和降鹽buffer以1:4的比例緩慢加入，要特別留意蛋白質在鹽濃度越低越容易聚集沉澱，同時溫度也會影響要特別留意。

(3.) 加入Millipore Amicon ultra-10K 濃縮管，同樣以3000 rpm、10°C、15 min來離心，觀察蛋白質狀態是否有聚集沉澱，若有則調整溫度再重複上述條件離心，直到找到蛋白質適合溫度才可增加離心時間。

(4.) 使用完畢後以 ddH_2O 和酒精清洗，最後保存在 20% 酒精中。

2.1.13 透析與螯合

(1.) 螯合buffer成分為50 mM HEPES、15 mM 8-HQSA、1 mM EDTA、pH 6.5。

(2.) 將透析膜浸入buffer中並搓開，先在下方夾上夾子。

(3.) 將蛋白加入，盡量不要有氣泡。

(4.) 在上方夾上夾子，並且和下面的方向不同，以增加接觸面積。

(5.) 將去鹽column用10 mM $NaPO_4$先清洗至少20ml。

(6.) 將透析去過金屬的蛋白通入column(蛋白的量不能大於1.4ml)，並在下方用eppendorf接，每管接10滴。

(7.) 取5 ml 10 mM $NaPO_4$通入，依照上述接法。

(8.) 再取5 ml 10 mM $NaPO_4$通入，大略將殘留物洗掉。

(9.) 最後用25 ml 10 mM $NaPO_4$將column洗乾淨。

(10.) 測量OD值，最多收集到wash 2，若wash 3、4濃度也很高，可以選擇再按照第一步驟重新再做一遍，確保裡面的鹽完全被去除。

2.1.14 晶體成長

(1.) 依序在點晶盤中加入250 µl 晶體成長特定溶液，蓋上蓋子防止揮發。

(2.) 撕兩條點晶膠帶在點晶架上(要一次撕好不能有摺痕，且要平整)。

(3.) 依據實驗需求點1~4點，以晶體成長特定溶液:蛋白=1:1或其他比例加入。

(4.) 先點1 µl晶體成長特定溶液，再加1 µl的蛋白(速度要快不然晶體

成長特定溶液可能會揮發掉，且不能有氣泡)。

(5.) 最後黏到點晶盤上，並用試鏡紙將周圍緊密的壓緊。

2.1.15 到國家同步輻射中心解蛋白質結構

(1.) 在顯微鏡下挑選和晶體大小差不多的 loop。

(2.) 將膠帶割下，並在顯微鏡下用loop小心的挑晶。

(3.) 之後放到液態氮中固定，用預先在液態氮中冷卻的夾子夾住，並連同液態氮一起拿到光束器前，才能將夾子拿出液面架到光束器上。

(4.) 最後一個出來的人按完警示鈕出來後，將門鎖上，再將鑰匙插入另一個控制器，等預備鈴響完，即可開始進行X光繞射。

(5.) 在電腦上設定好資料夾並打開程式。

(6.) 設定旋轉的角度、距離、曝光時間等，並在電腦上預跑。

(7.) 確認數值都在標準內即可開始跑。

(8.) 一樣在其他台電腦設定好資料夾，並開啟程式。

(9.) 和剛剛預跑過程差不多將收集到的資料利用軟體分析，最後經由傅立葉轉換得到空間中的電子密度資訊。

2.2 昆蟲細胞操作

為了避免原核生物可能無法正確表達真核生物的酵素，我們亦需要使用昆蟲細胞來表達與獲得人類與斑馬魚來源的酵素，以便解出結構了解其分子相關資訊。

2.2.1 昆蟲細胞培養

(1.) 將細胞快速解凍並加入含 10% FBS 的 medium (稀釋原先解凍的細胞液內的 DMSO)，種入 dish 或 flask 進行培養。

(2.) 第 2 天將 medium 全部去除，更換新的 10% FBS 的 medium，以完全去除細胞液內的 DMSO。

(3.) 每 2-3 天更換新的 10% FBS 的 medium，更換時保留些許大約 1-2 ml 原本舊的 10% FBS medium，剩餘部分才加入新的 10% FBS medium。

(4.) 若細胞數量過多可將細胞擴增培養到新的培養盤。

2.2.2 Transfection

(1.) Plasmid 濃度要在(0.1~2.0 μg/μl)。

(2.) 細胞在 well 內生長大約 70~90% 滿。

(3.) 將 plasmid 和 medium 混合，使整體濃度為(0.01μg/μl)。

(4.) 加入 Transfection reagent (和 DNA 的比例可為 1:1, 2:1, 3:1, 或

4:1)，pipetting 後，在室溫反應 30 分鐘。

(5.) 將反應好的 sample 加到 well 內(不需要將 growth medium 移除)，輕輕搖晃 30 秒。

(6.) 之後在 18-72 小時進行觀察。

第三章:實驗結果與討論

3.1 雙金屬的PaDHPase純化與製備

PaDHPase是一個活性區含有雙金屬的酵素。本實驗室前人構築的pET21b-PaDHPase質體，藉由轉質大腸桿菌來表達此基因產物，並且加入IPTG來大量表現目標蛋白,之後順利藉由親和性管柱層析方式，使用Ni-NTA column來純化，並且以不同濃度的imidazole來洗出，最後得到純的酵素(圖一)。

(A)

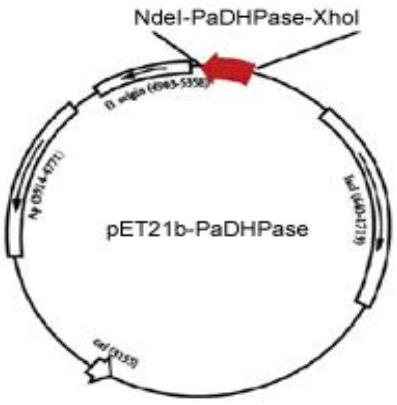

(B)

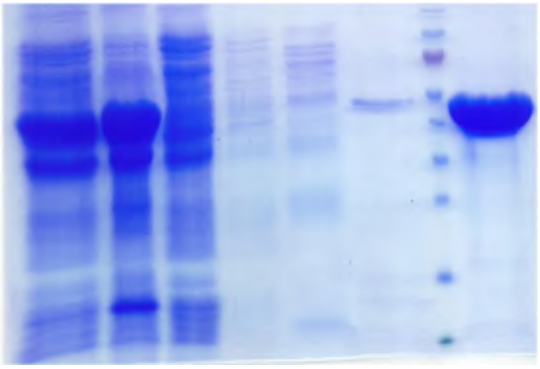

(C)

蛋白質表現與純化。(A)實驗室構築的PaDHPase質體。(B)利用Ni-NTA column純化的實際圖示。藉由Ni-NTA column內的固相擔體

結合，接著通入蛋白質液，由於目標蛋白事先加上6個His，因而會和Ni結合，間接使目標蛋白binding在column上，接著利用不同濃度的imidazole 和蛋白質競爭Ni的結合，使目標蛋白能在最後洗出。(C) 蛋白質純化後的膠圖。我們利用不同濃度的imidazole將binding在Ni-NTA column內的蛋白給洗出，圖中可見在內含200 mM imidazole溶液純化出目標蛋白PaDHPase (最右lane)。

3.2 雙金屬PaDHPase晶體的獲得與解出結構

經過數千種篩選，我們順利找到雙金屬 PaDHPase 結晶條件，並且藉由經由優化蛋白質晶體條件(圖二)，得到更加立體且大顆的晶體。

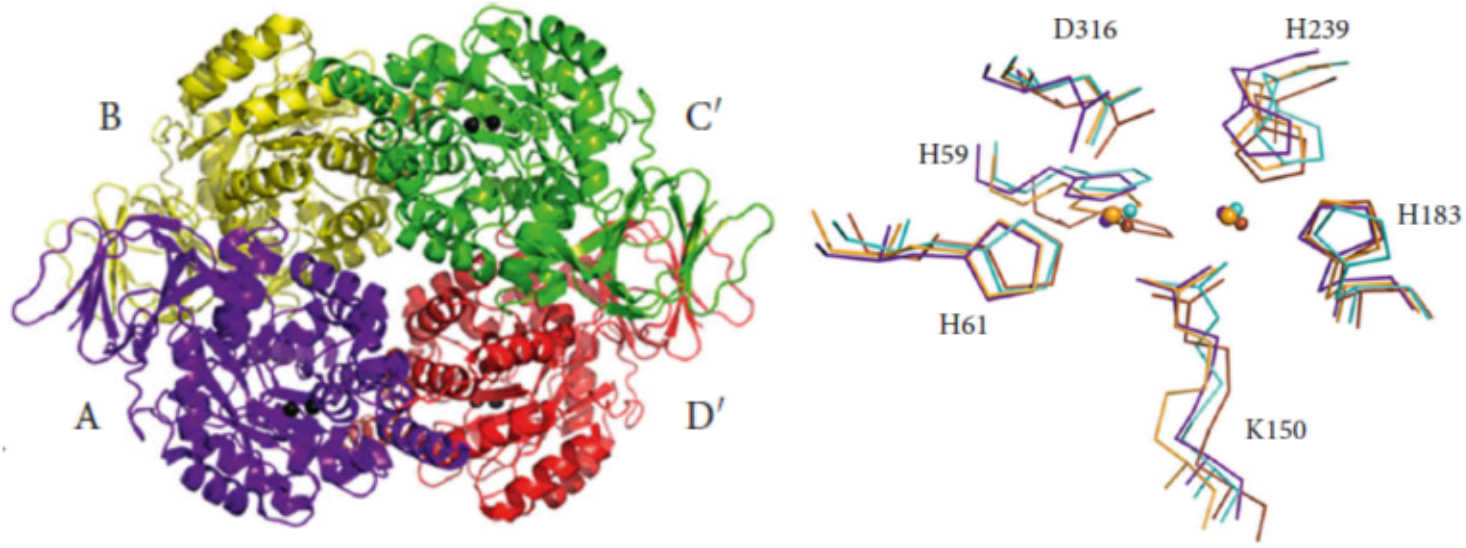

利用 X 光繞射並已解出解析度為 2.17 Å 的結晶結構(圖二)。

圖二：結晶結構。我們已解出 PaDHPase 的結晶結構，解析度為 2.17

Å。PaDHPase 與其他的 cyclic amidohydrolase 的活性區均含有四個 histidine，一個 aspartatate，一個轉譯後 COO 修飾的 post-carboxylated lysine，以及兩個金屬離子。

雙金屬 PaDHPase 的晶體成長條件篩選與優化

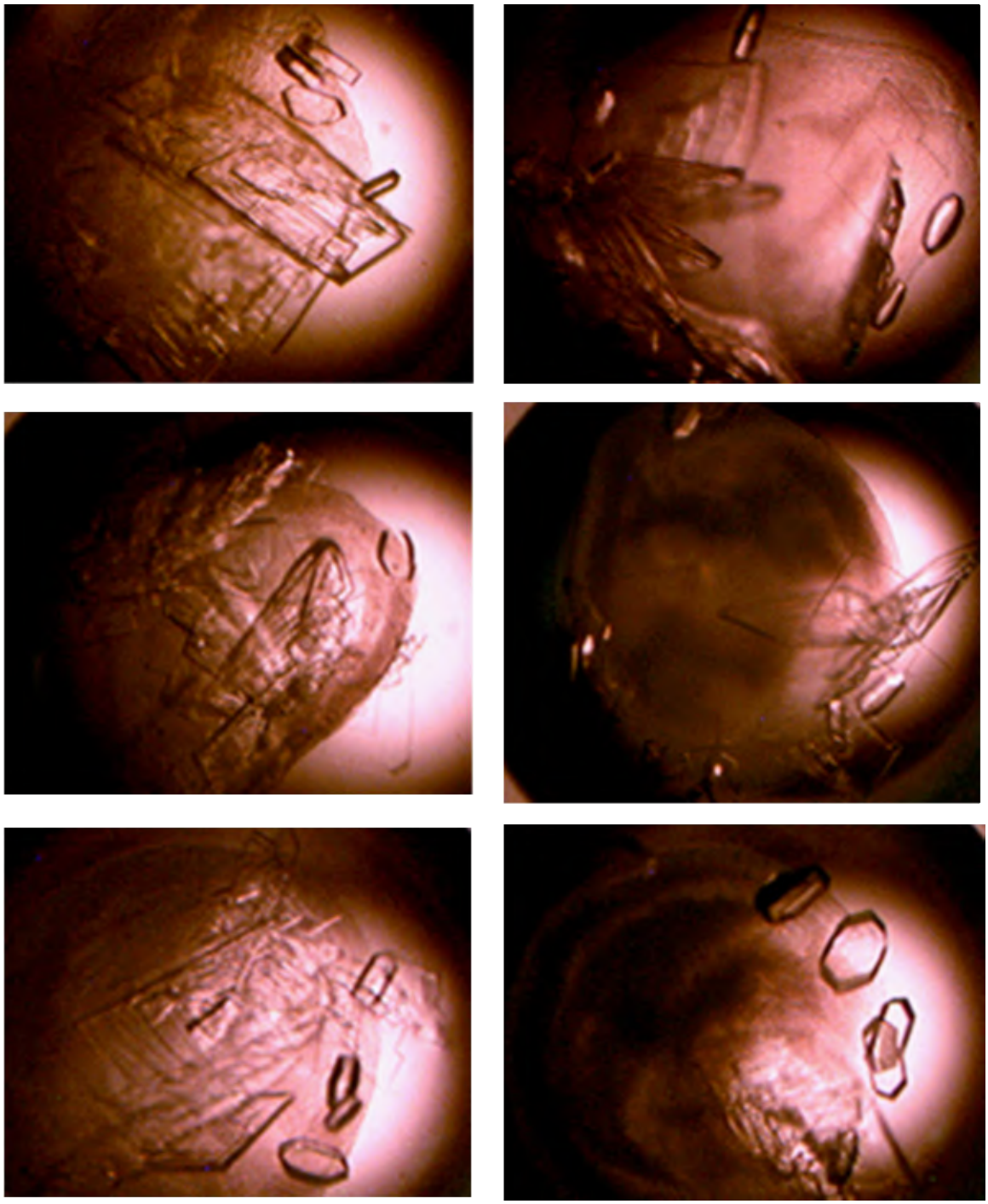

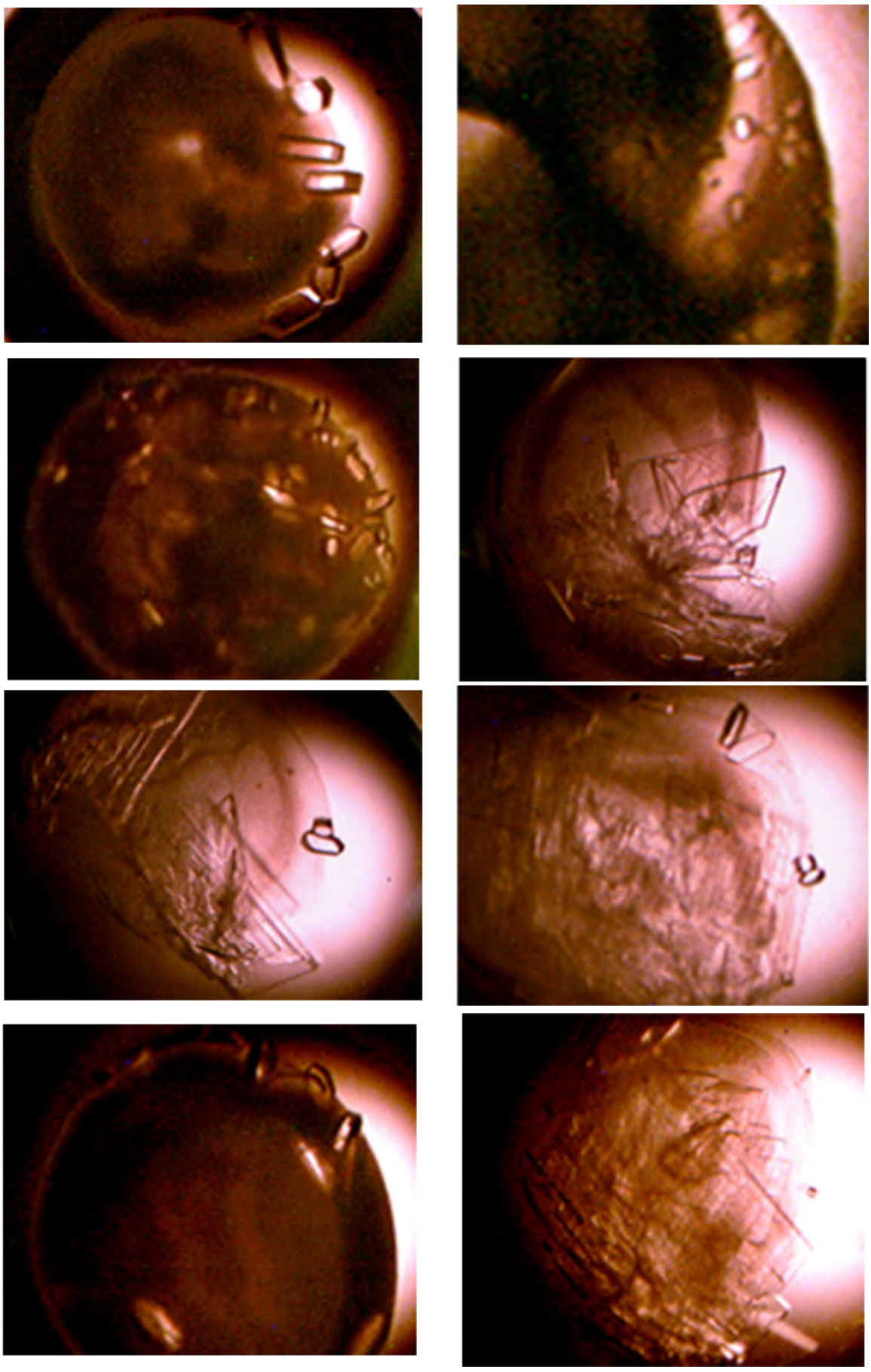


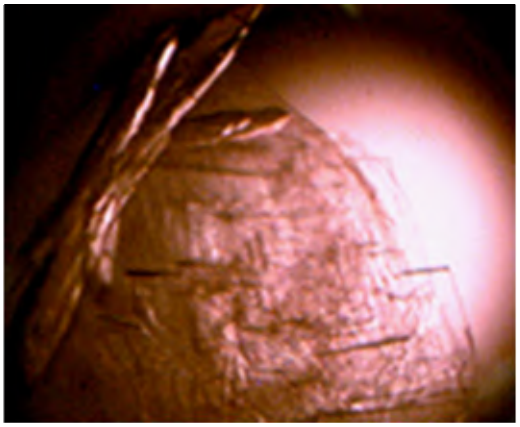
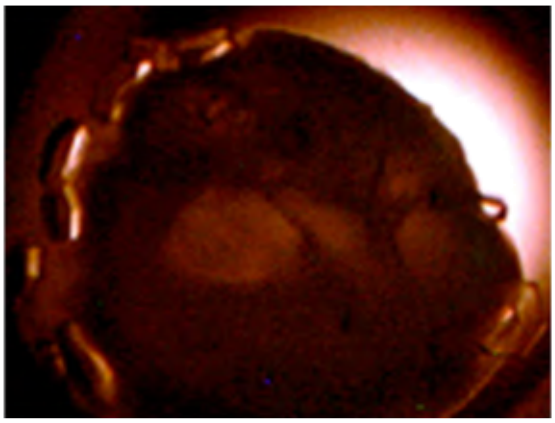
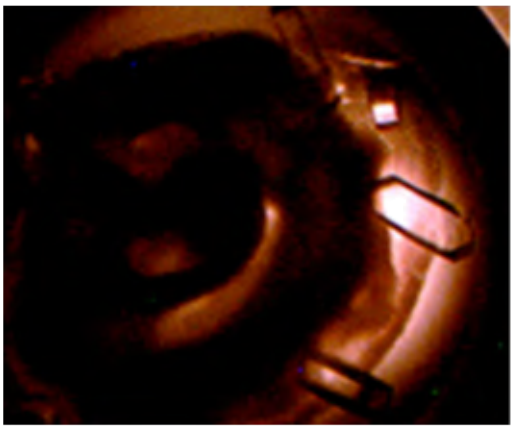
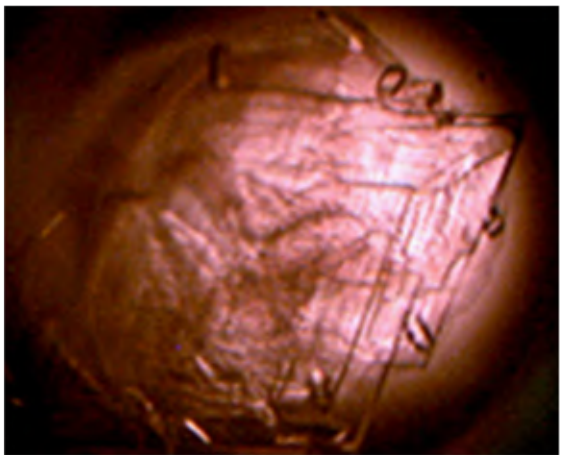
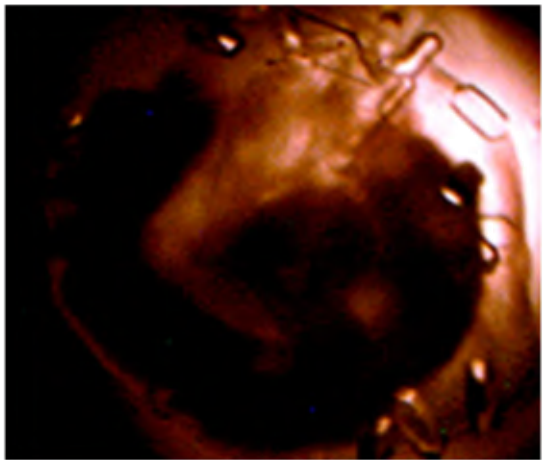
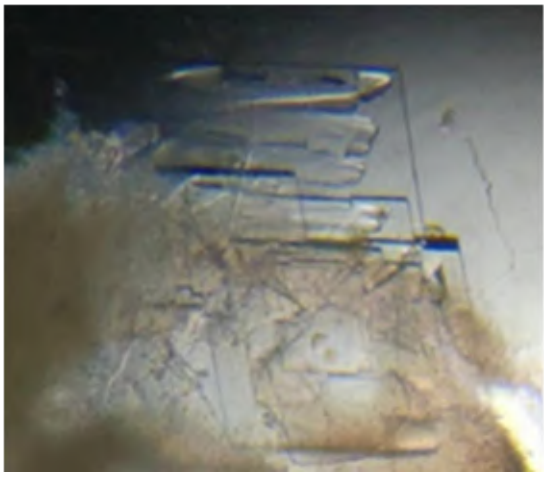
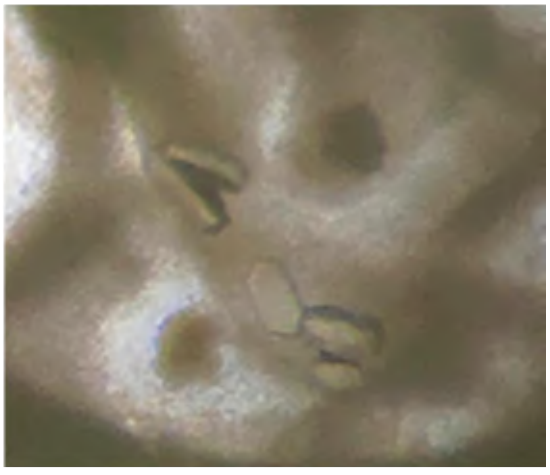

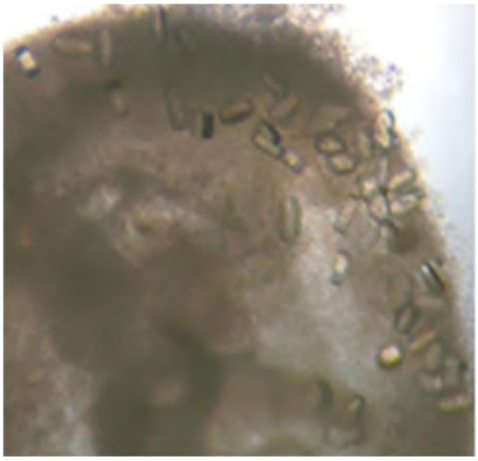
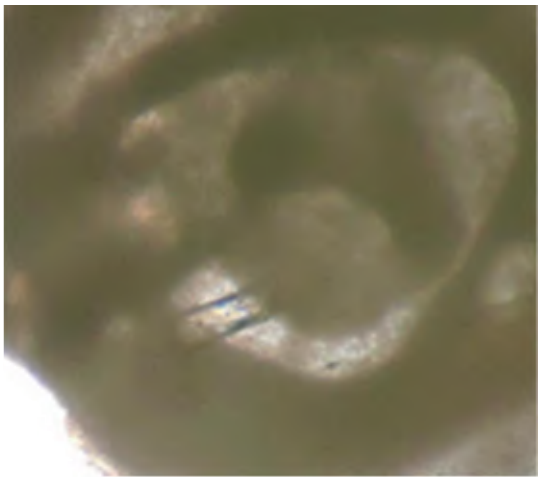
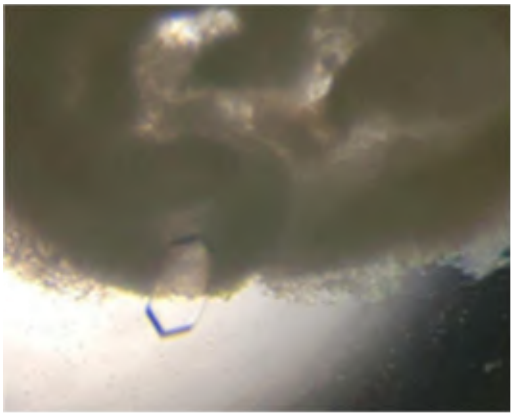
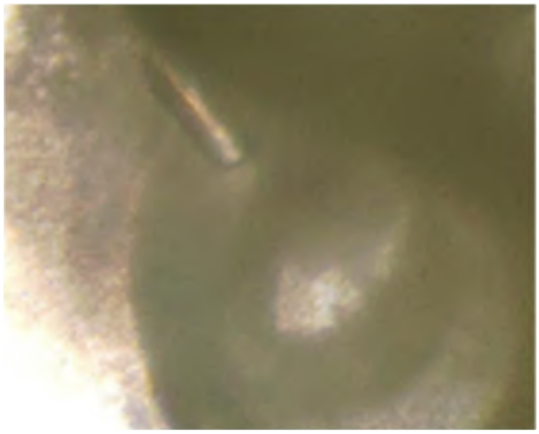
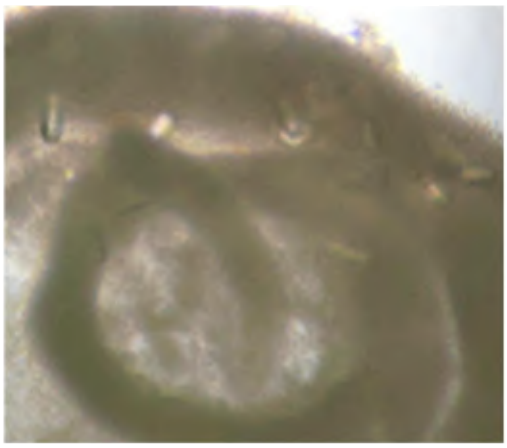
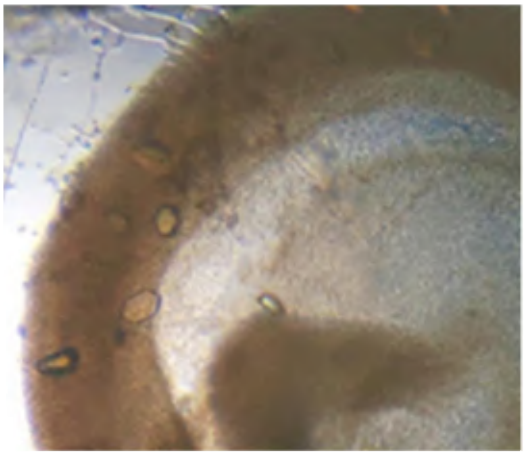
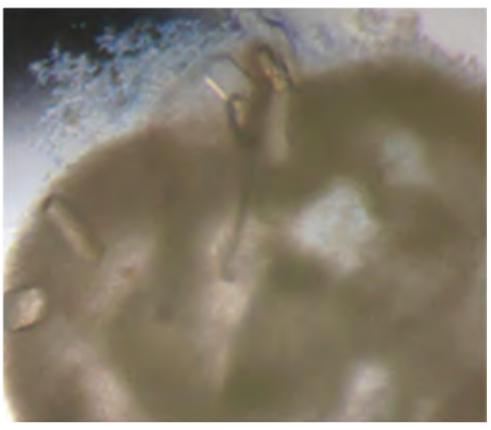
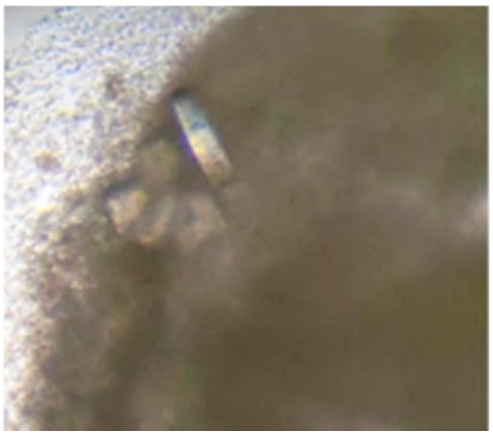

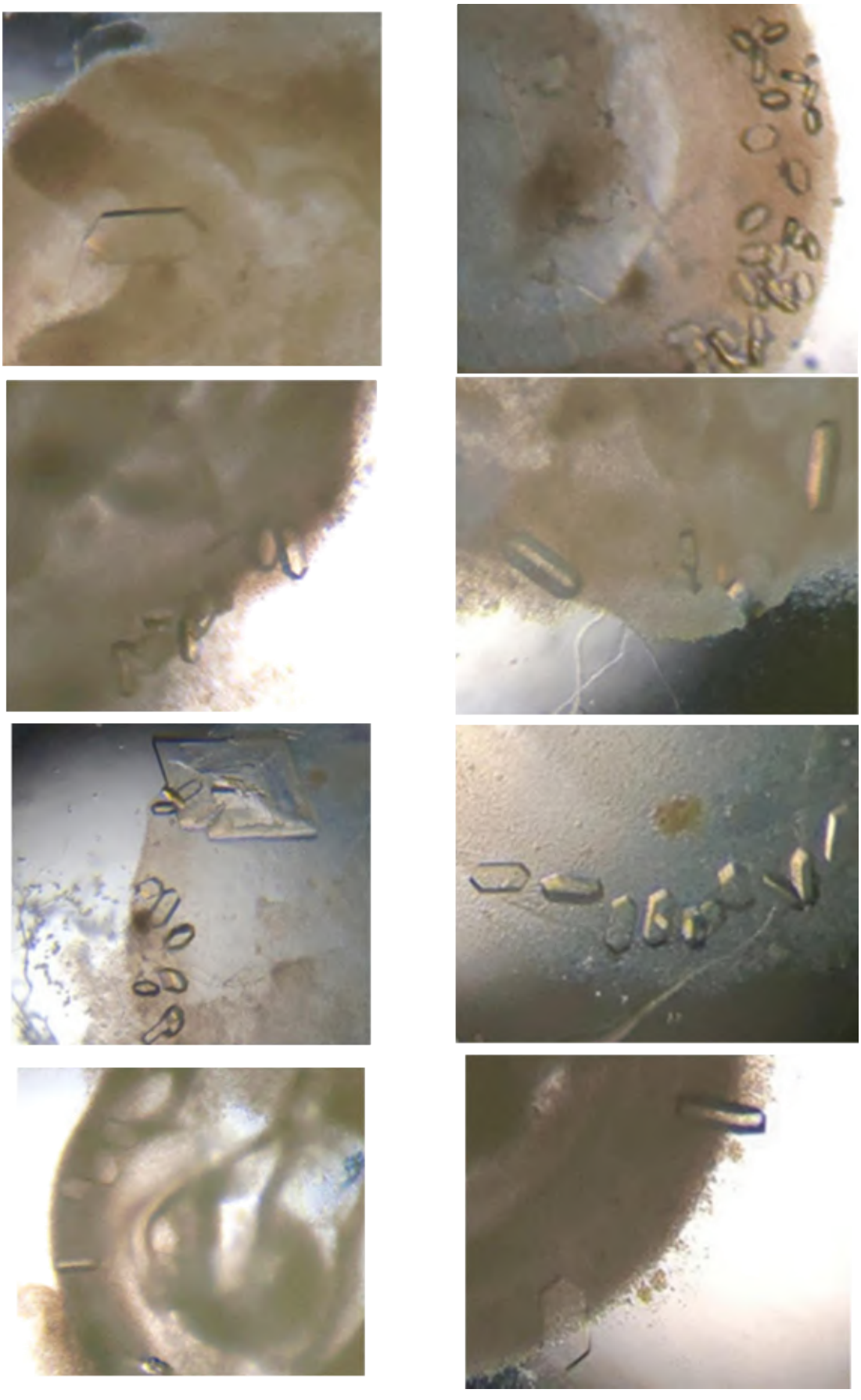

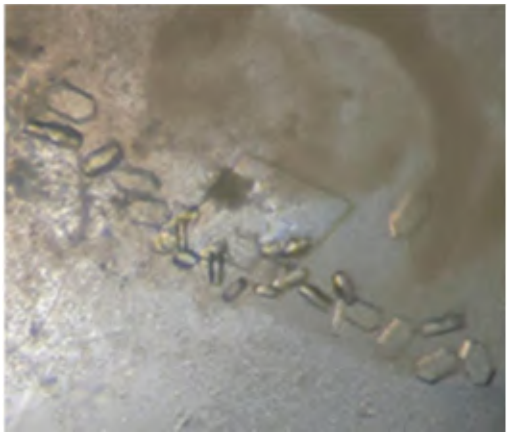

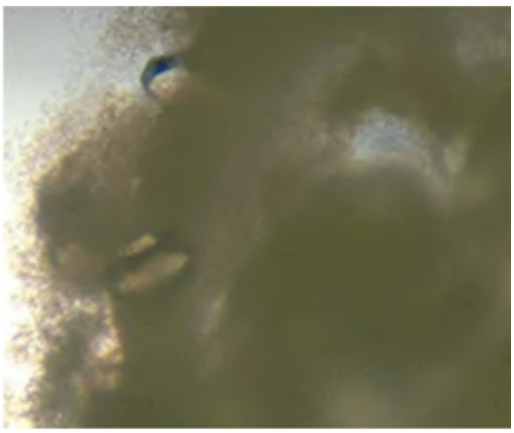

雙金屬 PaDHPase 晶體的篩選與優化。藉由不斷嘗試，微調原本長晶的條件，例如 PEG 濃度、pH 值、鹽類濃度等，或是調高原本的蛋白質濃度，也可以嘗試改變蛋白質和長晶條件溶液比例，從 1:1 改成 2:1 或更高，以利找尋晶體更適合的成長條件，而獲得晶型更大、更完整的晶體，有利後續收集 x 光繞射訊號解出結構時，有機會獲得解析度更高的數據。

3.3 PaDHPase 對於 pH 值依賴性的寡聚合現象

在篩選晶體條件並成功得到晶體的同時，我們發現和過去得到的晶體在相異極大的條件均有形成晶體，並且晶型也不相同，因此近一步藉由晶體結構以及膠體過濾色譜分析比較，發現在不同 pH 值分別形成不同聚體，推測此酵素可能因為不同的酸鹼環境改變化學鍵結，形成不同寡聚合現象。

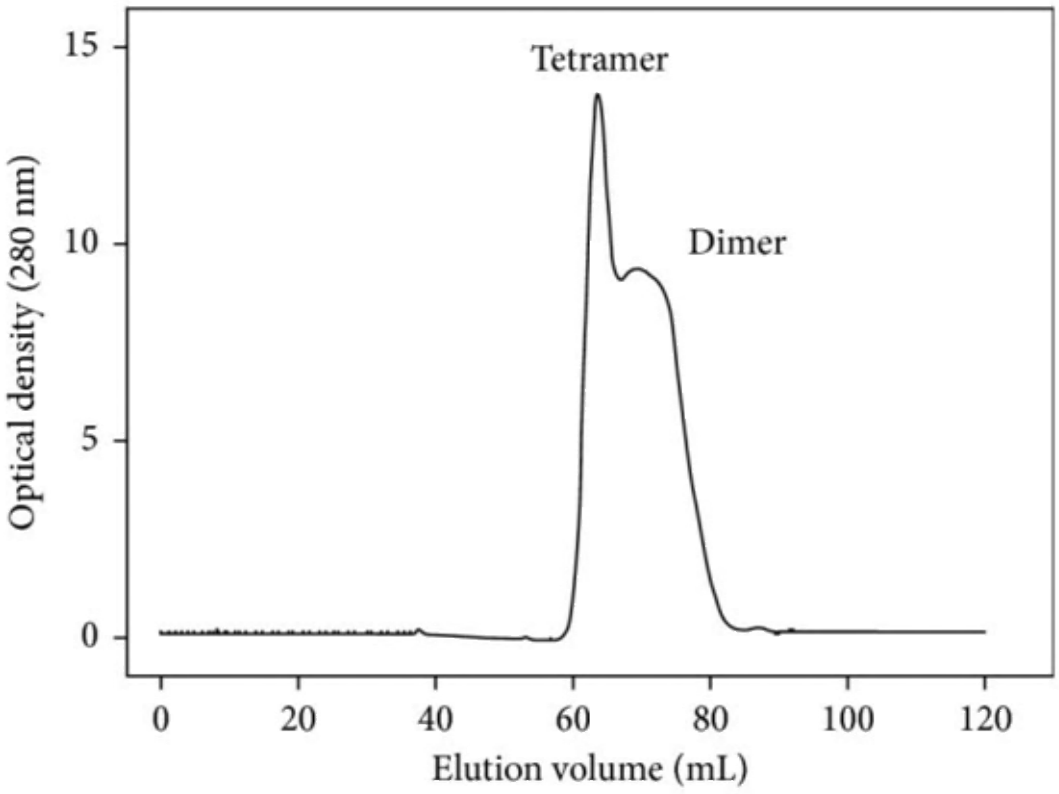

PaDHPase 在不同 pH 值的寡聚合現象。此次結構顯示為四套體而非原已知的雙套體，經過條件回推發現在晶體成長時的 pH 有所不同。pH 5.9 時，會形成四聚體；在 pH 為中性時，則形成二聚體。同時將純化好的 PaDHPase 蛋白質液體，利用膠體過濾法再次驗證，通過 buffer C (20 mM MES 和 100 mM NaCl，pH 5.9)，得到相對應分子量的訊號。正常單體的 PaDHPase 分子量為 53 kDa，而偵測到的兩個訊號分別為 105、180 kDa，恰巧約為單體的 2 倍和 4 倍。校正標準使用已知分子量的蛋白質：甲狀腺球蛋白（670 kDa）的，γ 球蛋白（158 kDa）的，卵清蛋白（44 kDa），肌紅蛋白（17 kDa），和維生素 B_{12}（1.35 kDa）。

3.4 單金屬PaDHPase的製備

PaDHPase是一個雙金屬的酵素。為了更加了解雙金屬中心對於DHPase的活性以及post-carboxylated lysine作用的重要性，我們嘗試藉由外在方式得到去金屬的PaDHPase。首先純化出雙金屬的PaDHPase，接著藉由自行配製的螯合劑溶液進行透析 (1 mM EDTA, 15 mM 8-HQSA, 50 mM MES, pH 6.5)。由於剛開始尚未確定透析時間，因此嘗試了幾種不同的時間，並且因為不確定透析過程中蛋白質是否會因為濃度過高而大量沉澱，所以也嘗試了不同濃度進行透析。透析之後會透過管柱層析去鹽後再進行濃縮。

我們將這些經不同透析狀況的蛋白質液利用質譜儀 (ICP-MS)分析，比較原先雙金屬 PaDHPase 和經過透析的差異。ICP-MS 顯示平均來說其中一顆金屬成功被去除，而測試酵素活性時發現，去除一顆金屬後的PaDHPase完全喪失活性。此時並不知道哪顆金屬被去除。

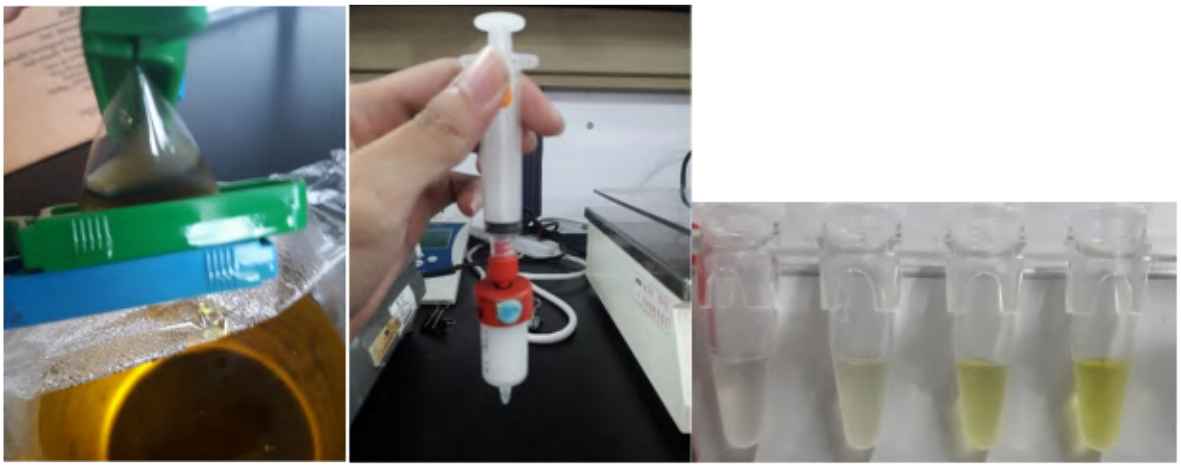

找尋與製備單金屬 PaDHPase。我們在嘗試不同的螯合劑條件，包括螯合劑種類、濃度與 pH 值後，我們發現在 1 mM EDTA, 15 mM 8-HQSA, 50 mM MES, pH 6.5 情況下透析雙金屬 PaDHPase 經 3 天可得到單金屬 PaDHPase; 單獨使用 EDTA 並無法螯合出 PaDHPase 的內含金屬。左圖:我們利用透析來浸置螯合劑於雙金屬 PaDHPase；中圖: 利用分子篩管柱層析去掉螯合劑(以及螯合出的金屬鹽溶液); 右圖:分管蒐集,此螯合劑配方為黃色,根據實驗結果我們僅蒐集前 1 mL 蛋白質溶液作為後續實驗所用(後來的結構證明這部分 PaDHPase 僅含一個金屬)。

3.5 單金屬PaDHPase結晶之獲得與結構之解出

為了更加確定究竟是活性區內的哪顆金屬被去除以及去除後如何影響酵素活性，因此我們欲藉由得到單金屬的 PaDHPase 晶體並解出結構，從結構方面來進一部探討。剛開始尚未確定透析時間，所以嘗試了幾種不同的時間,並且不確定透析過程中蛋白質是否會因為濃過高而大量沉澱,所以也嘗試了不同濃度進行透析，透過管柱層析後再進行濃縮。解出結構後，單金屬 PaDHPase 結晶結構解析度為 2.23 Å (表一)，發現僅剩一顆金屬(命名為 Znα) (圖 A)。同時發現和 Znα 作用的氨基酸包含: His59 (2.67 Å), His61 (2.72 Å), and D316 (2.29 Å)。

另外，更驚人的發現是當去除 Znß 我們發現原本 post-carboxylated lysine 轉變成正常帶正電的 lysine。因此結構的研究顯示此 post-carboxylation 並不是為了雙金屬中心而出現，即便此後修飾消失，仍有一金屬 Znα 不需羧化的氧原子來穩定。

我們將單金屬的 PaDHPase 和 TnDHPase 結構進行比較，發現單金屬的 TnDHPase (圖 B) 仍然具有 post-carboxylated lysine 的結構以及酵素活性，因此推測 post-carboxylated lysine 對於酵素活性有很大的影響，同時在 Znß 在 PaDHPase 的有無，也會間接影響 post-carboxylated lysine，所以 PaDHPase 後修飾的作用應該是由第二金屬 Znß 進入活性區來啟動。

單金屬 PaDHPase 結晶

PaDHPase 去金屬 3 次

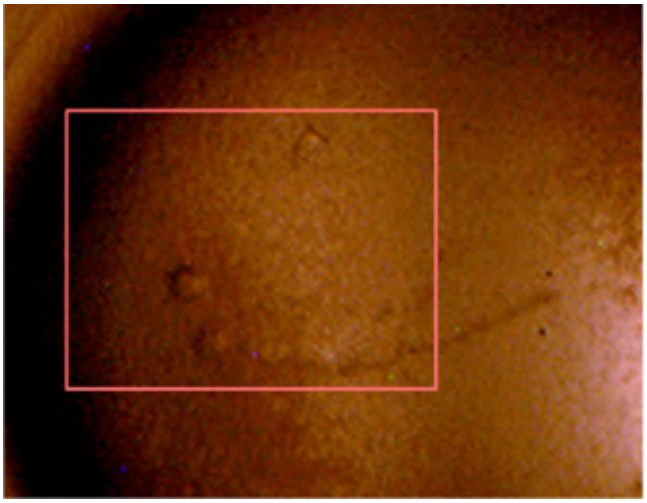

PaDHPase 去金屬 3 次

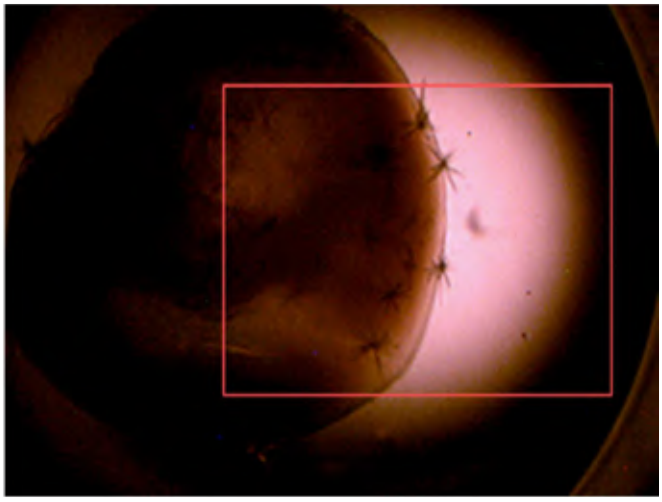

PaDHPase 去金屬 3 次

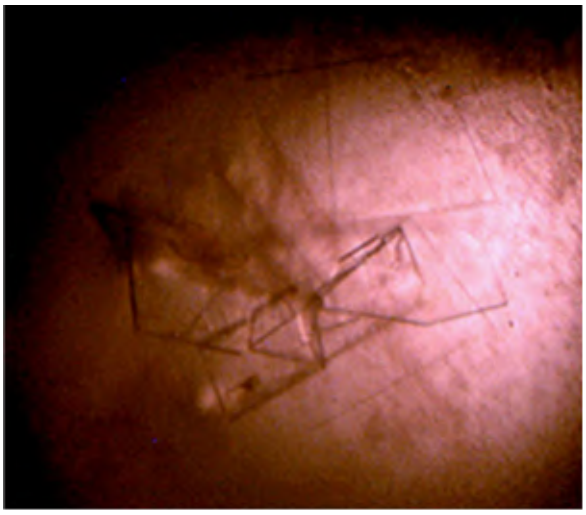

PaDHPase 去金屬 3 次

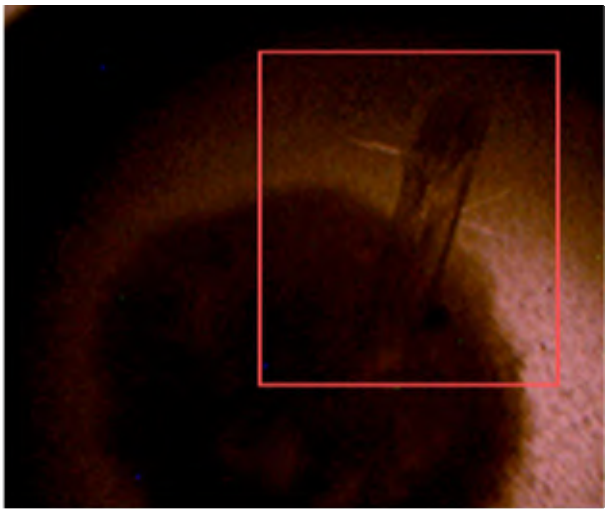

晶體名稱	長晶條件
PaDHPase 去金屬 3 次	30% PEG400, 100 mM MES, pH 6.5, 100 mM Magnesium Chloride
PaDHPase 去金屬 3 次	28% PEG550 MME, 100 mM MES, pH 6.5, 10 mM Zine Sulfate
PaDHPase 去金屬 3 次	25% PEG4000, 100 mM Tris-HCl, pH 8.5, 200 mM Calcium Chloride
PaDHPase 去金屬 3 次	30% PEG4000, 100 mM Tris-HCl, pH 8.5, 100 mM, Magnesium Chloride

PaDHPase 去金屬 3 次

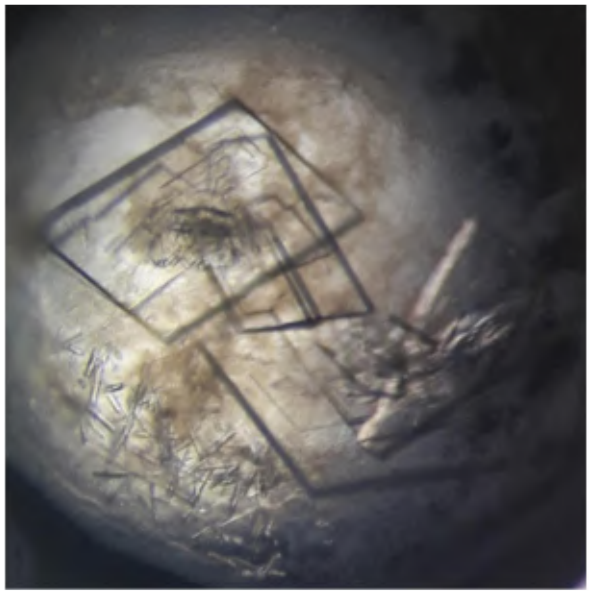

PaDHPase 去金屬 3 次

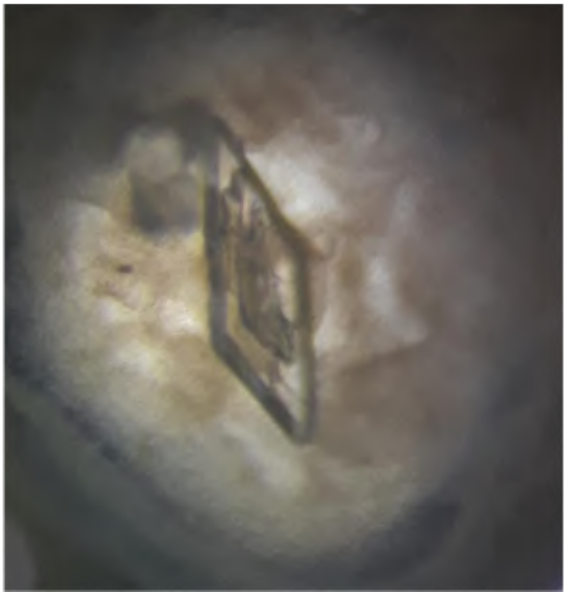

PaDHPase 去金屬 3 次

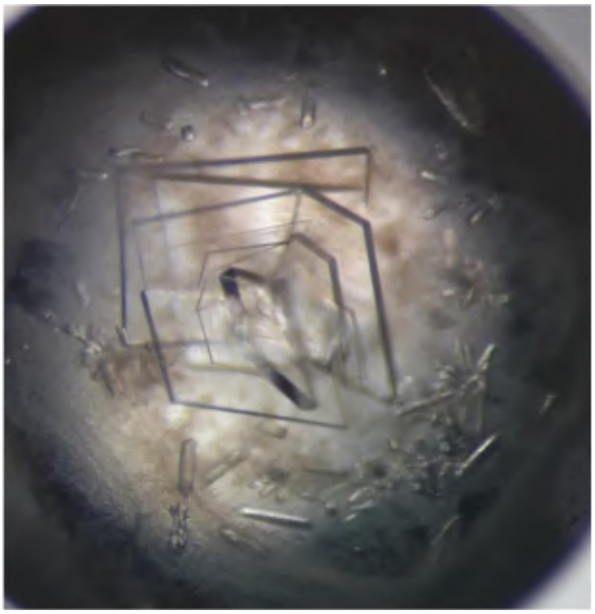

晶體名稱	長晶條件
PaDHPase 去金屬 3 次	22% PEG4000，200 mM Ammonium Sulfate，100 mM Sodium Acetate
PaDHPase 去金屬 3 次	20% PEG4000，100 mM Tris pH8.5，200 mM Calcium Acetate
PaDHPase 去金屬 3 次	20% PEG4000，100 mM Tris pH8.5，200 mM Calcium Acetate

單金屬 PaDHPase 晶體。藉由調高原本的蛋白質濃度，以及嘗試改變蛋白質和晶體成長溶液比例，從 1:1 改成 2:1，重新篩選長晶條件，成功將原本上圖細小如海膽尖刺或是薄片無厚度的晶體，經篩選重新找到新條件，獲得大顆且具有厚度的晶體。

繞射統計表

Data collection and refinement statistics.

Data collection		
Crystal	mono-Zn PaDHPase	huDHOase K1556A
Wavelength (Å)	0.975	0.975
Resolution (Å)	30–2.23	30–2.77
Space group	$P2_12_12$	$C222$
Cell dimension (Å)	$a=88.36\ \alpha=90$ $b=110.17\ \beta=90$ $c=112.66\ \gamma=90$	$a=88.84\ \alpha=90$ $b=108.63\ \beta=90$ $c=99.22\ \gamma=90$
Completeness (%)	99.8 (99.9)[a]	99.9 (99.7)[a]
$(I/\sigma I)$	12.9 (3.9)	23.68 (2.74)
R_{sym} or R_{merge} (%)	0.133 (0.491)	0.07 (0.498)
Redundancy	5.1 (5.2)	4.4 (4.4)
Refinement		
Resolution (Å)	29.28–2.23	29.8–2.77
No. reflections	54478	12440
R_{work}/R_{free}	0.1819/0.2323	0.2260/0.2889
No. atoms		
Protein	956	363
Zinc	1	1
Water	283	14
R.m.s deviation		
Bond lengths (Å)	0.008	0.011
Bond angles (°)	0.980	1.188
Ramachandran Plot		
In preferred regions	909 (95.48%)	335 (92.80%)
In allowed regions	35 (3.68%)	21 (5.82%)
Outliers	8 (0.84%)	5 (1.39%)
PDB entry	6AJD	5YZN

PaDHPase 單金屬(透析 3 次)

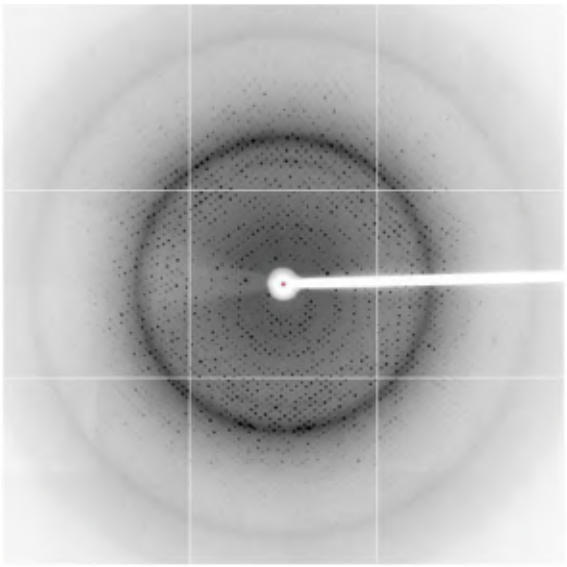

利用 loop 挑取右圖 PaDHPase 單金屬 (透析 3 次) 在該條件內晶型最立體且大顆的晶體，該晶體是在長晶條件為 (20% PEG 4000，100 mM Tris pH 8.5，200 mM Calcium Acetate) 的環境下形成之結晶，利用 x 光繞射進行繞射實驗收集繞射數據，在接收器距離 250 單位，光源釋放 5 秒，角度從 50 收到 170 度的情況下進行實驗 (Distnce: 250，Time: 5 s，Phi: 50~170)，最後得到析度為 2.23 Å。

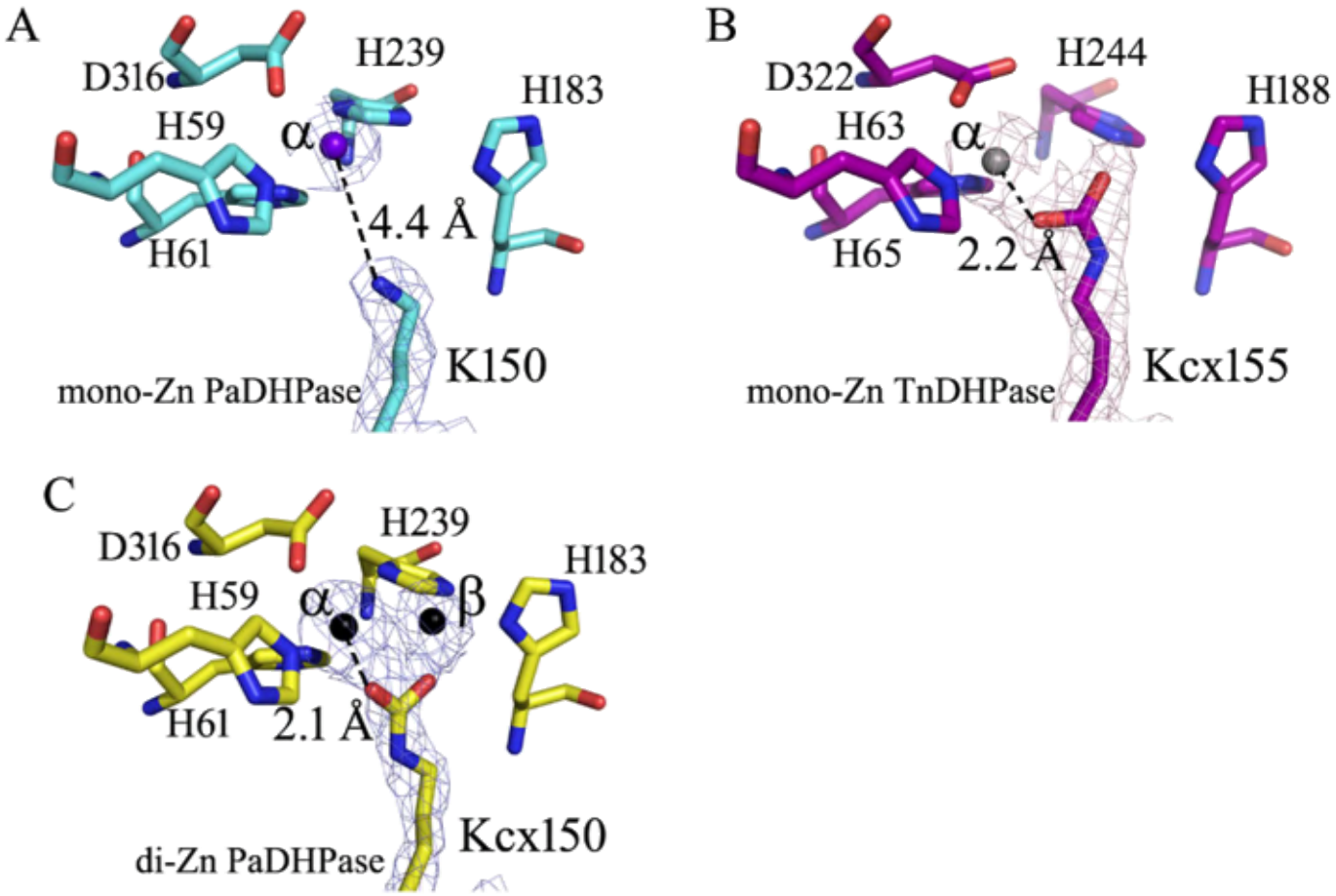

活性區的結構。(A) 單金屬 PaDHPase：Lysine 並無後修飾的現象，同時從結構上可以發現正常帶正電的 lysine 和金屬 Znα 距離過遠 (4.4Å) 而無作用力，表示 Znα 的穩固和 lysine 無關。(B)單金屬 TnDHPase：活性區內僅有一個金屬 Znα，不過其仍然具有 post-carboxylated lysine。(c) 雙金屬 PaDHPase：活性區內具有兩個金屬鋅離子(Znα 和 Znß)，並且具有後修飾的 post-carboxylated lysine。綜合圖 ABC，lysine 在單金屬 TnDHPase 和雙金屬 PaDHPase 均具有 post-carboxylation，但在單金屬 PaDHPase 卻沒有，而是原本正常帶

正電的 lysine。因此，可說明單金屬 PaDHPase 為何沒有活性而單金屬 TnDHPase 有活性，因為單金屬 PaDHPase 失去了後修飾的羧基。更多值得研究的問題包括為何相似的酵素何來不同的修飾機制？以及親核攻擊官能基 Asp316 並未遠離活性區為何單金屬 PaDHPase 完全失去活性？這些由此計畫執行後所帶出的新問題仍待下一階段的驗證。

3.6 藉由質譜分析單金屬PaDHPase

為了驗證單金屬和雙金屬PaDHPase的結構差異是否為真，我們亦使用了MALDI-TOF質譜儀的分析來比較。藉由將獲得晶體的單金屬和雙金屬PaDHPase並解出結構的同管蛋白質液利用MALDI-TOF 質譜儀分析其分子量並進行比較。理論上基因產物分子量會完全相同，除非有其他因素，如後修飾或剪切等。我們的結果顯示單金屬和雙金屬的 PaDHPase 分子量分別為 52952.87 和 52997.34，相差為44.47，恰巧為 COO 修飾的分子量差，剛好呼應結構上發現的，當僅有Znα時則無post-carboxylation。

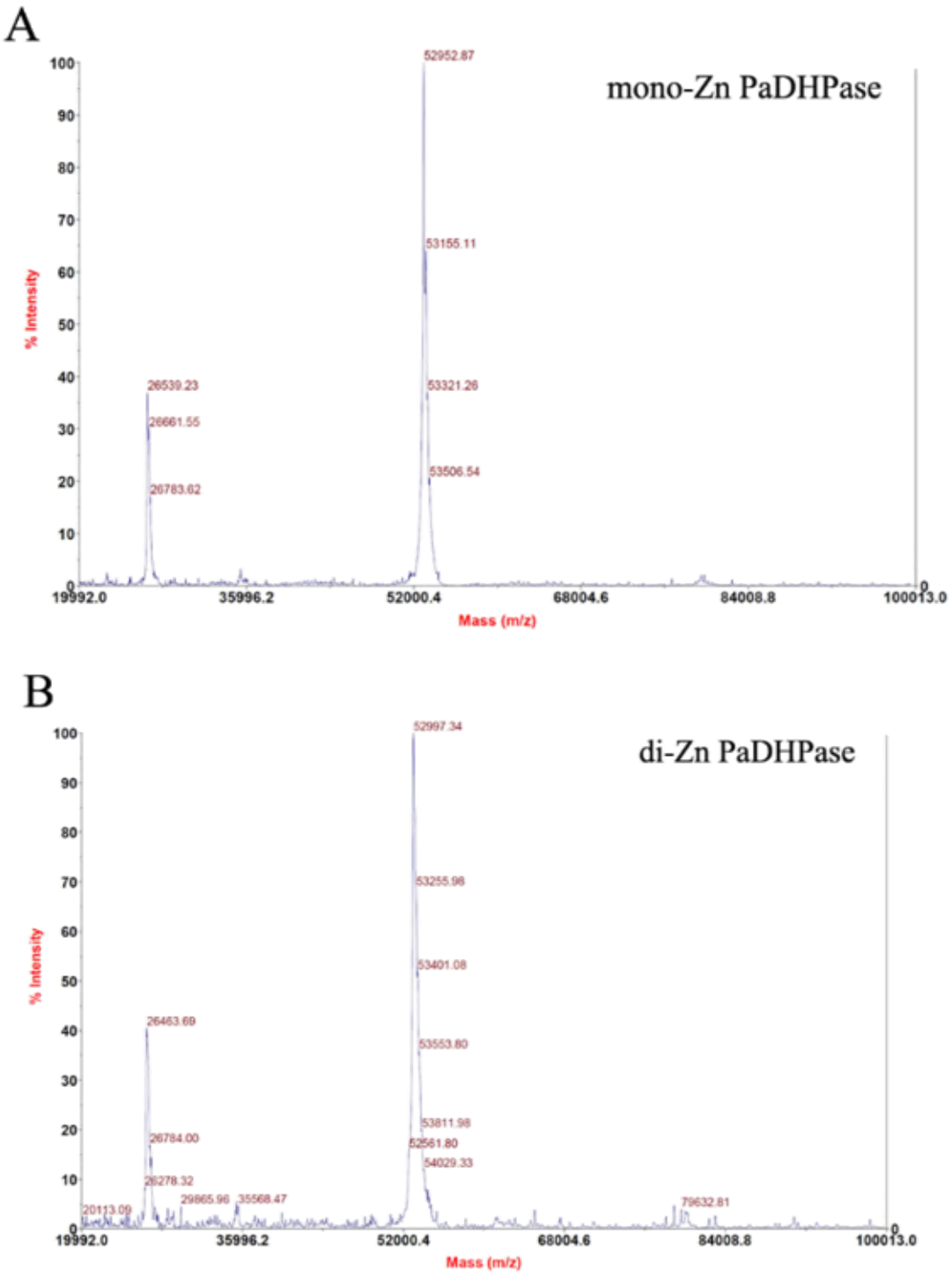

雙金屬 PaDHPase 與單金屬 PaDHPase 的質譜儀分析。我們利用付費方式送件分析這兩種 PaDHPase，發現分子量相差約 44 Da (52997-52953 = 44)，恰好就是 COO 修飾的分子量差。此結果與結晶結構相互呼應後修飾是由第二金屬進入活性區來啟動此化學後修飾。

意即沒有 Znß 就沒有後修飾。目前我們推論其化學反應應該是由帶正電的金屬極化 CO_2 的負電促使新共價鍵的形成，並接著參與雙金屬活性中心的自我組裝。

3.7 單金屬與雙金屬PaDHPase結構比較

進一步將單金屬與雙金屬 PaDHPase 活性區進行重疊，發現 His239 和 His183 角度上有些許旋轉，單金屬(cyan)的His239和His183角度上相較於雙金屬(yellow)分別移動 20.09º 和 12.95º，距離上則移動 1.14 和 0.58 Å。另外從結構上可觀察到羧化的Lys150在雙金屬以及未羧化的Lys150在單金屬其位置並無明顯不同。

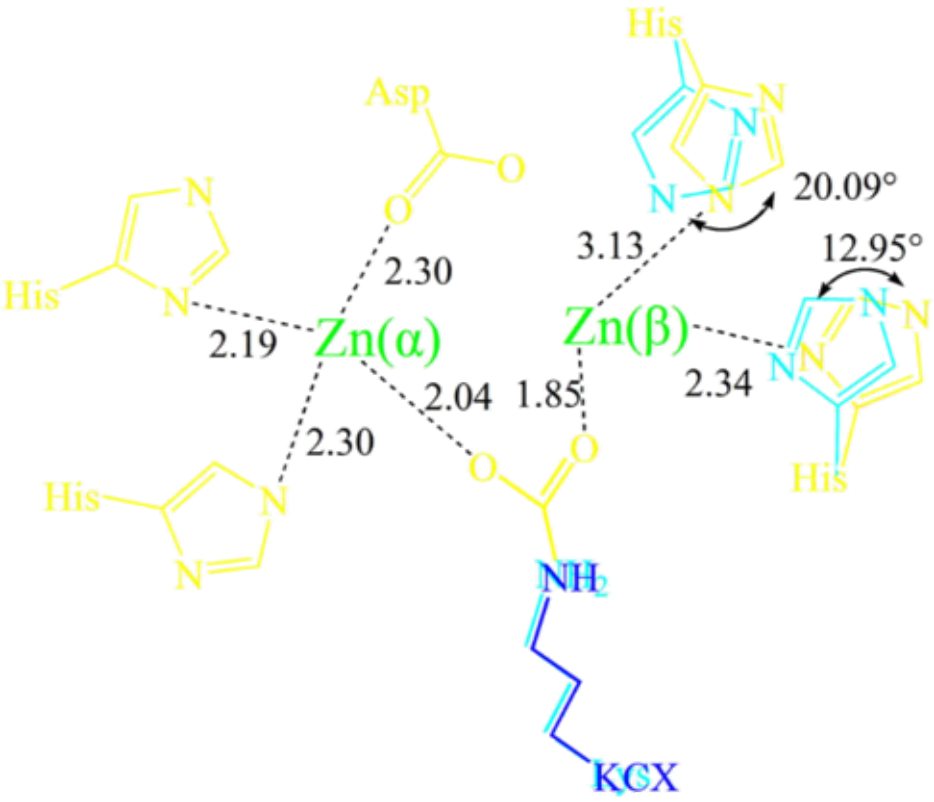

單金屬與雙金屬PaDHPase活性區結構比較。將單金屬與雙金屬PaDHPase活性區進行重疊，可以發現單金屬(cyan)的His239和His183角度上相較於雙金屬(yellow)分別移動20.09º和12.95º，距離上移動1.14和0.58 Å，顯示第二個金屬鋅進入活性區才能使活性區穩固。

3.8 huDHOase K1556A之結構 (human DHOase K1556A)

除了DHPase之外，cyclic amidohydrolase家族的其他成員活性區內是否也需要雙金屬才能穩固活性區，因此我們嘗試利用相同方法藉由將雙金屬huDHOase透析並希望得到晶體，不過此方法並未成功，經篩選無法獲得有效晶體。接著我們嘗試將 huDHOase 進行 K1556A 之突變並經過多次篩選後順利順利得到晶體，並且這個點突變的 huDHOase 亦解出結構。huDHOase K1556A結構的解析度為2.77 Å (PDB entry 5YNZ)。從結構上看到 huDHOase K1556A 的突變活性區內仍然保有一個金屬Znα，與單金屬PaDHPase相同。因此過去認為post-carboxylated lysine能穩固活性區的雙金屬可能不完全正確，同時從結構上也能發現在活性區內的雙金屬，Znß 相較於Znα 比較不穩定而容易跑出，這點和單金屬PaDHPase極為相似，即 Znß 和post-carboxylated lysine之間的影響有很大的關聯。

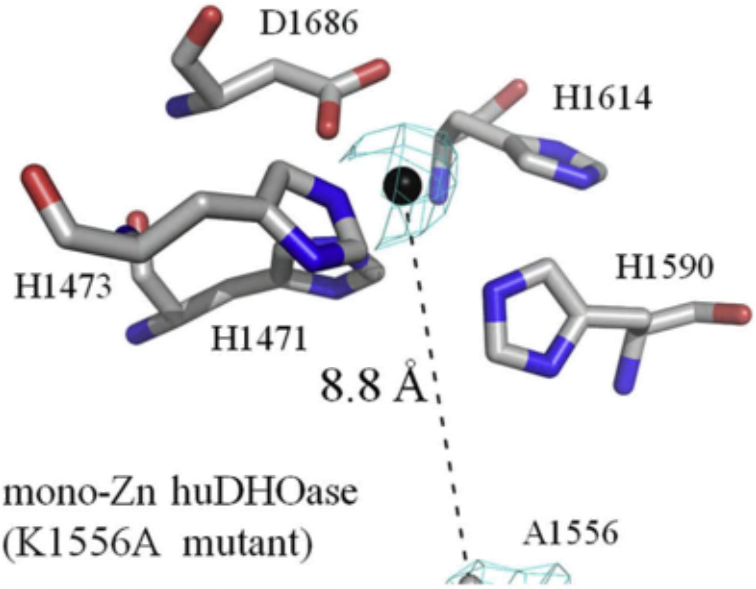

huDHOase K1556A之結構。當將post-carboxylated lysine進行突變後發現Znα仍然在活性區內，而Znß則消失，因此過去認為post-carboxylated lysine能穩固活性區的雙金屬可能不完全正確。即便沒有此後修飾，Znα仍可存在。另外，和單金屬 PaDHPase 相似，若無 Znß 則無 post-carboxylated lysine，因此Znß和post-carboxylated lysine之間的影響有很大的關聯。此結果亦顯示post-carboxylation可透過 Znß 調控，並且是一個可逆反應，端取決於Znß的存在與否。

3.9 其他複合結晶結構與點突變結構

目前已知 PaDHPase 活性區內的金屬 Znß 在活性區內扮演比較重要的角色，在單金屬PaDHPase結構中可發現，若無Znß則無post-carboxylated lysine，因此目前我們正在嘗試幾種抑制劑，例如某臨床藥物以及自行篩選具抑制活性的化合物，期望能得到共結晶的結

構(圖a)，並透過分子結構了解抑制機制以利進行藥物設計及優化。

同時，在上述發現雙金屬中心的穩固並非直接和post-carboxylated lysine相關，再加上cyclic amidohydrolase家族活性區內的氨基酸又都相同，也激起我們想更加了解活性區內胺基酸和雙金屬之間的關聯及影響，藉由點突變的結晶結構觀察活性區及雙金屬的變化，同時測量活性，以利更加了解影響此酵素活性的原因。

(圖a)

DHPase+抑制劑1

DHPase+抑制劑2

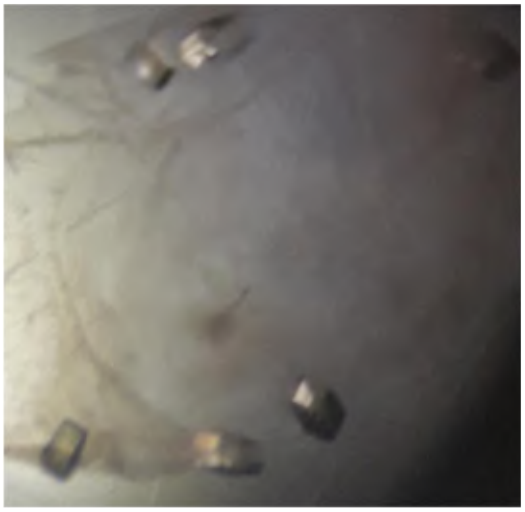

DHPase+抑制劑3

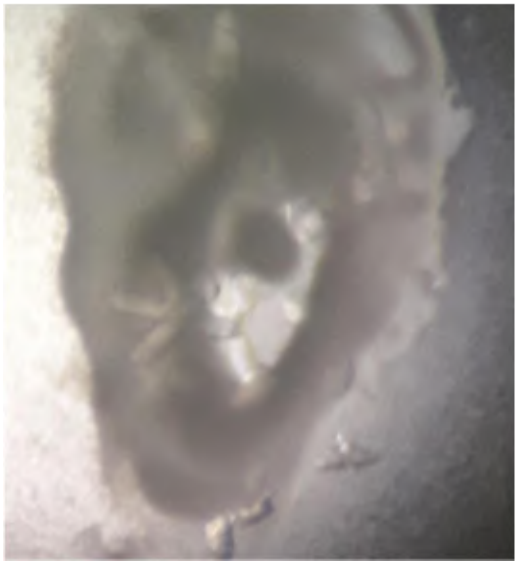

DHPase+抑制劑4

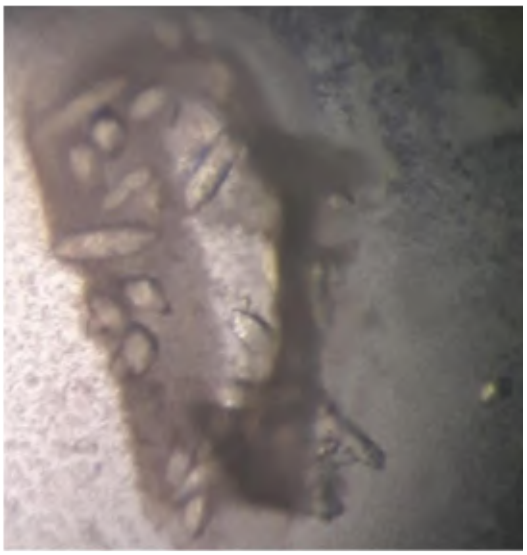

晶體名稱	長晶條件
DHPase+抑制劑1	10% PEG 8000，100 mM HEPES pH7.5，200 mM Calcium Acetate
DHPase+抑制劑2	10% PEG 8000，100 mM HEPES pH7.5，200 mM Calcium Acetate
DHPase+抑制劑3	17%PEG20000，100mM Tris pH8.5，100mM Magnesium Chloride
DHPase+抑制劑4	17%PEG8000，100mM Tris pH8.5，100mM Magnesium Chloride

DHPase+抑制劑4

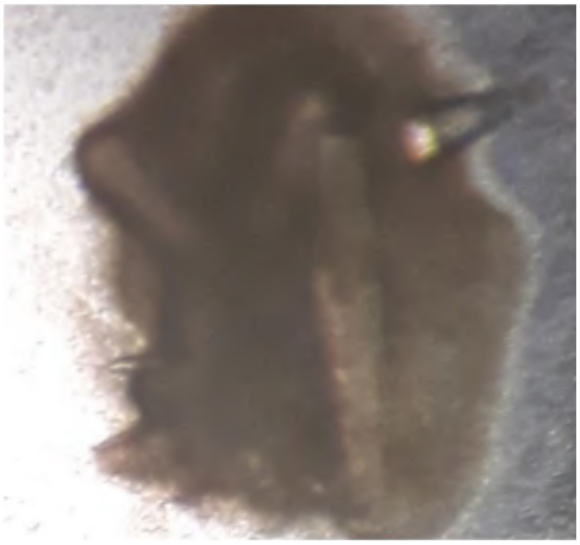

DHPase+抑制劑4

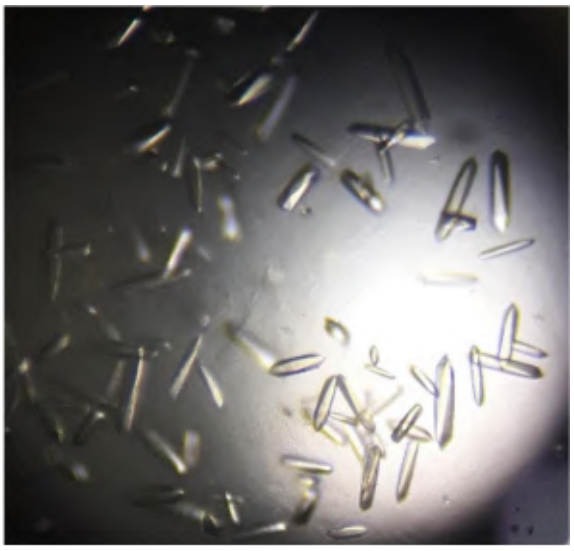

DHPase+抑制劑5

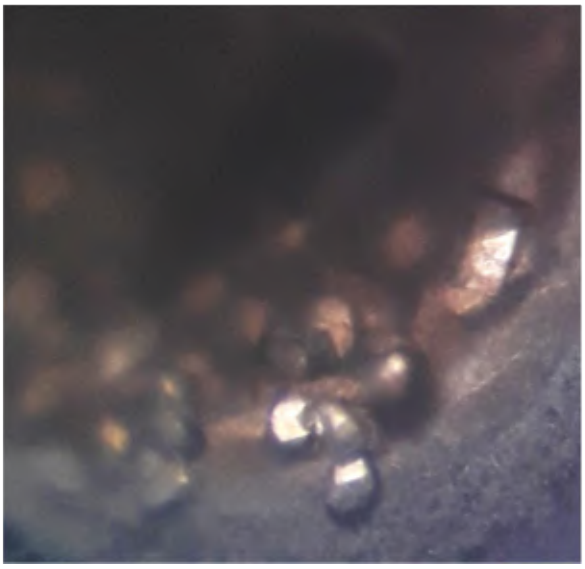

晶體名稱	長晶條件
DHPase+抑制劑4	18% PEG8000，100mM HEPES pH7.5，200mM Calcium Acetate
DHPase+抑制劑4	1.5mM Ammonium Sulfate，15% Glycerol，100mM Tris pH8.5
DHPase+抑制劑5	25% PEG4000，100mM Tris pH8.5，200mM Calcium Chloride

(圖b)

DHPase 突變株1

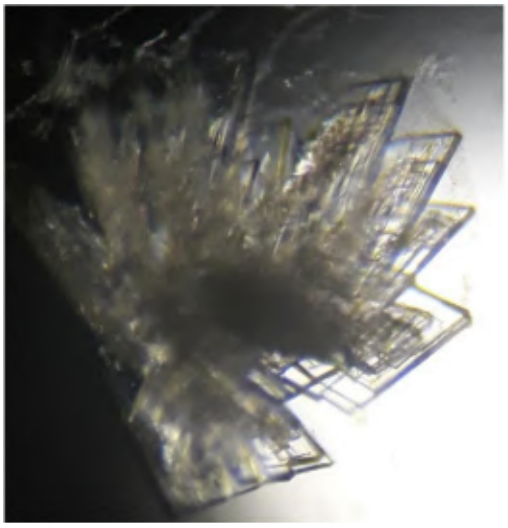

DHPase 突變株1（優化）

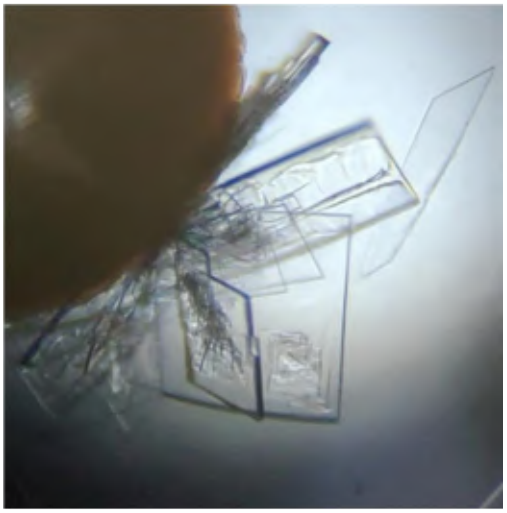

DHPase 突變株1（優化）

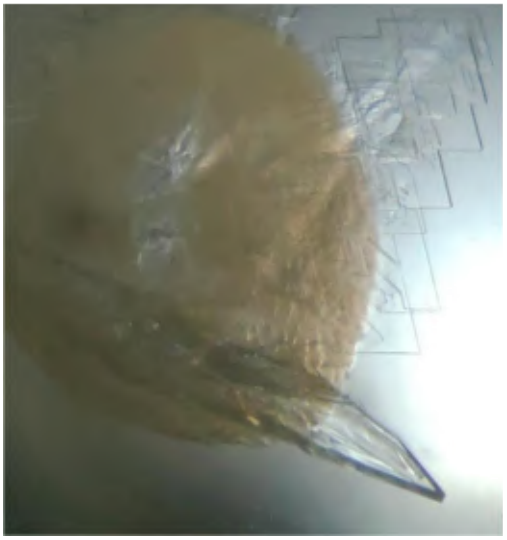

DHPase 突變株1（優化）

晶體名稱	長晶條件
DHPase 突變株1	18% PEG8000，100mM HEPES pH7.5，200mM Calcium Acetate
DHPase 突變株1(優化)	20% PEG8000，100mM HEPES pH7.5，200mM Calcium Acetate
DHPase 突變株1(優化)	16% PEG8000，100mM HEPES pH7，200mM Calcium Acetate
DHPase 突變株1(優化)	20% PEG8000，100mM HEPES pH7.5，200mM Calcium Acetate

(圖b)

DHPase 突變株2

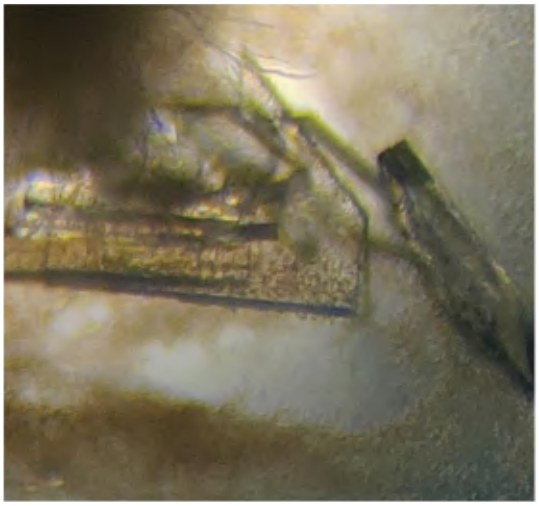

DHPase 突變株2（優化）

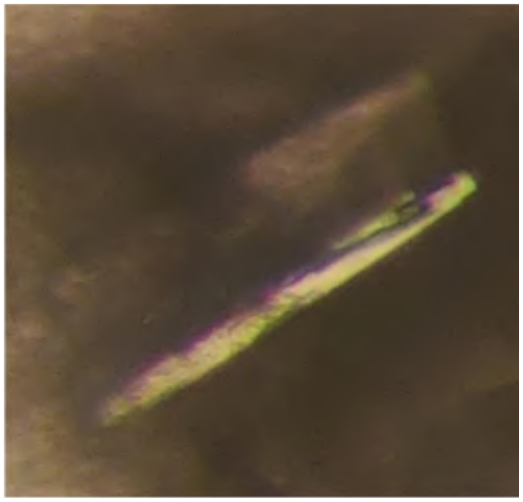

DHPase 突變株2（優化）

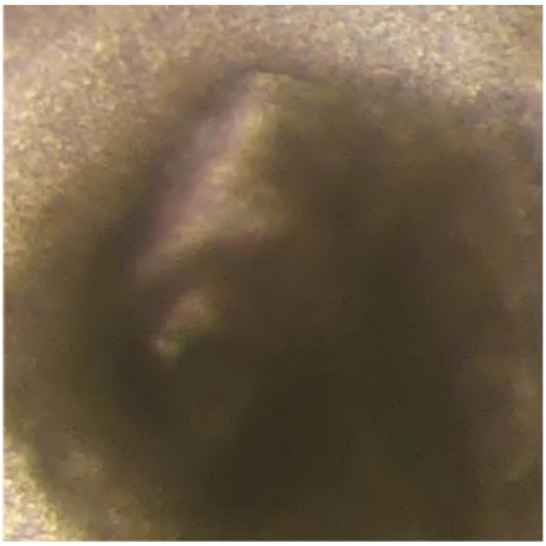

DHPase 突變株2（優化）

晶體名稱	長晶條件
DHPase 突變株2	18% PEG8000，100mM HEPES pH7.5，200mM Calcium Acetate
DHPase 突變株2(優化)	16% PEG8000，100mM HEPES pH7，200mM Calcium Acetate
DHPase 突變株2(優化)	18% PEG8000，100mM HEPES pH7，200mM Calcium Acetate
DHPase 突變株2(優化)	18% PEG8000，100mM HEPES pH7，200mM Calcium Acetat

DHPase 突變株1	DHPase 突變株2(優化)
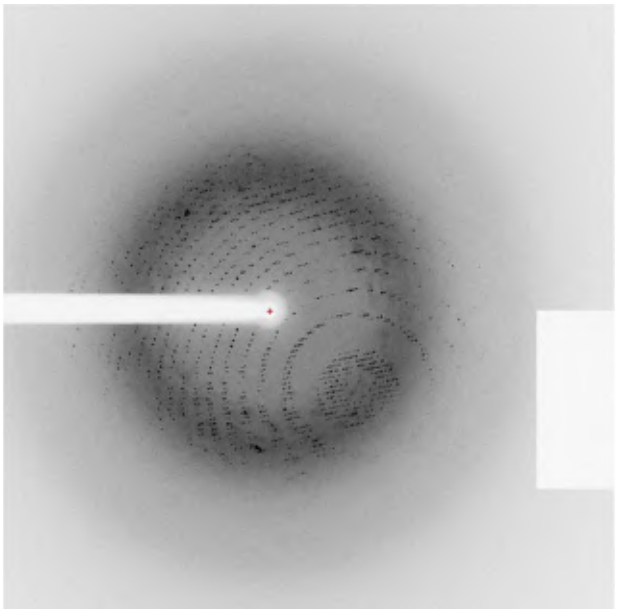	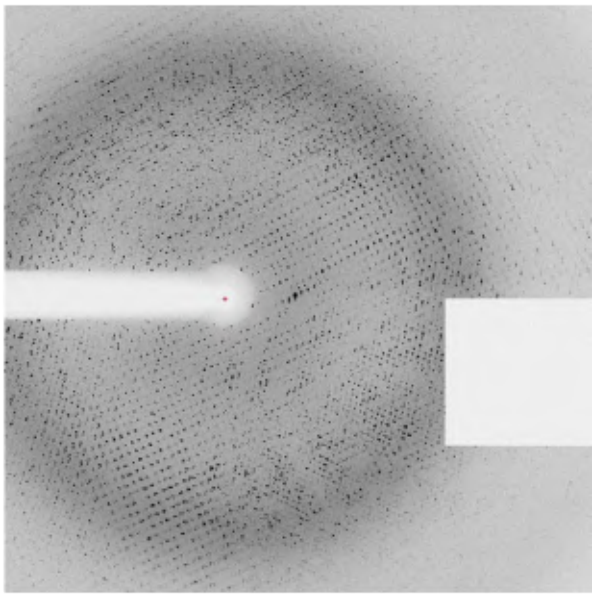
利用loop挑取DHPase 突變株1，在該條件內晶型最立體且大顆的晶體，該晶體是在長晶條件為 (20% PEG 8000，100 mM HEPES, pH7.5，200 mM Calcium Acetate)的環境下形成之結晶，利用x光繞射進行繞射實驗收集繞射數據，在接收器距離170單位，光源釋放0.1秒，角度從92收到170度，且每0.2度收一張圖。	利用loop挑取DHPase 突變株2 (優化)，在該條件內晶型最立體且大顆的晶體，該晶體是在長晶條件為(16% PEG 8000，100 mM HEPES, pH7，200 mM Calcium Acetate)的環境下形成之結晶，利用x光繞射進行繞射實驗收集繞射數據，在接收器距離200單位，光源釋放2秒，角度從95收到205度，且每0.5度收一張圖。

(圖c)

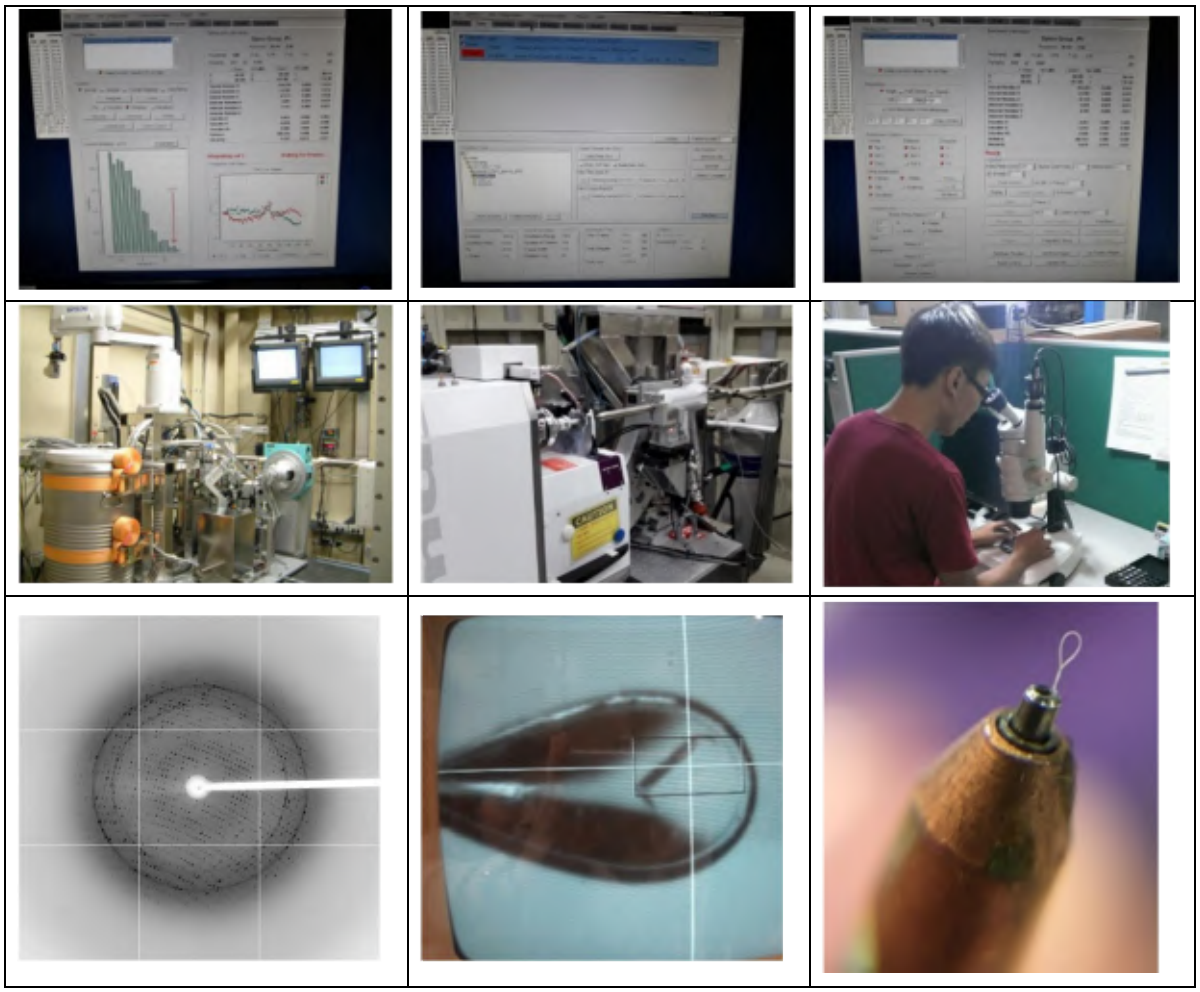

其他複合結構與點突變結構亦正在解析。(a) PaDHPase 與抑制劑共結晶。嘗試了幾種抑制劑的共結晶，目前正在解析中。(b) PaDHPase 點突變之晶體。嘗試了活性區內幾個胺基酸的突變，目前結構亦正在解析。(c)實際操作之圖片。上圖: 使用電腦軟體來解析複合晶體; 中圖: 利用顯微鏡觀察晶體與使用同步輻射光來收集繞射數據; 下圖: 使用晶體環撈晶體上光束線分析繞射強度。

3.10 其他家族成員結晶結構

Cyclic amidohydrolase 家族的其他成員活性區如 ALLase 與 DHOase 和 PaDHPase 幾乎一樣，但這些酵素活性區的後修飾機制是否和 PaDHPase 相同，即當僅有一個金屬鋅在活性區則無法形成 post-carboxylated lysine 仍未知。單金屬酵素具有活性與否，包括必須要第二個金屬 Znß 進入活性區才能穩固活性區，這部分的資訊亦仍然未知。

因此，我們透過螯合劑溶液 (1 mM EDTA, 15 mM 8-HQSA, 50 mM MES, pH 6.5) 透析，希望藉由執行此 PaDHPase 計畫的成功來進行下一階段 ALLase 與 DHOase 的新結果，所以我們嘗試將傷寒沙門氏菌 (*Salmonella enterica* serovar Typhimurium; Sty)的 ALLase (圖 a) 和 huDHOase 進行去金屬程序，冀能利用結晶結構獲得後修飾資訊與金屬中心相關資訊(圖 b)。

目前雖然有得到看起來疑似像蛋白質晶體的晶體，也試著利用 x 光繞射進行分析，不過得到的結果不是繞射點解析度太差，就是完全沒有繞射點，又或者是該晶體其實是鹽，因此現在仍然在嘗試重新優化實驗條件或是可能需要改用其他實驗方法。

所以目前有嘗試將 huDHOase 活性區的 post-carboxylated lysine 進行某些突變並獲得晶體結構，探討 Znß 和 post-carboxylated lysine

以及其他金屬結合胺基酸如 His 與 Asp 突變的關聯性。

StyALLase 去金屬酵素製備方式目前利用和 PaDHPase 相同的方式進行去金屬並長成晶體，不過收集的繞射圖訊號卻不如預期，嘗試了三個不同條件的不同晶體但得到的繞射圖卻是空的完全沒有點，因此目前可能會找尋其他實驗方法。然而，部分晶體卻在長時間的成長下，出現令人驚喜的繞射結果。此部分並非我們原在此計畫的研究目標，我們將在下階段繼續完成此結果。

另外，除了人類 huDHOase 外(我們僅得到 huDHOase K1556A 突變株結構，單金屬 huDHOase 無法獲得有效晶體)，我們亦嘗試不同來源的 DHOase，如從綠點魚(HsDHOase)以及酵母菌來源(ScDHOase)來下手。HsDHOase 已完成去金屬製備，目前已進入晶體成長階段。從得到的晶體中選了三個看起來比較立體且大小可以用 loop 挑起的晶體進行繞射實驗。嘗試了三個不同條件的不同晶體目前得到的繞射圖中一個是空的，暗示堆疊不一致; 而另外兩個解析度不好，但暗示有機會優化晶體成長條件，因此正在將此有繞射點但解析度不佳的條件進行優化，微調長晶條件或是提高蛋白質濃度，希望能得到比較良好的晶體繞射圖；另一部份則往點突變方向探討，嘗試利用點突變晶體結構來探討影響酵素活性的可能原因。ScDHOase 的部分同樣使用相同手法去金屬以及點晶，不過目前均無得到任何 ScDHOase 的晶體，

未來可能會提高蛋白質濃度再重新嘗試將蛋白質拿來點晶，希望藉由提高蛋白質濃度，達到晶體形成。

ScDHOase 去金屬(透析 3 次)

Inject 3	Wash 1	Wash 2	Wash 3	Wash 4	Wash 5	Wash 6	Wash 7	Wash 10	
X	X	0.17	0.28	0.34	0.06			●	●表示出現顏色
Inject 3	Wash 1	Wash 2	Wash 3	Wash 4	Wash 5	Wash 6	Wash 7	Wash 10	
X	0.02	0.31	0.3	0.28	0.05			●	

HsDHOase 去金屬(透析 3 次)

Inject 3	Wash 1	Wash 2	Wash 3	Wash 4	Wash 5	Wash 6	Wash 7	Wash 9	
X	0.13	0.48	0.44	0.12	0.05	0.01		●	●表示出現顏色
Inject 3	**Wash 1**	**Wash 2**	**Wash 3**	**Wash 4**	**Wash 5**	**Wash 6**	**Wash7**	**Wash 10**	
X	X	0.18	0.5	0.07	0.04	0.04		●	

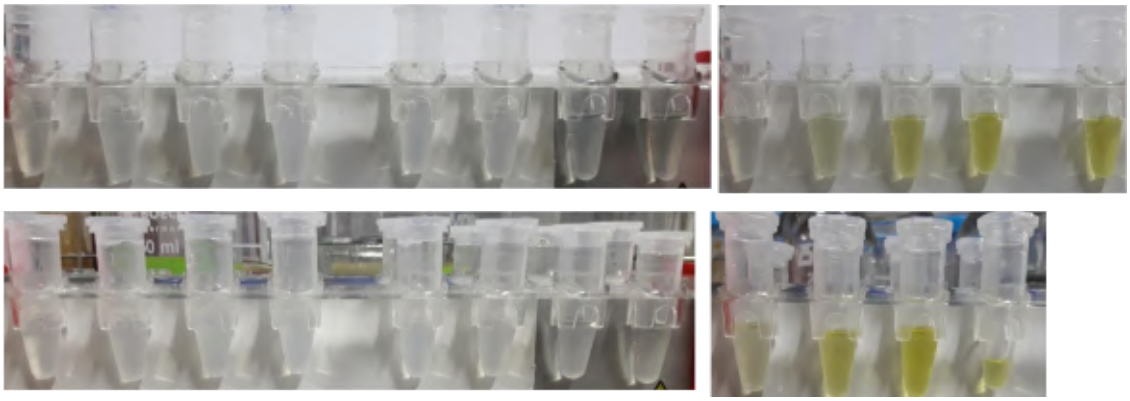

StyALLase 去金屬(透析 3 次)

Inject 3	Wash 1	Wash 2	Wash 3	Wash 4	Wash 5	Wash 6	Wash 7	Wash 10	
0.01	0.16	0.56	0.62	0.21	0.07	0.03		●	●表示出現顏色
Inject 3	**Wash 1**	**Wash 2**	**Wash 3**	**Wash 4**	**Wash 5**	**Wash 6**	**Wash 7**	**Wash 9**	
X	0.12	0.53	0.38	0.21	0.06	0.02		●	

Cyclic amidohydrolase 家族其他酵素成員透析螯合金屬程序。利用分子篩管柱層析去掉螯合劑(以及螯合出的金屬鹽溶液)並且採用分管蒐集。此螯合劑配方為黃色，根據實驗結果我們僅蒐集前幾管紅色標示之濃度的蛋白質溶液作為後續實驗所用，避免溶液內含有金屬螯合的複合物。

StyALLase 去金屬(透析 3 次)

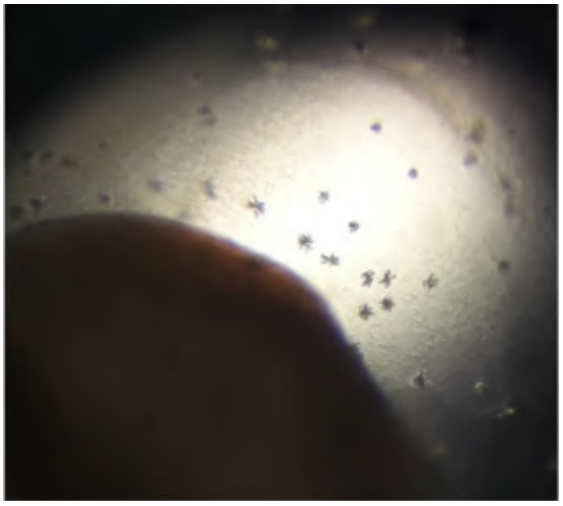

StyALLase 去金屬(透析 4 次)

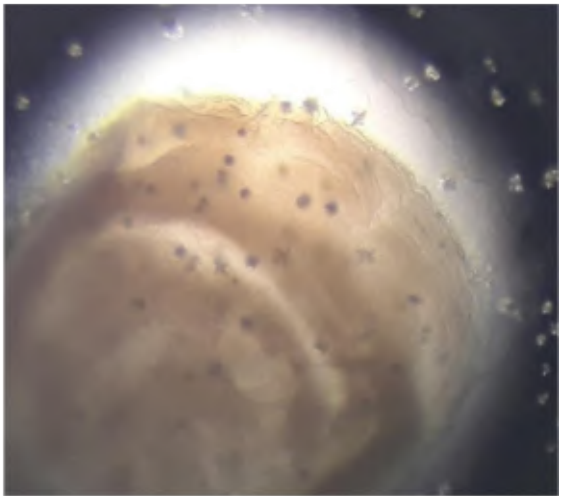

StyALLase 去金屬(透析 3 次)

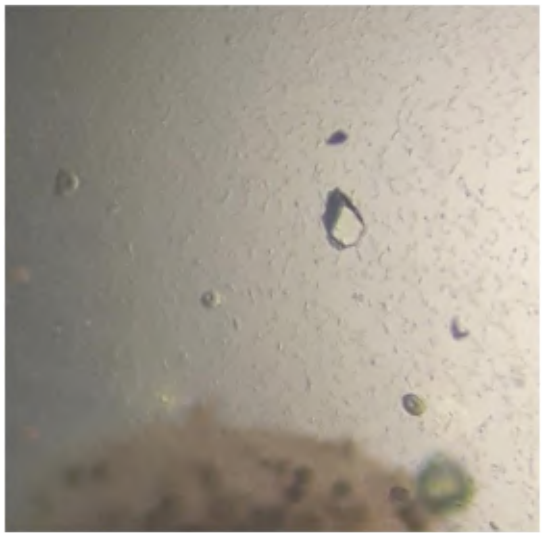

StyALLase 去金屬(透析 4 次)

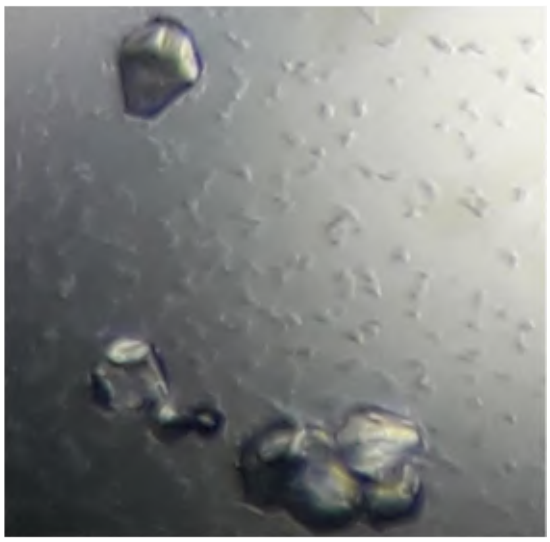

StyALLase 去金屬(透析 4 次)

晶體名稱	成長條件
StyALL 去金屬(透析 3 次)	35%　PEG4000
StyALL 去金屬(透析 4 次)	35%　PEG4000
StyALL 去金屬(透析 3 次)	10%PEG8000，100mM HEPES，pH7.5，200mM Calcium Acetate
StyALL 去金屬(透析 4 次)	10%PEG8000，100mM HEPES，pH7.5，200mM Calcium Acetate
StyALL 去金屬(透析 3 次)	10%PEG8000，100mM MES，pH6.5，200mM Zinc Acetate

StyALLase 去金屬(透析 3 次)

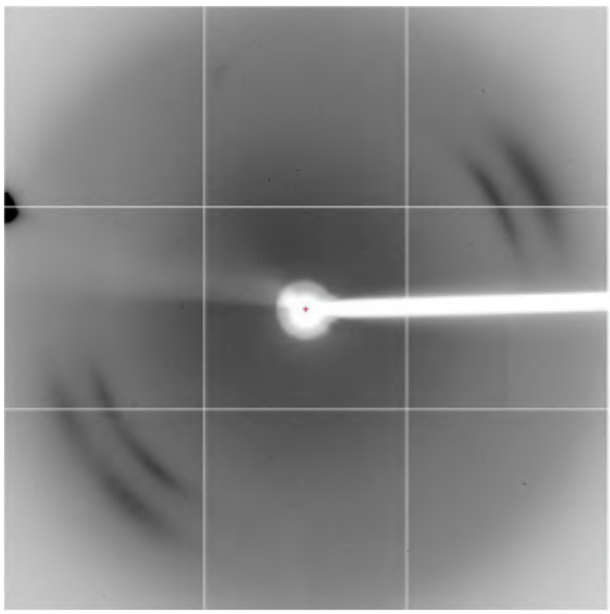

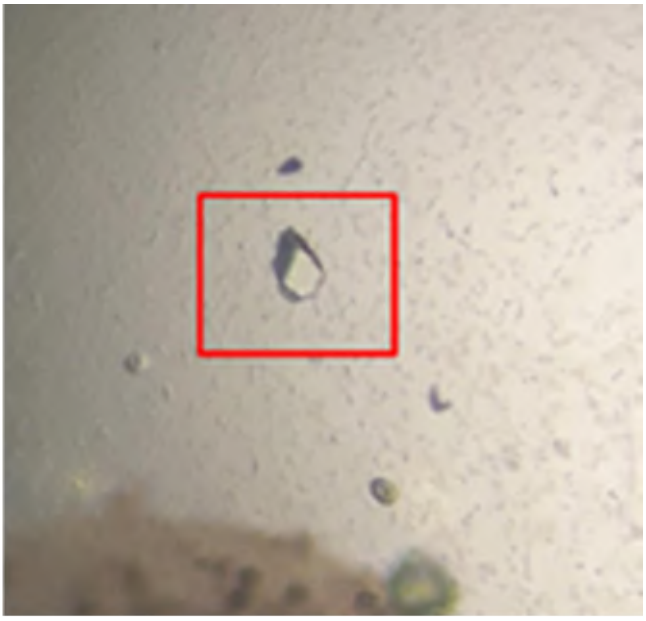

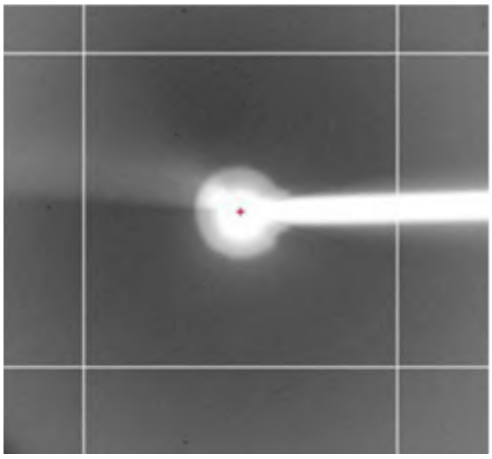

*進一步將上圖繞射點圖中心低解析度區放大，明顯看到連低解析度區域也沒有任何繞射點，整個晶體內部是空的。

利用 loop 挑取右圖 StyALLase 去金屬(透析 3 次)在該條件內晶型最立體且大顆的晶體，該晶體是在長晶條件為(10% PEG 8000，100 mM HEPES，pH7.5，200 mM Calcium Acetate)的環境下形成之結晶，利用 x 光繞射進行繞射實驗收集繞射數據，在接收器距離 500，光源釋放 60 秒，角度 45 度的情況向進行實驗(Distnce: 500，Time: 60 s，Phi: 45)，偵測結果如左圖發現晶體繞射結果是空的，無繞射點。

StyALLase 去金屬(透析 4 次)

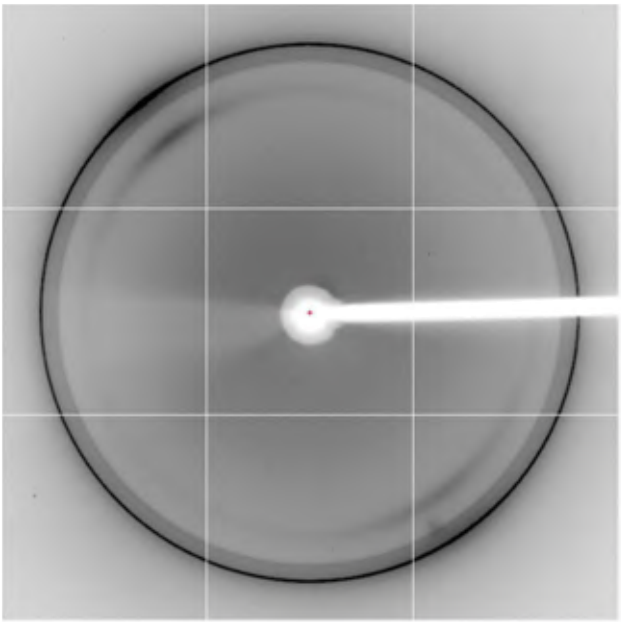

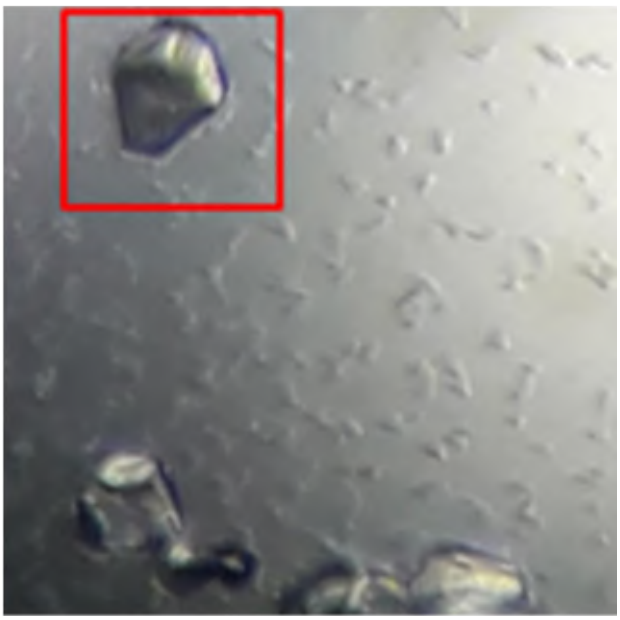

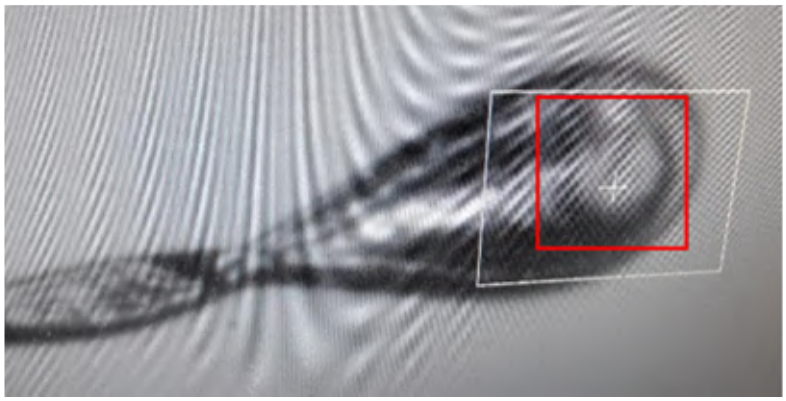

利用 loop 挑取右圖 StyALLase 去金屬(透析 4 次)在該條件內晶型最立體且大顆的晶體，該晶體是在長晶條件為(10% PEG 8000，100 mM HEPES，pH7.5，200 mM Calcium Acetate)的環境下形成之結晶，利用 x 光繞射進行繞射實驗收集繞射數據，在接收器距離 500，光源釋放 60 秒，角度 225 度的情況向進行實驗(Distnce: 500，Time: 60s，Phi: 225)，偵測結果如左圖發現晶體繞射結果是空的，無繞射點。

StyALLase 去金屬(透析 4 次)

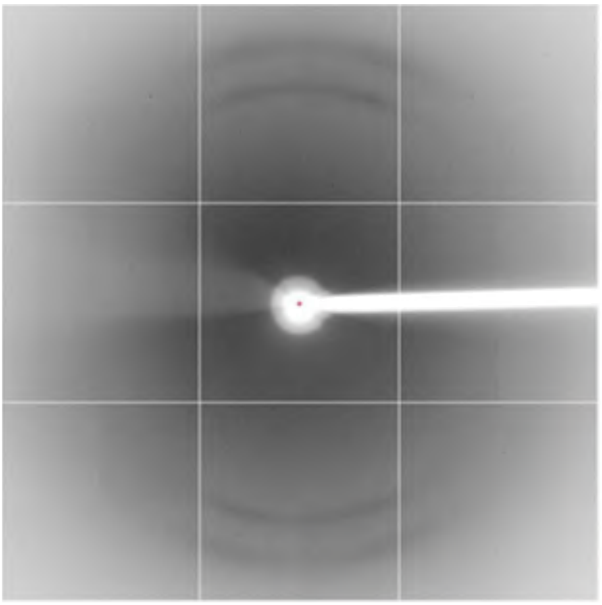

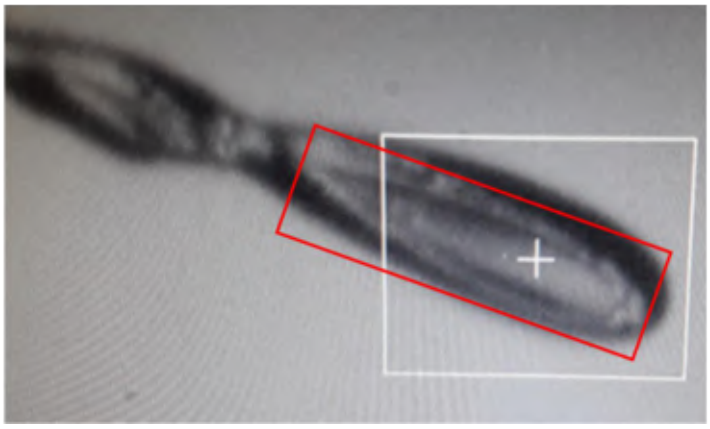

利用 loop 挑取右圖 StyALLase 去金屬(透析 4 次)在該條件內晶型最立體且大顆的晶體，該晶體是在長晶條件為(10% PEG 8000，100 mM HEPES，pH7.5，200 mM Calcium Acetate)的環境下形成之結晶，利用 x 光繞射進行繞射實驗收集繞射數據，在接收器距離 500，光源釋放 60 秒，角度 225 度的情況向進行實驗(Distnce: 500，Time: 60s，Phi: 225)，偵測結果如左圖發現晶體繞射結果是空的，無繞射點。

HsDHOase 去金屬(透析 3 次)

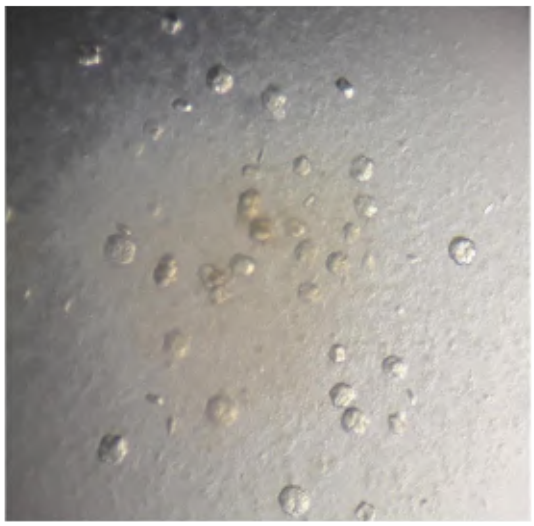

HsDHOase 去金屬(透析 4 次)

HsDHOase 去金屬(透析 3 次)

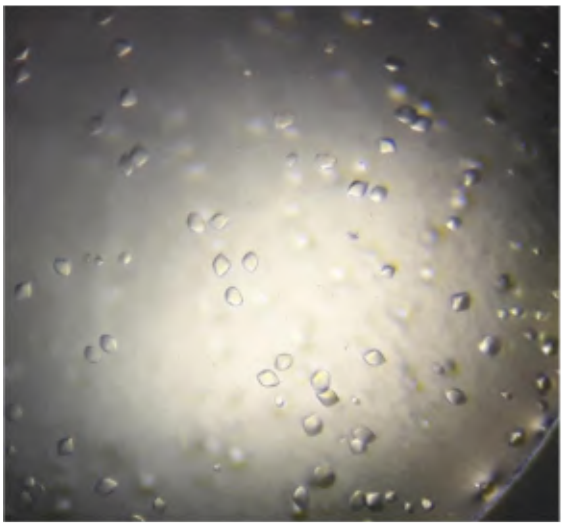

HsDHOase 去金屬(透析 4 次)

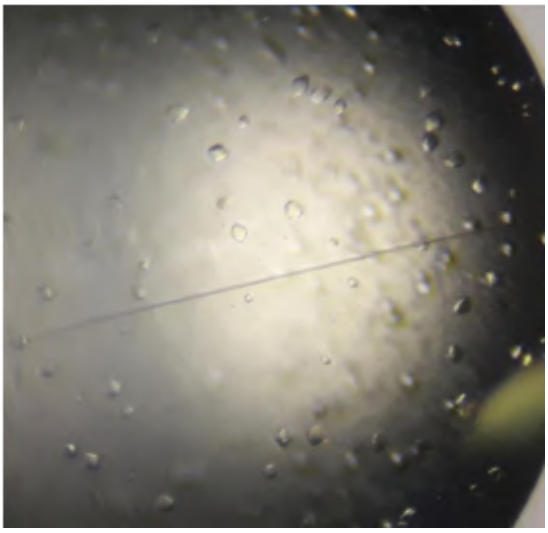

晶體名稱	成長條件
HsDHOase 去金屬(透析 3 次)	15% PEG8000，50 mM Ammonium Sulfate，100 mM Sodium Citrate
HsDHOase 去金屬(透析 4 次)	15% PEG8000，50 mM Ammonium Sulfate，100 mM Sodium Citrate
HsDHOase 去金屬(透析 3 次)	30% PEG400，100 mM MES pH6.5，100 mM Sodium Acetate
HsDHOase 去金屬(透析 4 次)	30% PEG400，100 mM MES pH6.5，100 mM Sodium Acetate

HsDHOase 去金屬(透析 3 次)

HsDHOase 去金屬(透析 4 次)

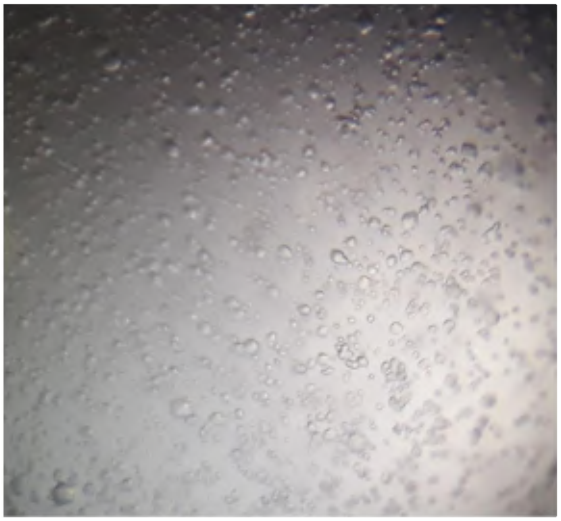

HsDHOase 去金屬(透析 3 次)

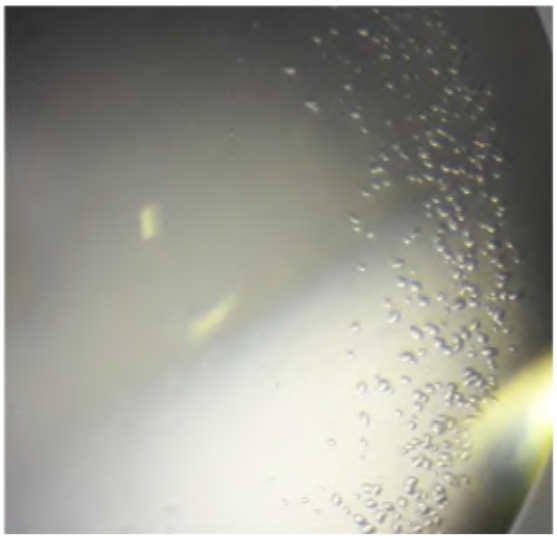

HsDHOase 去金屬(透析 4 次)

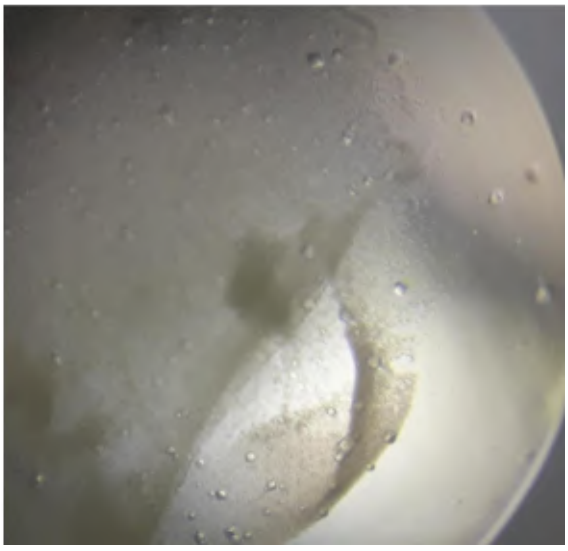

晶體名稱	成長條件
HsDHOase 去金屬(透析 3 次)	1.6M Magnesium Sulfate，100 mM MES pH6.5
HsDHOase 去金屬(透析 4 次)	1.6M Magnesium Sulfate，100 mM MES pH6.5
HsDHOase 去金屬(透析 3 次)	800mM Potassium/sodium Tartrate，100mM HEPES pH7.5
HsDHOase 去金屬(透析 4 次)	800mM Potassium/sodium Tartrate，100mM HEPES pH7.5

HsDHOase 去金屬(透析 3 次)

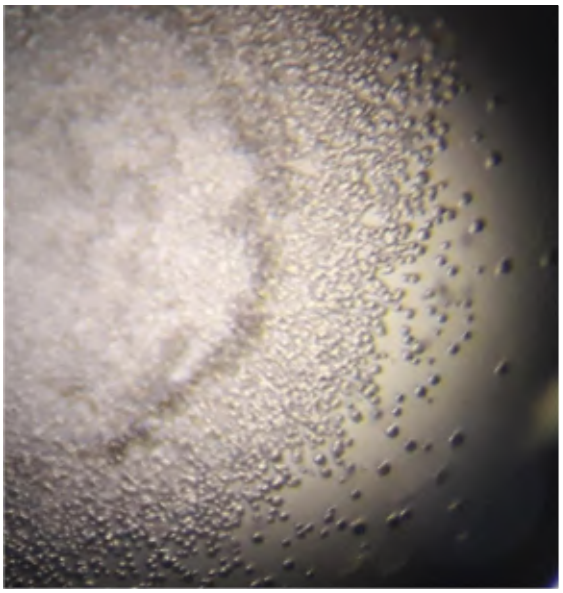

HsDHOase 去金屬(透析 4 次)

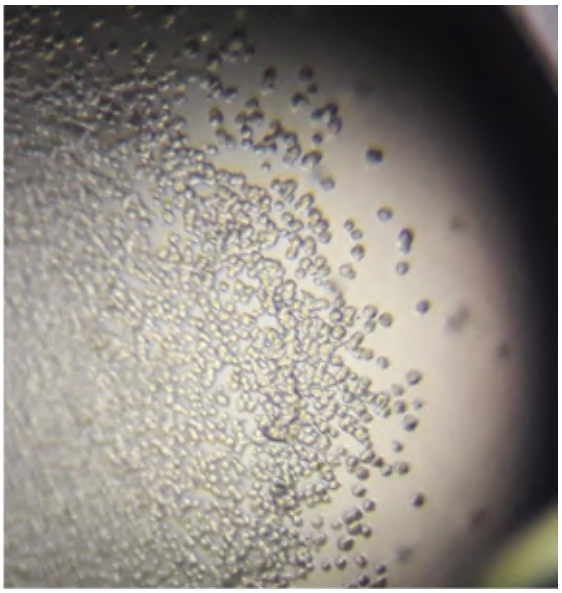

HsDHOase 去金屬(透析 4 次)

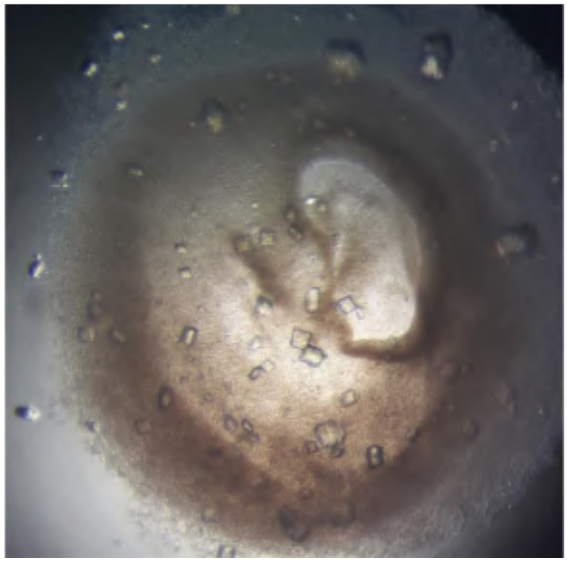

晶體名稱	成長條件
HsDHOase 去金屬(透析 3 次)	1.2 M Ammonium Sulfate，3% 2-Propanol，50 mM Sodium Citrate
HsDHOase 去金屬(透析 4 次)	1.2 M Ammonium Sulfate，3% 2-Propanol，50 mM Sodium Citrate
HsDHOase 去金屬(透析 4 次)	500 mM Ammonium Sulfate，1 M Lithium Sulfate，100 mM Sodium Citrate

HsDHOase 去金屬(透析 3 次)

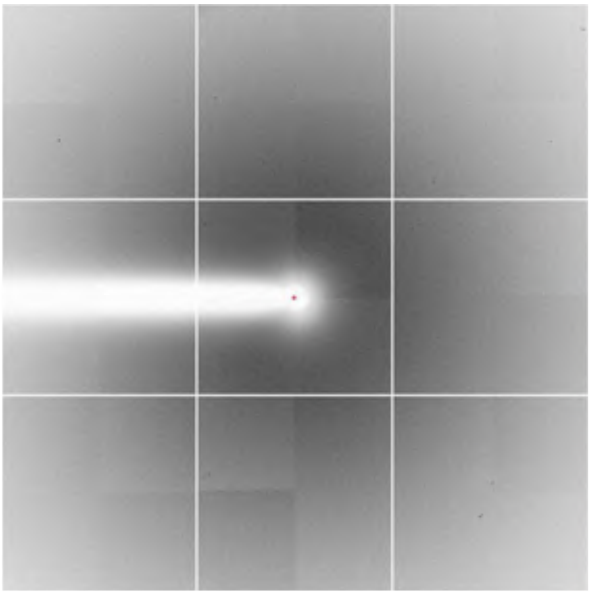

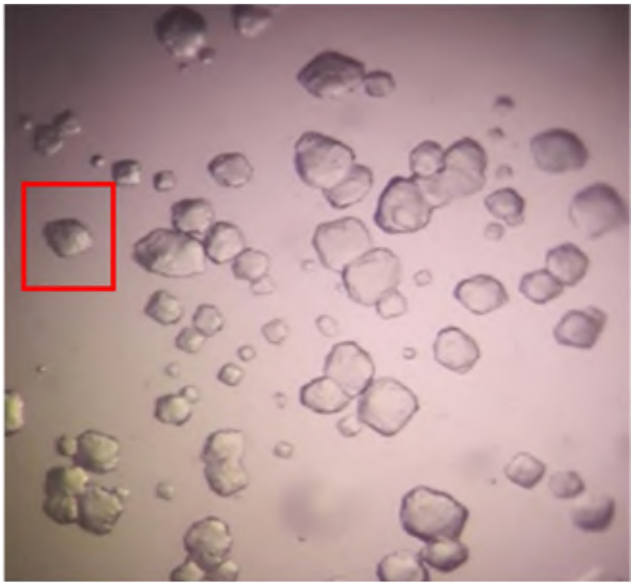

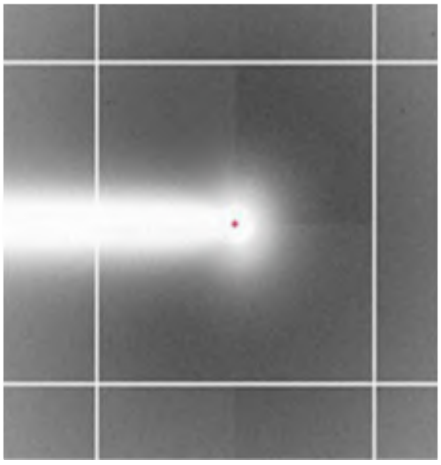

*進一步將上圖繞射點圖中心低解析度區放大，明顯看到連低解析度區域也沒有任何繞射點，整個晶體內部是空的。

利用 loop 挑取右圖 HsDHOase 去金屬(透析 3 次)在該條件內晶型最立體且大顆的晶體，該晶體是在長晶條件(15% PEG 8000，50 mM Ammonium Sulfate，100 mM Sodium Citrate)的環境下形成之結晶，利用 x 光繞射進行繞射實驗收集繞射數據，在接收器距離 500，光源釋放 20 秒，角度 267 度的情況向進行實驗(Distnce: 500，Time: 20s，Phi: 267)，偵測結果如左圖發現晶體繞射結果是空的，無繞射點。

HsDHOase 去金屬(透析 3 次)

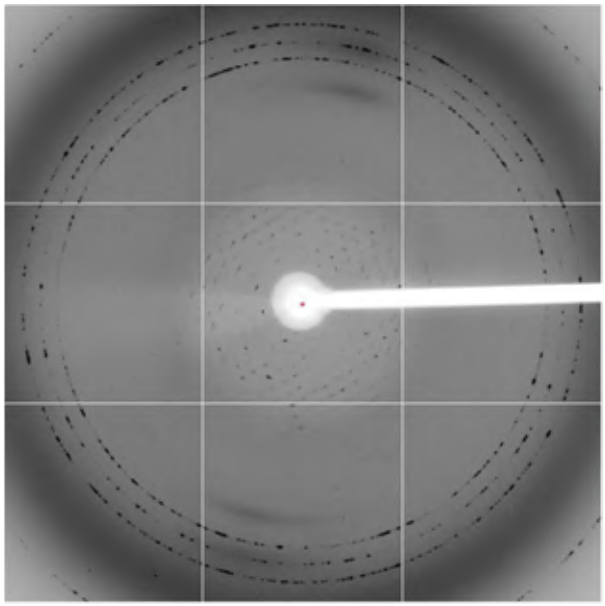

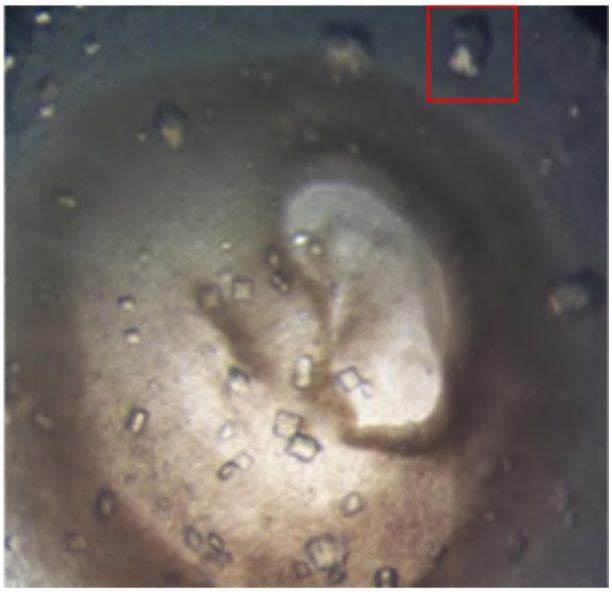

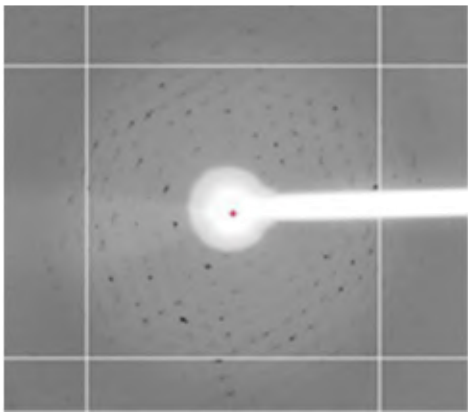

*進一步將上圖繞射點圖中心低解析度區放大，明顯看到低解析度區域(約 7–10 Å)，雖然有繞射點了不過強度不夠且在低解析度區無法順利解出結構，不過可以進一步在優化此長晶條件。

利用 loop 挑取右圖 HsDHOase 去金屬(透析 3 次)在該條件內晶型最立體且大顆的晶體，該晶體是在長晶條件(500 mM Ammonium Sulfate，1 M Lithium Sulfate，100 mM Sodium Citrate)的環境下形成之結晶，利用 x 光繞射進行繞射實驗收集繞射數據，在接收器距離 500，光源釋放 50 秒，角度 2 度的情況向進行實驗(Distnce: 500，Time: 50s，Phi: 2)，偵測結果發現雖有繞射點但強度不夠且集中在低解析度區。

HsDHOase 去金屬(透析 3 次)

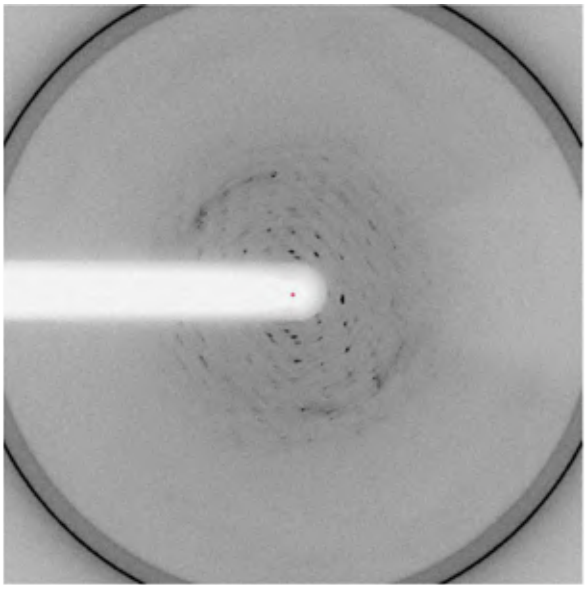

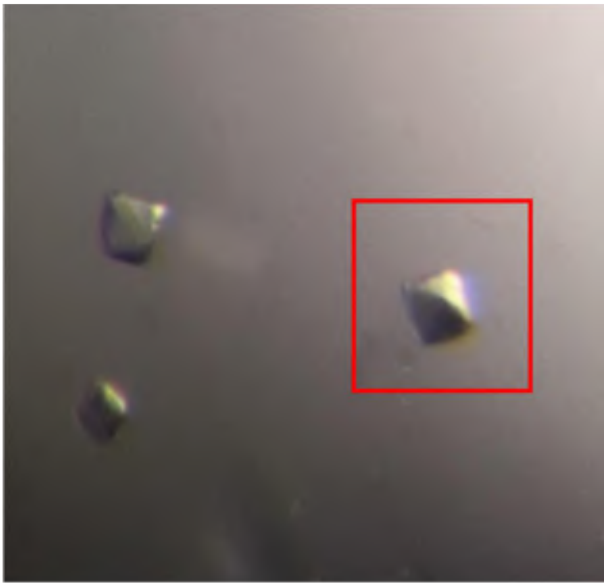

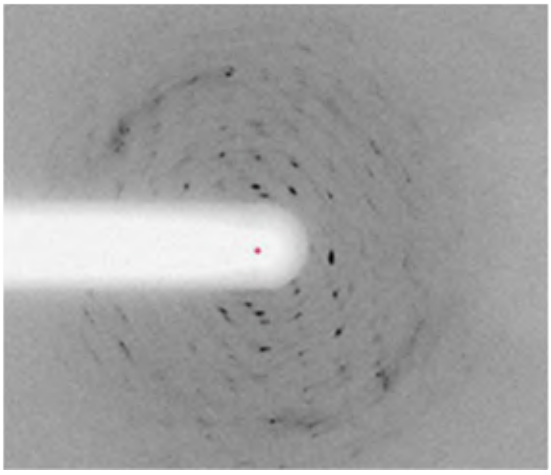

*進一步將上圖繞射點圖中心低解析度區放大，明顯看到低解析度區域(約 7–10 Å)，雖然有繞射點了不過強度不夠且在低解析度區，同時繞射點有拖曳，無法順利解出結構，不過可以進一步在優化此長晶條件。

利用 loop 挑取右圖 HsDHOase 去金屬(透析 3 次)在該條件內晶型最立體且大顆的晶體，該晶體是在長晶條件(30% PEG400，100 mM MES pH 6.5，100 mM Sodium Acetate)的環境下形成之結晶，利用 x 光繞射進行繞射實驗收集繞射數據，在接收器距離 300，光源釋放 1 秒，角度 90 度的情況向進行實驗(Distnce: 500，Time: 1s，Phi: 90)，偵測結果發現雖有繞射點集中在低解析度區且有拖曳。

3.11 利用真核細胞表現 ALLase

事實上 ALLase 還未有成功的真核重組蛋白質的報導，原核生物如大腸桿菌似乎無法功能性的表達真核 ALLase，例如實驗室已試過阿拉伯芥的 ALLase 於大腸桿菌表達無活性。我們試試看藉由培養昆蟲細胞來表現真核來源的 ALLase，來探討真核和原核表現的 ALLase 活性區與功能之差異，並且希望更進一步活用在其他酵素如真核的 DHPase 與 DHOase 的重組蛋白質製備上。也希望排除是否因表達生物的不同，是否會因為某些原因(如特別的修飾或折疊因子)而使酵素活性出現差異。因此目前嘗試使用 High Five 昆蟲細胞進行實驗。

High Five（BTI-Tn-5B1-4）是一種昆蟲細胞品系。High Five 細胞已成為使用桿狀病毒或轉染進行重組蛋白表達的最常用細胞系之一，並且在許多情況下已經證明比其他鱗翅目細胞系如 Sf9 細胞表達更多的重組蛋白。它們可以在沒有血清的情況下生長，並且可以以鬆散的附著狀態或懸浮培養。High Five 細胞能產生豐富的 miRNA、siRNA 和 piRNA，使其適合所有此類研究。

剛開始使用的質體和轉殖入大腸桿菌表現的質體相同，不過 transfection 到 High Five 昆蟲細胞的效果並不明顯，同時剛開始設計的酵素無外加 His 使後續實驗無法有效明確的分離出目標蛋白，只收集到混合多種原先細胞內的雜蛋白，而無法真正確定酵素的活性。之

後我們就改變方法構築了另一質體，並在目標蛋白質序列後端外加 6 個 His 以利純化分離目標蛋白。

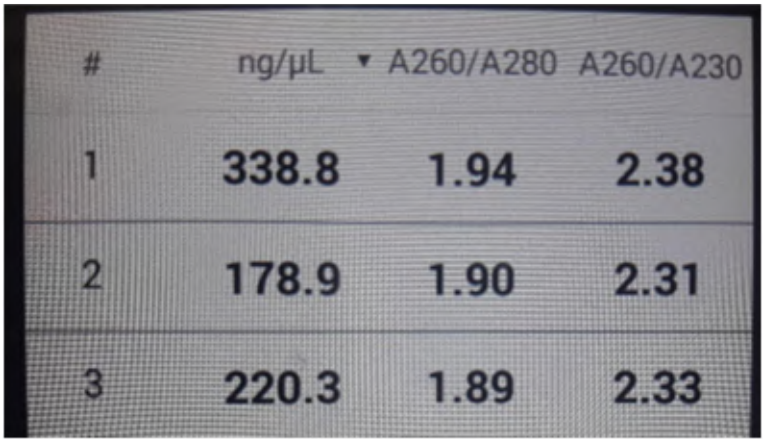

#	ng/μL	A260/A280	A260/A230
1	338.8	1.94	2.38
2	178.9	1.90	2.31
3	220.3	1.89	2.33

藉由含去內毒素的 Kit 來抽取質體，最後測量到抽出的質體濃度。

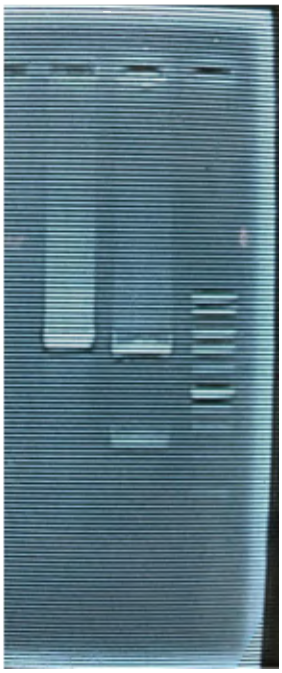

左圖:實際 DNA 膠圖。之前 ALLase 的序列沒有外加 6 個 His ，無法容易的進一步將破細胞後的上清液純化出 ALLase，所以後續測量酵素活性時，也無法明確確定是否是測到目標酵素還是細胞內其他物質干擾，所以後續我們改利用外加 6 個 His 的 ALLase，並利用 pFast Bac

質體來搭載。右圖:由於不確定上圖抽出的質體是因為太濃而有點拖曳，還是其實並非抽到目標，因此進行雙切的檢驗，添加原先設計的質體內的兩個酵素切點，跑膠後觀察是否有被切出。

第一代(1-1)	第一代(1-2)
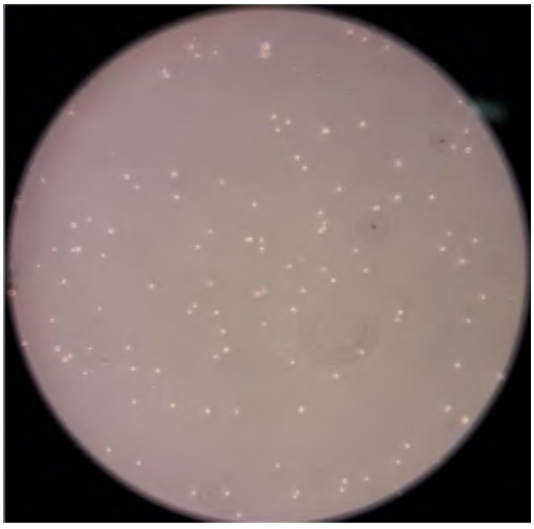	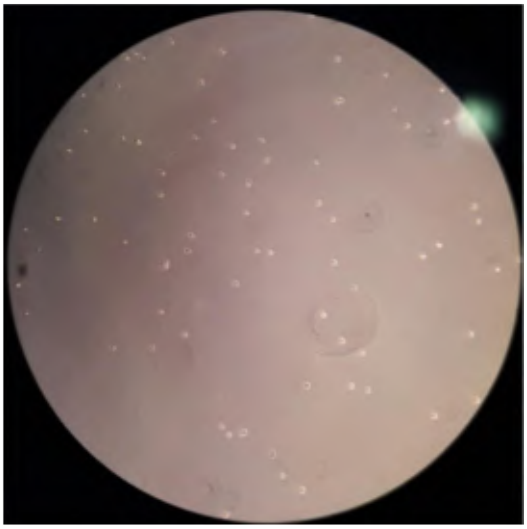
第一代(1-1)	第一代(1-2)
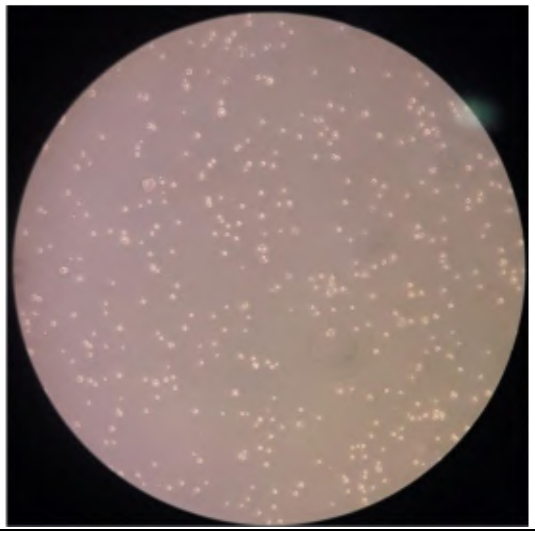	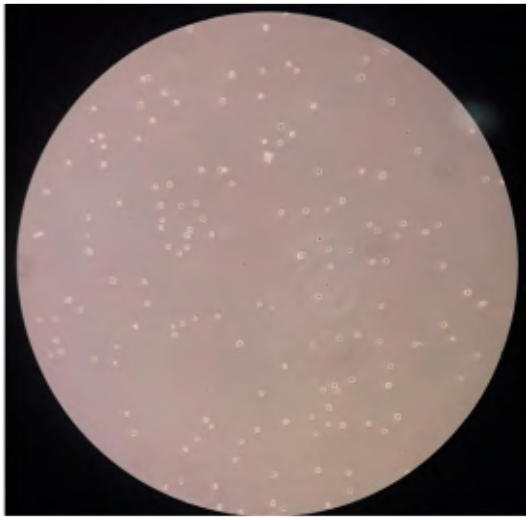
第二代(2-1-1)	第二代(2-1-2)

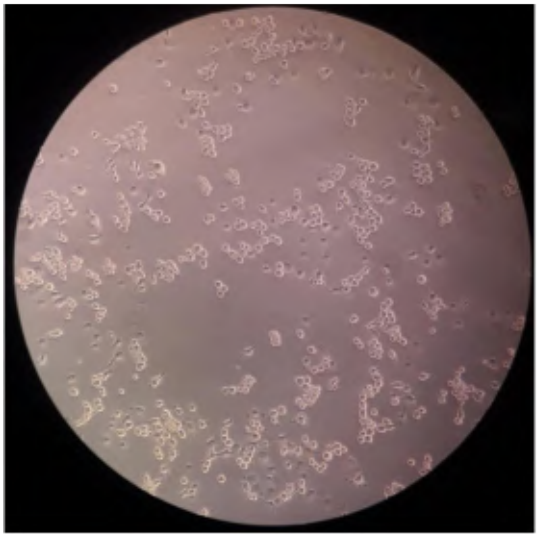	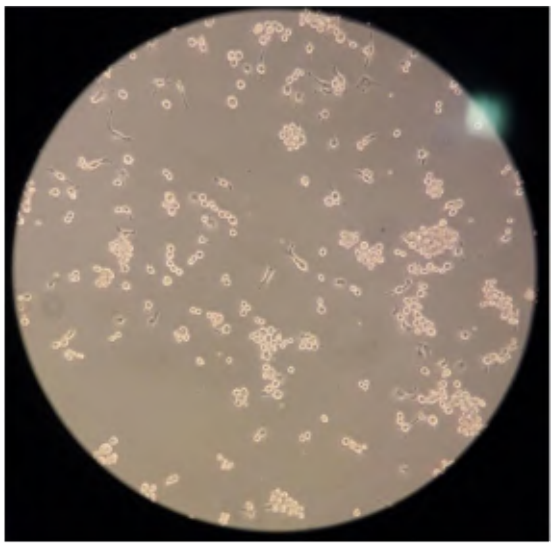
第二代(2-2-1)	第二代(2-2-2)
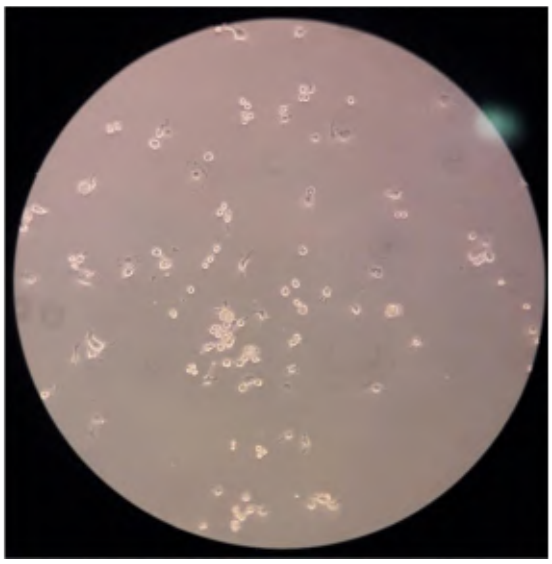	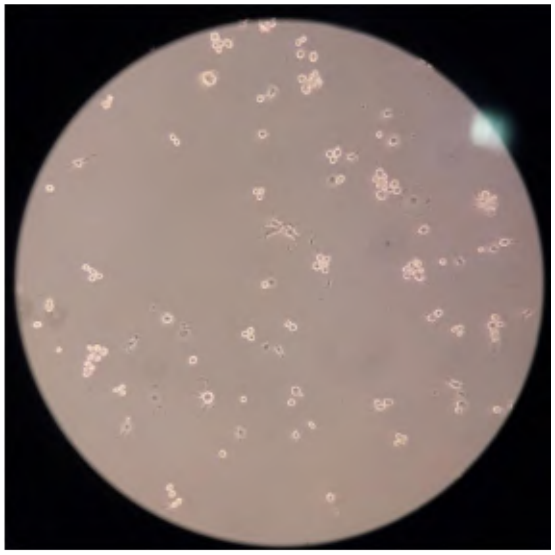
第二代(2-1-1)	第二代(2-1-2)

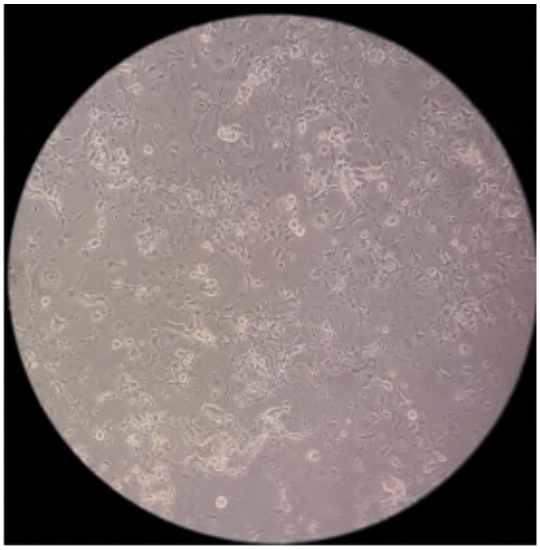	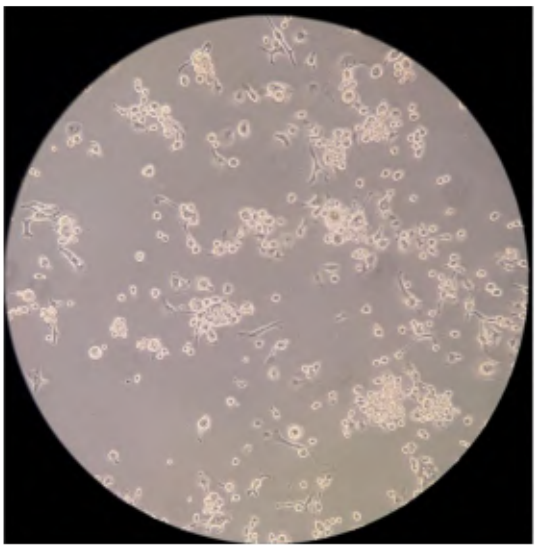
第二代(2-2-1)	第二代(2-2-2)
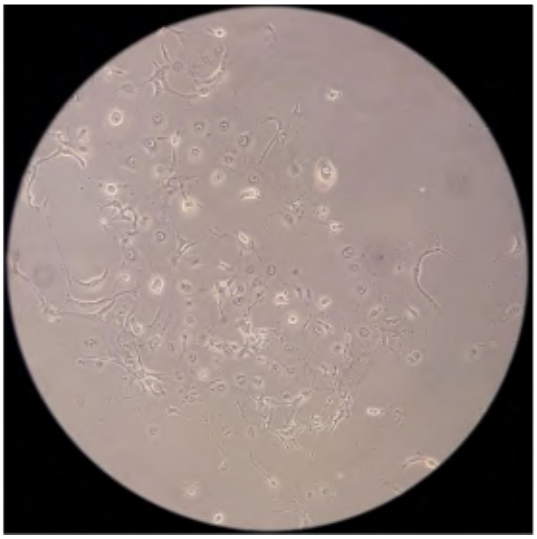	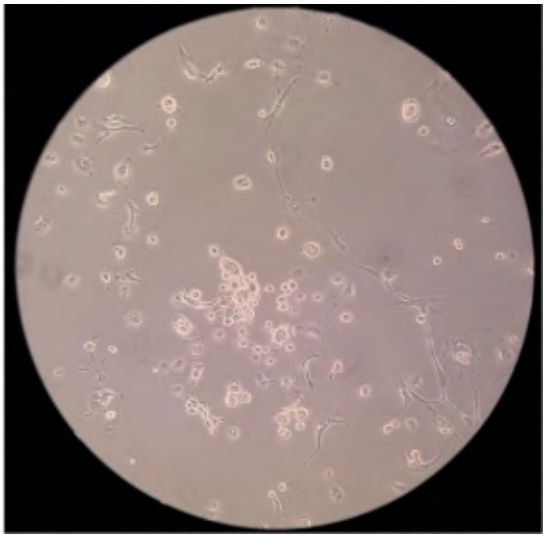
第二代(2-1-1)	第二代(2-1-2)

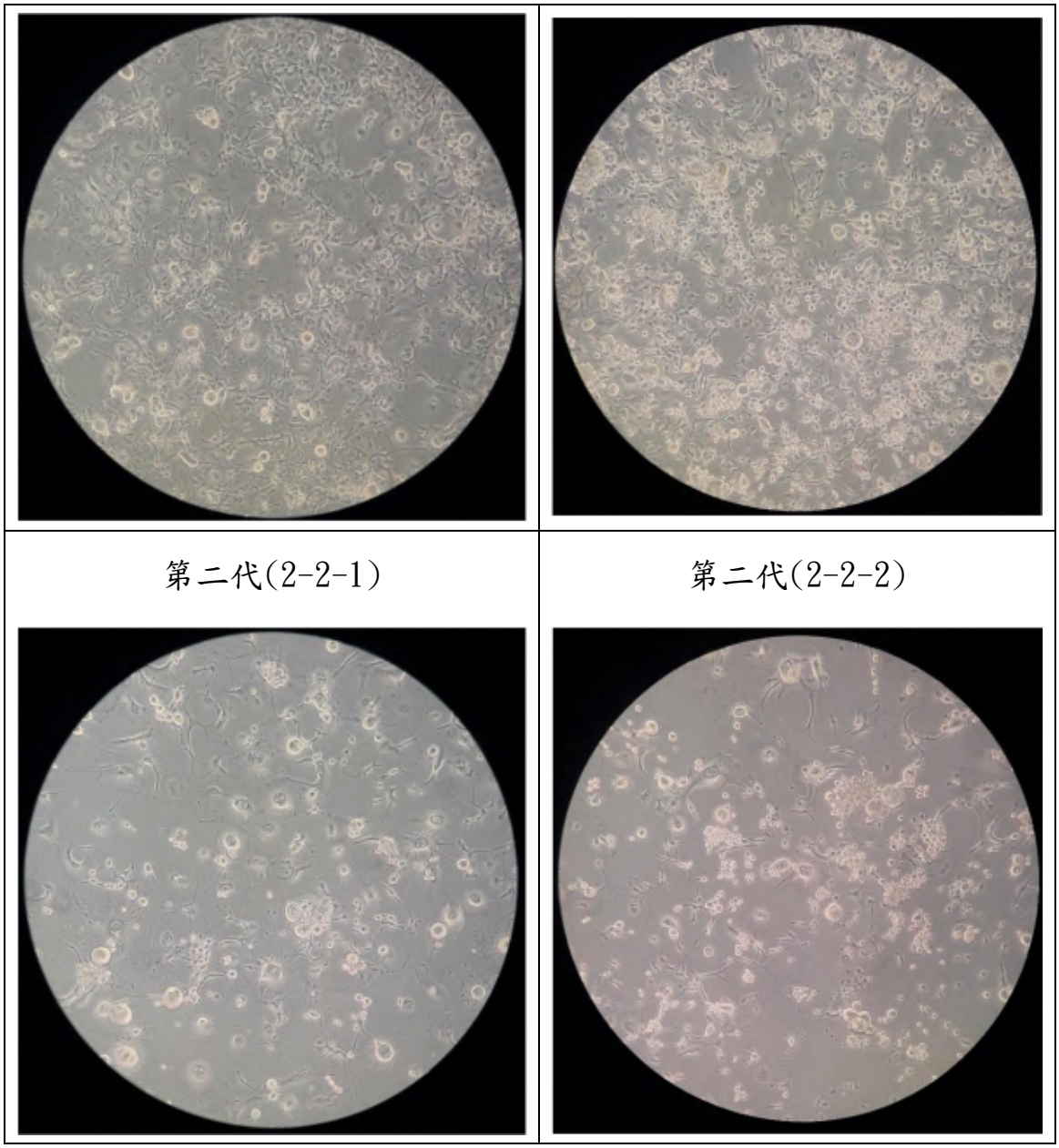

High Five 昆蟲細胞培養。將細胞解凍到 2 個 25T flask 培養，接著每 2-3 天觀察並更換 medium，當培養到 7-8 分滿則可分別擴增成 2 盤，或改更換成 75T flask 繼續培養，當細胞數達到一定程度後則可開始進一步進行後續 transfection 的實驗。

Transfection 第 1 天

Control(無 transfect)	Control(無 transfect)
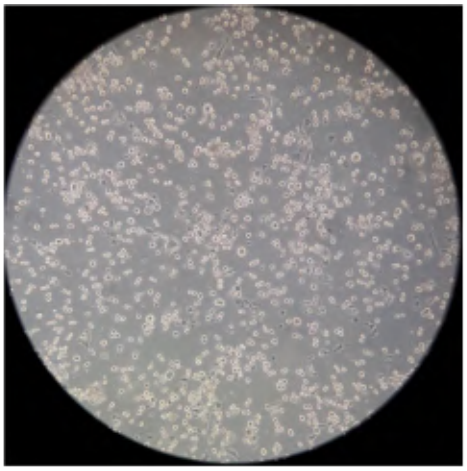	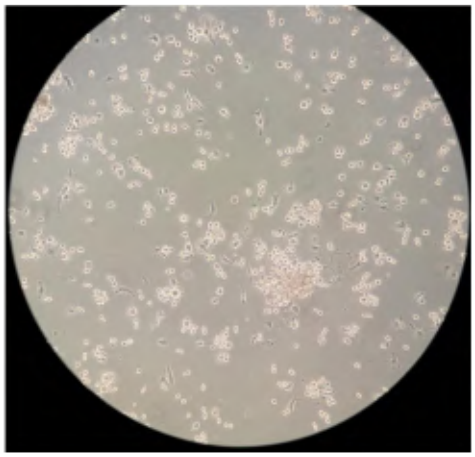
Transfect 質體 1 (1:1)	Transfect 質體 1 (1:2)
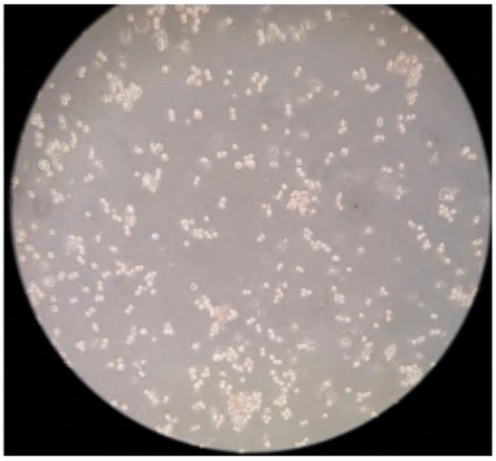	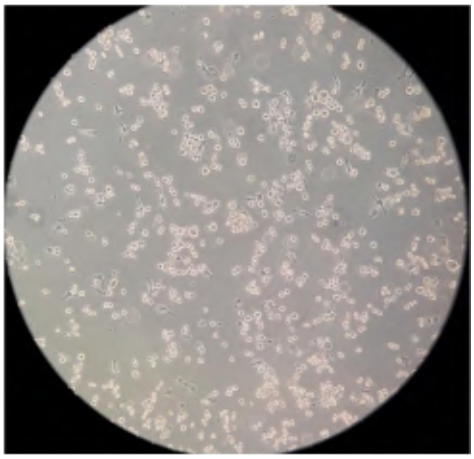
Transfect 質體 2 (1:1)	Transfect 質體 2 (1:2)
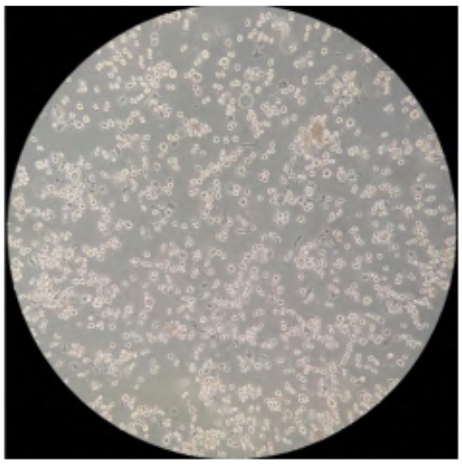	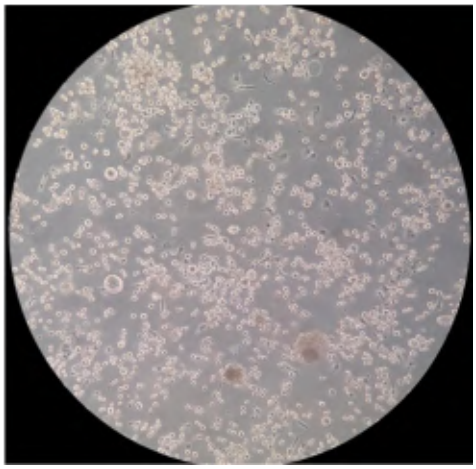

Transfect 第 2 天

Control(無 transfect)	Control(無 transfect)
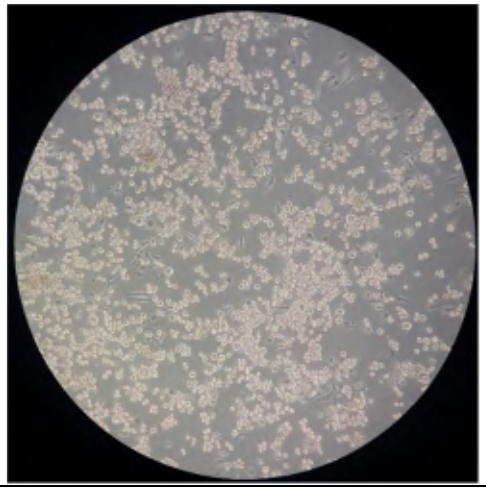	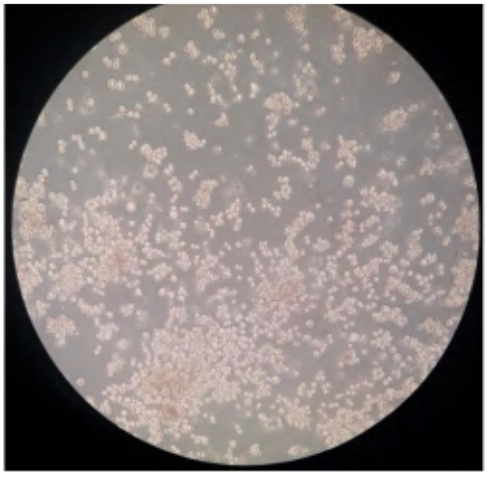
Transfect 質體 1 (1:1)	Transfect 質體 1 (1:2)
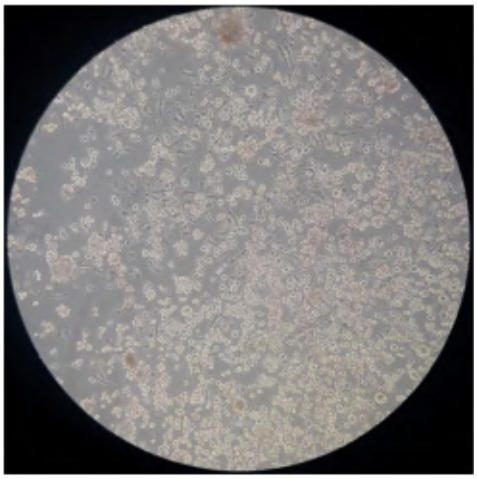	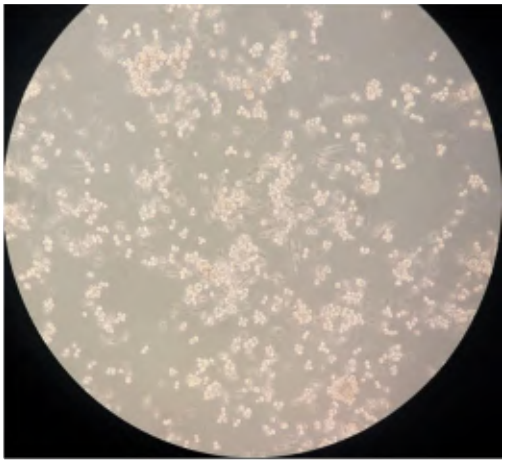
Transfect 質體 2 (1:1)	Transfect 質體 2 (1:2)
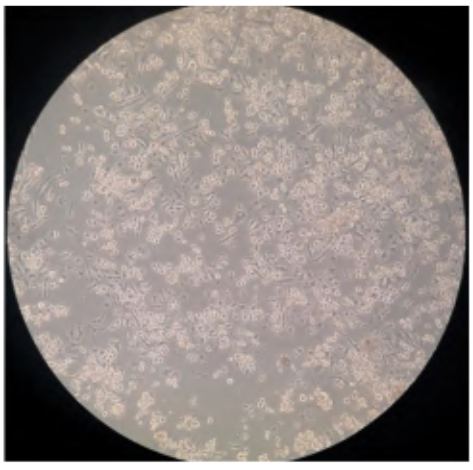	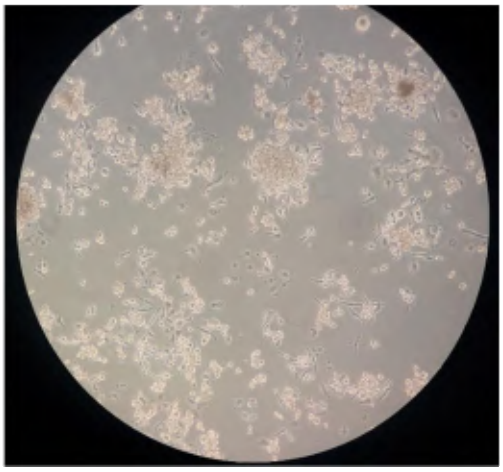

Transfect 第 3 天

Control(無 transfect)	Control(無 transfect)
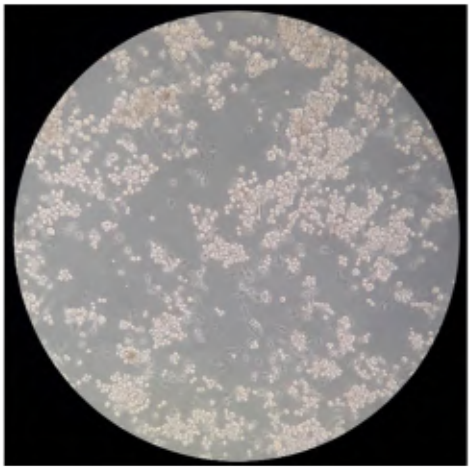	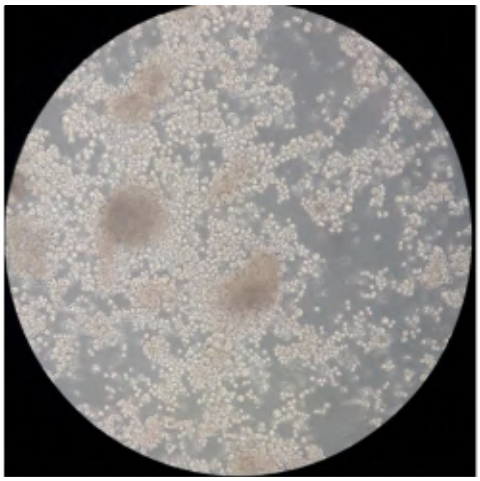
Transfect 質體 1 (1:1)	Transfect 質體 1 (1:2)
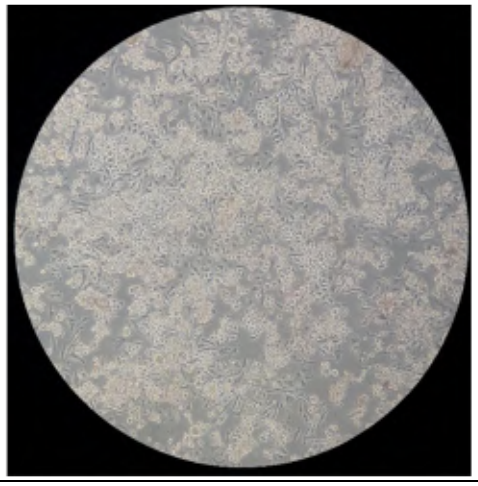	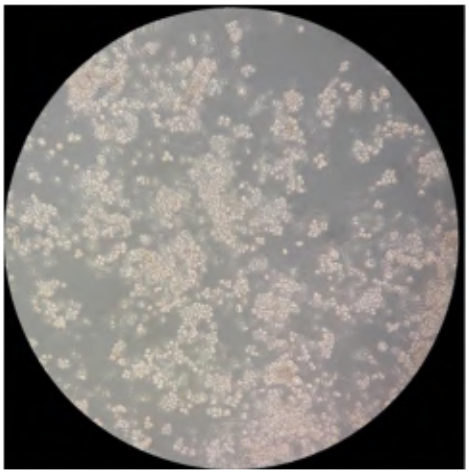
Transfect 質體 2 (1:1)	Transfect 質體 2 (1:2)
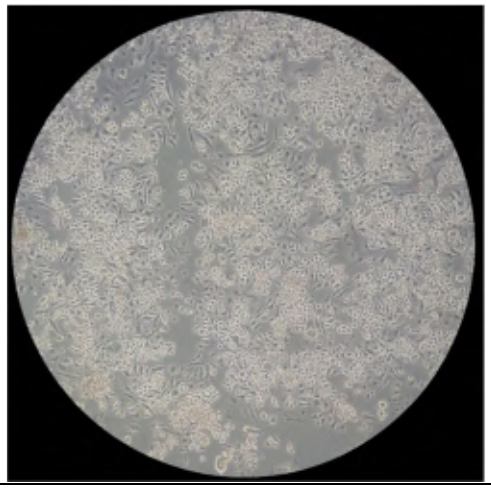	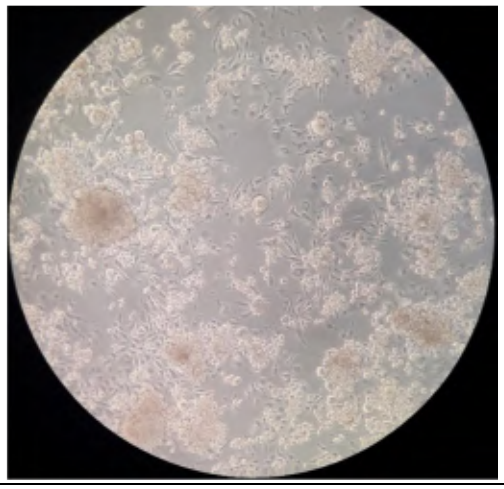

Transfect 第 3 天 (照螢光)

Control(無 transfect) 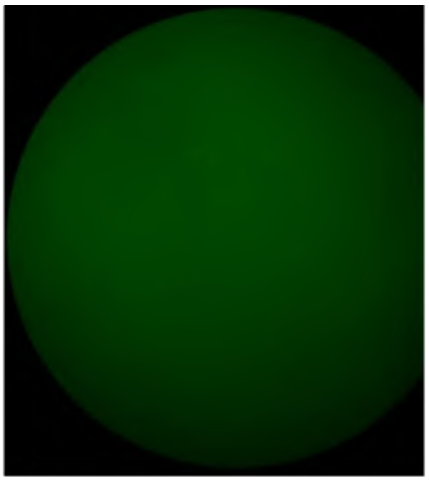	Control(無 transfect) 
Transfect 質體 1 (1:1) 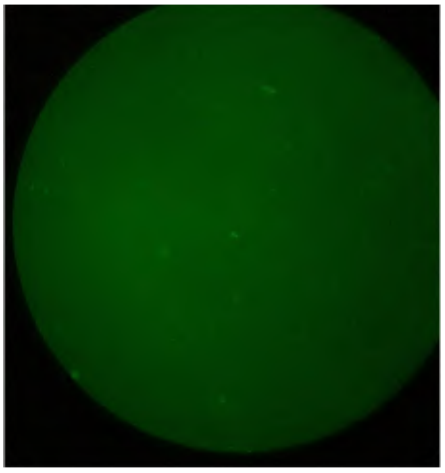	Transfect 質體 1 (1:2) 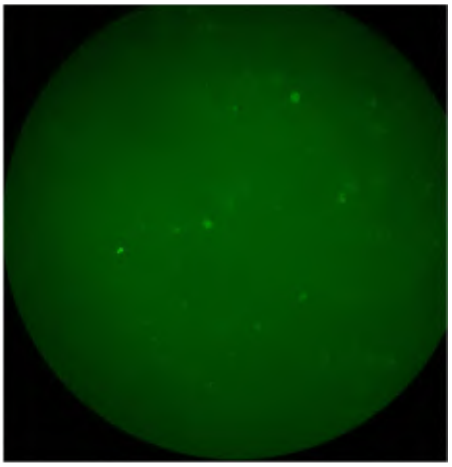
Transfect 質體 2 (1:1) 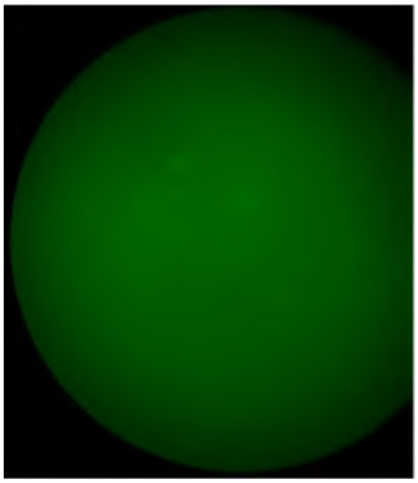	Transfect 質體 2 (1:2) 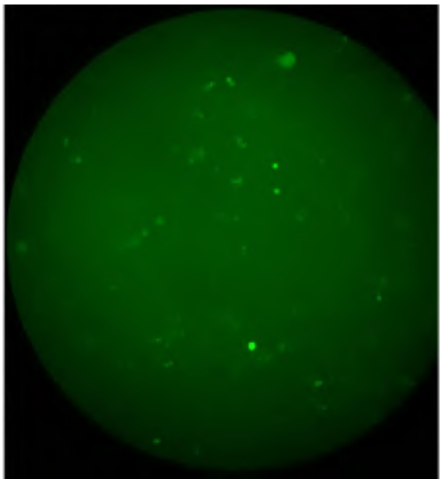

第四章:結論

本計畫內容成功如原計畫書所預期解出數個不同套體、不同金屬含量的 DHPase 的結晶結構，本人並在此計畫區間發表3篇 SCI 論文 [27, 31, 35]，其中2篇與此計畫密切相關，本人皆為第一作者 [27, 31]; 另一篇則在行有餘力的空檔與實驗室其他夥伴合作合著，本人為第二作者 [35]。此計畫結果報告出如何利用特別成分的螯合劑製備單金屬PaDHPase，並獲得單金屬以及比較雙金屬PaDHPase的結晶結構，並且從結構以及膠體過濾色譜分析中發現，雙金屬PaDHPase對於pH值依賴性具有寡聚合現象 [27]。另外，比較單金屬及雙金屬 PaDHPase 活性區發現當僅有一個金屬Znα在活性區時，此時lysine 並無後修飾的作用，且酵素也不具有活性，必須由第二個金屬 Znß 進入活性區，由帶正電的金屬極化CO_2的負電促使新共價鍵的形成，並接著參與雙金屬活性中心的自我組裝，才能穩固活性區使酵素具有活性 [31]。同時，huDHOase K1556A的結晶結構也能更進一步證明，在雙金屬活性區中，Znß 和罕見的 post-carboxylated lysine 具有很大關聯性。這些結果帶出了下一階段的研究課題，包括此各酵素家族成員在活性區的各項結構與活性是否一致? 由於部分不含金屬活性中心的ALLase已被報導 [36, 37]，在演化過程中這些酵素是否仍必須具雙金屬中心且需賴氨酸的後修飾仍待更多研究結果結論之。

最後，目前仍在繼續進行 PaDHPase 與抑制劑的共結晶以及活性區中負責金屬結合胺基酸的點突變的研究，希望透過共結晶結構，從分子結構來完全了解其抑制機制，並希望能夠根據此結構進行下一階段的藥物設計優化。另外，希望獲得活化區突變株的結晶結構，來更完整了解影響此酵素活性的原因，並進一步探討在演化過程中為何會導向cyclic amidohydrolase家族成員其活性區完全的保留4個His、1個Asp和1個post-carboxylated lysine。

期待未來能完全了解此酵素，包括工業上用其生產具旋光性特異性的抗生素前驅物。另外藉由結構與功能性研究能開發出相關抑制劑抑制此酵素活性，間接抑制綠膿桿菌甚或其他超級細菌的生長及代謝，成為新型的標靶抗生素藥物，達到另類新抗生素藥物研發的方向，為社會對抗抗藥性細菌甚或癌細胞增添可能的臨床應用希望。

第五章:參考文獻

[1] D.R. Evans, H.I. Guy, Mammalian pyrimidine biosynthesis: fresh insights into an ancient pathway, J Biol Chem, 279 (2004) 33035-33038.
[2] J.M. Clemente-Jimenez, S. Martinez-Rodriguez, F. Rodriguez-Vico, F.J. Heras-Vazquez, Optically pure alpha-amino acids production by the "Hydantoinase Process", Recent Pat Biotechnol, 2 (2008) 35-46.
[3] H.E. Schoemaker, D. Mink, M.G. Wubbolts, Dispelling the myths--biocatalysis in industrial synthesis, Science, 299 (2003) 1694-1697.
[4] Z. Gojkovic, L. Rislund, B. Andersen, M.P. Sandrini, P.F. Cook, K.D. Schnackerz, J. Piskur, Dihydropyrimidine amidohydrolases and dihydroorotases share the same origin and several enzymatic properties, Nucleic Acids Res, 31 (2003) 1683-1692.
[5] G.J. Kim, H.S. Kim, Identification of the structural similarity in the functionally related amidohydrolases acting on the cyclic amide ring, Biochem J, 330 (Pt 1) (1998) 295-302.
[6] W.F. Peng, C.Y. Huang, Allantoinase and dihydroorotase binding and inhibition by flavonols and the substrates of cyclic amidohydrolases, Biochimie, 101 (2014) 113-122.
[7] Y.Y. Ho, Y.H. Huang, C.Y. Huang, Chemical rescue of the post-translationally carboxylated lysine mutant of allantoinase and dihydroorotase by metal ions and short-chain carboxylic acids, Amino Acids, 44 (2013) 1181-1191.
[8] Y.H. Huang, C.Y. Huang, Creation of a putative third metal binding site in type II dihydroorotases significantly enhances enzyme activity, Protein Pept Lett, 22 (2015) 1117-1122.
[9] A. Grande-Garcia, N. Lallous, C. Diaz-Tejada, S. Ramon-Maiques, Structure, functional characterization, and evolution of the dihydroorotase domain of human CAD, Structure, 22 (2014) 185-198.
[10] J.B. Thoden, G.N. Phillips, Jr., T.M. Neal, F.M. Raushel, H.M. Holden, Molecular structure of dihydroorotase: a paradigm for catalysis through the use of a binuclear metal center, Biochemistry, 40 (2001) 6989-6997.
[11] C.Y. Huang, C.C. Hsu, M.C. Chen, Y.S. Yang, Effect of metal binding and posttranslational lysine carboxylation on the activity of recombinant hydantoinase, J Biol Inorg Chem, 14 (2009) 111-121.

[12] C.Y. Huang, Y.P. Chao, Y.S. Yang, Purification of industrial hydantoinase in one chromatographic step without affinity tag, Protein Expr Purif, 30 (2003) 134-139.
[13] C.Y. Huang, Y.S. Yang, Discovery of a novel N-iminylamidase activity: substrate specificity, chemicoselectivity and catalytic mechanism, Protein Expr Purif, 40 (2005) 203-211.
[14] C.Y. Huang, Y.S. Yang, A novel cold-adapted imidase from fish Oreochromis niloticus that catalyzes hydrolysis of maleimide, Biochem Biophys Res Commun, 312 (2003) 467-472.
[15] C.Y. Huang, Y.S. Yang, The role of metal on imide hydrolysis: metal content and pH profiles of metal ion-replaced mammalian imidase, Biochem Biophys Res Commun, 297 (2002) 1027-1032.
[16] Y.C. Hsieh, M.C. Chen, C.C. Hsu, S.I. Chan, Y.S. Yang, C.J. Chen, Crystal structures of vertebrate dihydropyrimidinase and complexes from Tetraodon nigroviridis with lysine carbamylation: metal and structural requirements for post-translational modification and function, J Biol Chem, 288 (2013) 30645-30658.
[17] Z. Xu, Y. Liu, Y. Yang, W. Jiang, E. Arnold, J. Ding, Crystal structure of D-Hydantoinase from Burkholderia pickettii at a resolution of 2.7 Angstroms: insights into the molecular basis of enzyme thermostability, J Bacteriol, 185 (2003) 4038-4049.
[18] J. Abendroth, K. Niefind, D. Schomburg, X-ray structure of a dihydropyrimidinase from Thermus sp. at 1.3 A resolution, J Mol Biol, 320 (2002) 143-156.
[19] S.M. Runser, P.C. Meyer, Purification and biochemical characterization of the hydantoin hydrolyzing enzyme from Agrobacterium species. A hydantoinase with no 5,6-dihydropyrimidine amidohydrolase activity, Eur J Biochem, 213 (1993) 1315-1324.
[20] B. Lohkamp, B. Andersen, J. Piskur, D. Dobritzsch, The crystal structures of dihydropyrimidinases reaffirm the close relationship between cyclic amidohydrolases and explain their substrate specificity, J Biol Chem, 281 (2006) 13762-13776.
[21] X.Y. Zhang, L.X. Niu, Y.W. Shi, J.M. Yuan, The flexibility of the non-conservative region at the C terminus of D-hydantoinase from Pseudomonas putida YZ-26 is extremely limited, Appl Biochem Biotechnol, 144 (2008) 237-247.
[22] L. Niu, X. Zhang, Y. Shi, J. Yuan, Subunit dissociation and stability alteration of D hydantoinase deleted at the terminal amino acid residue,

Biotechnol Lett, 29 (2007) 303-308.
[23] C.Y. Huang, Inhibition of a putative dihydropyrimidinase from *Pseudomonas aeruginosa* PAO1 by flavonoids and substrates of cyclic amidohydrolases, PLoS One, 10 (2015) e0127634.
[24] C.T. Tzeng, Y.H. Huang, C.Y. Huang, Crystal structure of dihydropyrimidinase from Pseudomonas aeruginosa PAO1: Insights into the molecular basis of formation of a dimer, Biochem Biophys Res Commun, 478 (2016) 1449-1455.
[25] J.A. Marsh, H. Hernandez, Z. Hall, S.E. Ahnert, T. Perica, C.V. Robinson, S.A. Teichmann, Protein complexes are under evolutionary selection to assemble via ordered pathways, Cell, 153 (2013) 461-470.
[26] D.S. Goodsell, A.J. Olson, Structural symmetry and protein function, Annu Rev Biophys Biomol Struct, 29 (2000) 105-153.
[27] J.H. Cheng, C.C. Huang, Y.H. Huang, C.Y. Huang, Structural Basis for pH-Dependent Oligomerization of Dihydropyrimidinase from Pseudomonas aeruginosa PAO1, Bioinorg Chem Appl, 2018 (2018) 9564391.
[28] I.S. Park, R.P. Hausinger, Requirement of carbon dioxide for in vitro assembly of the urease nickel metallocenter, Science, 267 (1995) 1156-1158.
[29] E. Jabri, M.B. Carr, R.P. Hausinger, P.A. Karplus, The crystal structure of urease from Klebsiella aerogenes, Science, 268 (1995) 998-1004.
[30] J. Murn, Y. Shi, The winding path of protein methylation research: milestones and new frontiers, Nat Rev Mol Cell Biol, 18 (2017) 517-527.
[31] J.H. Cheng, Y.H. Huang, J.J. Lin, C.Y. Huang, Crystal structures of monometallic dihydropyrimidinase and the human dihydroorotase domain K1556A mutant reveal no lysine carbamylation within the active site, Biochem Biophys Res Commun, 505 (2018) 439-444.
[32] P.M. Wilson, P.V. Danenberg, P.G. Johnston, H.J. Lenz, R.D. Ladner, Standing the test of time: targeting thymidylate biosynthesis in cancer therapy, Nat Rev Clin Oncol, 11 (2014) 282-298.
[33] K. Bush, Alarming beta-lactamase-mediated resistance in multidrug-resistant Enterobacteriaceae, Curr Opin Microbiol, 13 (2010) 558-564.
[34] M.A. Fischbach, C.T. Walsh, Antibiotics for emerging pathogens, Science, 325 (2009) 1089-1093.
[35] K.L. Chen, Cheng, J.H., Lin, C.Y., Huang, Y.H., Huang, C.Y.,

Characterization of single-stranded DNA-binding protein SsbB from Staphylococcus aureus: SsbB cannot stimulate PriA helicase, RSC Adv., 8 (2018) 28367-28375.
[36] K. Kim, M.I. Kim, J. Chung, J.H. Ahn, S. Rhee, Crystal structure of metal-dependent allantoinase from Escherichia coli, J Mol Biol, 387 (2009) 1067-1074.
[37] I. Ramazzina, L. Cendron, C. Folli, R. Berni, D. Monteverdi, G. Zanotti, R. Percudani, Logical identification of an allantoinase analog (puuE) recruited from polysaccharide deacetylases, J Biol Chem, 283 (2008) 23295-23304.

附錄

其他水解酵素純化之膠圖

HsDHOase　4瓶 震3次　12%下膠

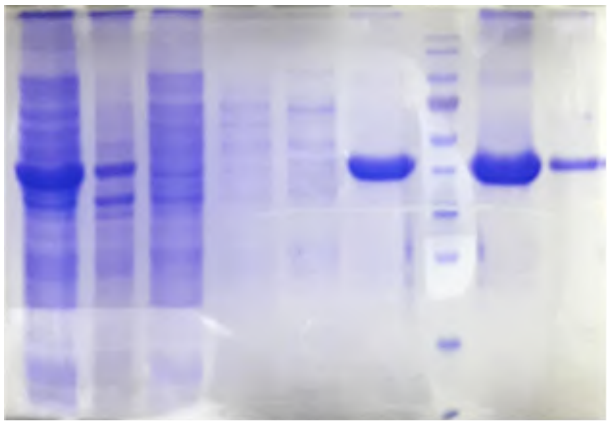

ScDHOase 4瓶 震3次 12%下膠

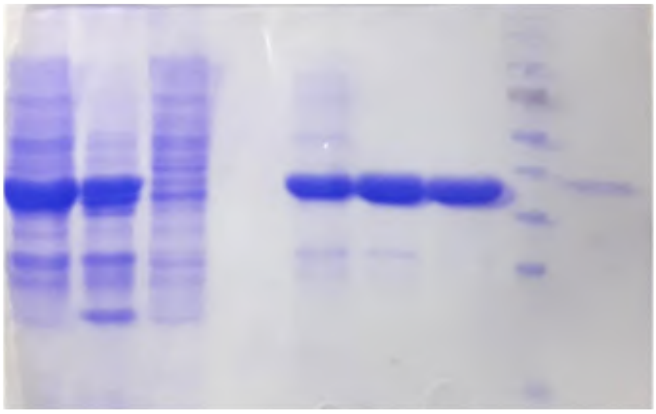

HsDHOase　4瓶 震3次　12%下膠

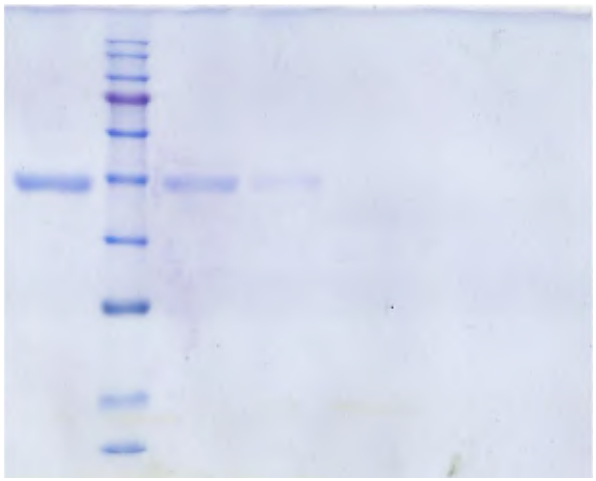

ScDHOase 4瓶 震3次 12%下膠

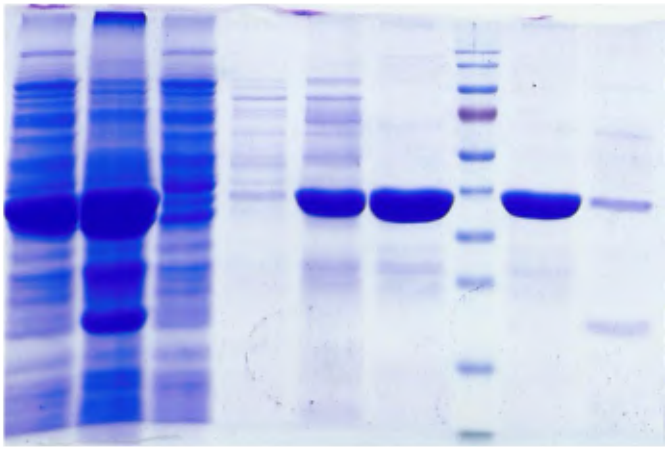

在此計畫執行區間的論文發表

Biochemical and Biophysical Research Communications 505 (2018) 439–444

Contents lists available at ScienceDirect

Biochemical and Biophysical Research Communications

journal homepage: www.elsevier.com/locate/ybbrc

Crystal structures of monometallic dihydropyrimidinase and the human dihydroorotase domain K1556A mutant reveal no lysine carbamylation within the active site

Jen-Hao Cheng [a], Yen-Hua Huang [a], Jing-Jie Lin [a, b], Cheng-Yang Huang [a, c, *]

[a] School of Biomedical Sciences, Chung Shan Medical University, No.110, Sec.1, Chien-Kuo N. Rd., Taichung City, Taiwan
[b] School of Medicine, College of Medicine, Chung Shan Medical University, No. 110, Sec. 1, Chien-Kuo N. Rd., Taichung City, Taiwan
[c] Department of Medical Research, Chung Shan Medical University Hospital, No.110, Sec.1, Chien-Kuo N. Rd., Taichung City, Taiwan

ARTICLE INFO

Article history:
Received 13 September 2018
Accepted 23 September 2018
Available online 27 September 2018

Keywords:
Dihydropyrimidinase
Dihydroorotase
Lysine carbamylation
Imidase
Allantoinase
Metalloenzyme

ABSTRACT

Dihydropyrimidinase (DHPase) is a member of the cyclic amidohydrolase family, which also includes allantoinase, dihydroorotase (DHOase), hydantoinase, and imidase. Almost all of these zinc metalloenzymes possess a binuclear metal center in which two metal ions are bridged by a post-translational carbamylated Lys. Crystal structure of *Tetraodon nigroviridis* DHPase reveals that one zinc ion is sufficient to stabilize Lys carbamylation. In this study, we found that one metal coordination was not sufficient to fix CO_2 to the Lys in bacterial DHPase. We prepared and characterized mono-Zn DHPase from *Pseudomonas aeruginosa* (PaDHPase), and the catalytic activity of mono-Zn PaDHPase was not detected. The crystal structure of mono-Zn PaDHPase determined at 2.23 Å resolution (PDB entry 6AJD) revealed that Lys150 was no longer carbamylated. This finding indicated the decarbamylation of the Lys during the metal chelating process. To confirm the state of Lys carbamylation in mono-Zn PaDHPase in solution, mass spectrometric (MS) analysis was carried out. The MS result was in agreement with the theoretical value for uncarbamylated PaDHPase. Crystal structure of the human DHOase domain (huDHOase) K1556A mutant was also determined (PDB entry 5YNZ), and the structure revealed that the active site of huDHOase K1556A mutant contained one metal ion. Like mono-Zn PaDHPase, oxygen ligands of the carbamylated Lys were not required for Znα binding. Considering the collective data from X-ray crystal structure and MS analysis, mono-Zn PaDHPase in both crystalline state and solution was not carbamylated. In addition, structural evidences indicated that post-translational carbamylated Lys was not required for Znα binding in PaDHPase and in huDHOase.

1. Introduction

Post-translational modification (PTM) on proteins has a regulatory role in many essential cellular processes by altering the functional properties of proteins at a relatively low energy cost [1]. PTMs are typically reversible and may need a specific enzyme to add covalent modification [1]. Post-translational Lys carbamylation, i.e., a chemical reaction to add a carboxyl group to the ε-amino group of a Lys, was discovered more than 20 years ago [2]. This modification on Lys creates a new amino acid that changes the side chain from positive to negative charge at neutral pH and also lengthens the side chain [3–5]. A carbamylated Lys within the active site of urease provides an oxygen ligand to each nickel, thereby explaining the need for carbon dioxide in activation of the apoenzyme and suggesting a role for di-metal binding [6]. To date, more than 300 protein structures with Lys carbamylation, such as pyruvate carboxylase, β-lactamase, ribulose-1,5-bisphosphate carboxylase/oxygenase (RuBisCO), phosphodiesterase, hydantoinase, urease, dihydroorotase (DHOase), allantoinase, and dihydropyrimidinase (DHPase), can be found in the Protein Data Bank.

DHPase catalyzes the reversible cyclization of dihydrouracil to *N*-carbamoyl-β-alanine in the second step of the pyrimidine degradation pathway [7]. DHPase [3,8,9] is a member of the cyclic amidohydrolase family [10,11], which also includes allantoinase [4,12,13], DHOase [4,14–17], hydantoinase [5,18], and imidase [19–21]. Almost all of these zinc enzymes contain the binuclear

* Corresponding author. School of Biomedical Sciences, Chung Shan Medical University, No. 110, Sec. 1, Chien-Kuo N. Rd., Taichung City, Taiwan.
E-mail address: cyhuang@csmu.edu.tw (C.-Y. Huang).

https://doi.org/10.1016/j.bbrc.2018.09.153
0006-291X/

metal center that consists of four His, one Asp, and one post-translational carbamylated Lys residues. Post-carbamylated Lys is required for enzyme activity and self-assembly of binuclear metal center [4,5]. Metals in DHPase can be removed by some chelators [3]. The active site of apo-DHPase can be restored via titration with metal ions, which restores activity [3]. Crystal structure of *Tetraodon nigroviridis* DHPase (TnDHPase) reveals that one zinc ion is sufficient to stabilize Lys carbamylation [3]. Thus, vertebrate DHPase may only need one zinc ion for catalytic reaction [3]. It remains unclear whether or not only one metal is also sufficient for stabilizing Lys carbamylation and normal function in bacterial DHPase. Because molecular evidence is lacking, Lys carbamylation in other mono-Zn DHPase and cyclic amidohydrolase such as DHOase also remains to be elucidated.

In the present study, we prepared and characterized mono-Zn *Pseudomonas aeruginosa* DHPase (PaDHPase). Unlike mono-Zn TnDHPase, mono-Zn PaDHPase activity was undetectable. To find the reason, we determined the crystal structure of mono-Zn PaDHPase at 2.23 Å resolution. Crystal structure of the human DHOase domain (huDHOase) K1556A mutant was also determined, and the structure revealed that the active site of huDHOase K1556A mutant contained one metal ion. X-ray crystal structure and mass spectrometric (MS) analysis revealed that mono-Zn PaDHPase in crystalline state and solution was not carbamylated. Thus, no enzyme activity was found.

2. Materials and methods

2.1. Protein expression and purification of PaDHPase

Construction of the PaDHPase expression plasmid has been reported [8]. The recombinant PaDHPase was purified using the protocol described previously for SSB-like proteins [22–25]. Briefly, *E. coli* BL21(DE3) cells were transformed with the expression vector and overexpression of the expression plasmids was induced by incubating with 1 mM isopropyl thiogalactopyranoside. The protein was purified from the soluble supernatant by Ni^{2+}-affinity chromatography (HiTrap HP; GE Healthcare Bio-Sciences), eluted with Buffer A (20 mM Tris-HCl, 250 mM imidazole, and 0.5 M NaCl, pH 7.9). Protein purity remained at >97% as determined by SDS-PAGE (Mini-PROTEAN Tetra System; Bio-Rad, CA, USA).

2.2. huDHOase K1556A mutant

In mammals, DHOase is found as part of the large multifunctional protein, carbamoyl phosphate synthetase (CPSase)/aspartate transcarbamoylase (ATCase)/DHOase protein (CAD) [26]. Construction of huDHOase (aa 1456–1846 of CAD protein) expression plasmid has been reported [27]. The huDHOase K1556A mutant was generated using a QuikChange Site-Directed Mutagenesis kit according to the manufacturer's protocol (Stratagene, LaJolla, CA). The presence of the mutation was verified by DNA sequencing. The oligonucleotide primers used for this mutant were as follows: 5′-TCTGCAGCCGGGCTGGCGCTTTACCTCAAT-3′ and 5′-CTCATTGAGG-TAAAGCGCCAGCCCGGCTGC-3′. The underlined sequences denote the mutated amino acid. The recombinant huDHOase K1556A mutant protein was purified using the protocol described for PaDHPase.

2.3. Preparation of mono-Zn PaDHPase

Purified PaDHPase was dialyzed against a chelating buffer (50 mM MES, 50 mM EDTA, and 15 mM 8-HQSA, pH 6.5; Buffer B) at room temperature for 3 days. The resultant enzyme solution was then dialyzed against a dialysis buffer (20 mM HEPES and 100 mM NaCl, pH 7.0; Buffer C).

2.4. Crystallography

Before crystallization, mono-Zn PaDHPase and huDHOase K1556A mutant were concentrated to 20 mg/mL in Buffer C. Crystals of mono-Zn PaDHPase were grown at room temperature by hanging drop vapor diffusion in 25% PEG 4000, 100 mM Tris-HCl, 200 mM calcium chloride, pH 8.5. Crystals of huDHOase K1556A mutant were grown in 2 M sodium chloride, 100 mM MES, 200 mM sodium acetate, pH 6.5. Data were collected using an ADSC Quantum-315r CCD area detector at SPXF beamline BL13C1 at NSRRC (Taiwan, ROC). All data integration and scaling were carried out using HKL-2000 [28]. The crystal structures of mono-Zn PaDHPase and huDHOase K1556A mutant were determined with the molecular replacement software Phaser-MR [29] using di-Zn PaDHPase (PDB entry 5E5C) [30] and huDHOase (PDB entry 4BY3) [31] as models, respectively. Models was built and refined with PHENIX [32] and Coot [33].

2.5. MS analysis

The carbamylated and decarbamylated PaDHPases were analyzed via matrix-assisted laser desorption/ionization time-of-flight mass spectrometry (MALDI-TOF MS) using the protocol described previously [34]. The cinnamic acid derivative α-cyano-4-hydroxycinnamic acid (CHCA) matrixes were dissolved in 50% acetonitrile with 0.1% formic acid. One μL of sample was mixed with an equal volume of CHCA, then 1 μL of analyte solution was deposited onto a stainless steel sample plate, air-dried, and analyzed in a Voyager-DE Pro MALDI-TOF mass spectrometer equipped with a pulsed nitrogen laser set at 337 nm (Applied Biosystems, CA). All mass spectra were acquired in the linear positive ion mode with delayed extraction. The extraction and guide wire voltages were set at 20 kV and 0.2%. The mass calibration was achieved using ion peaks of BSA. Data analysis was performed by Data Explorer software (Applied Biosystems).

3. Results and discussion

3.1. Preparation of mono-Zn PaDHPase

PaDHPase is a di-Zn enzyme [30]. To determine the importance of the binuclear metal center in PaDHPase activity and the relationship between post-translational Lys carbamylation and the metals within the active site of PaDHPase, mono-Zn PaDHPase was prepared and characterized. After analysis using inductively coupled plasma mass spectrometry [4,5], we found that one metal ion in di-Zn PaDHPase was removed by incubating with chelator buffer containing 15 mM 8-HQSA and 50 mM EDTA for 3 days. EDTA alone is a poor chelator for removal of metal in PaDHPase. Unlike TnDHPase, however, the activity of mono-Zn PaDHPase was undetected.

3.2. Crystal structure of mono-Zn PaDHPase

To determine which metal ion in di-Zn PaDHPase was removed by the chelator buffer and to study the metal removing effect on the enzyme structure-activity relationship, mono-Zn PaDHPase was crystallized through hanging drop vapor diffusion for structure determination. The crystal structure of mono-Zn PaDHPase at a resolution of 2.23 Å (Table 1) showed one zinc atom (designated as Znα) in the active site (Fig. 1A). Znα was coordinated with His59 (2.67 Å), His61 (2.72 Å), and D316 (2.29 Å). Three water molecules were also found near Znα. H239, which was originally involved in

Table 1
Data collection and refinement statistics.

Data collection		
Crystal	mono-Zn PaDHPase	huDHOase K1556A
Wavelength (Å)	0.975	0.975
Resolution (Å)	30–2.23	30–2.77
Space group	$P2_12_12$	$C222$
Cell dimension (Å)	$a = 88.36$ $\alpha = 90$	$a = 88.84$ $\alpha = 90$
	$b = 110.17$ $\beta = 90$	$b = 108.63$ $\beta = 90$
	$c = 112.66$ $\gamma = 90$	$c = 99.22$ $\gamma = 90$
Completeness (%)	99.8 (99.9)[a]	99.9 (99.7)[a]
⟨I/σI⟩	12.9 (3.9)	23.68 (2.74)
R_{sym} or R_{merge} (%)	0.133 (0.491)	0.07 (0.498)
Redundancy	5.1 (5.2)	4.4 (4.4)
Refinement		
Resolution (Å)	29.28–2.23	29.8–2.77
No. reflections	54478	12440
R_{work}/R_{free}	0.1819/0.2323	0.2260/0.2889
No. atoms		
Protein	956	363
Zinc	1	1
Water	283	14
R.m.s deviation		
Bond lengths (Å)	0.008	0.011
Bond angles (°)	0.980	1.188
Ramachandran Plot		
In preferred regions	909 (95.48%)	335 (92.80%)
In allowed regions	35 (3.68%)	21 (5.82%)
Outliers	8 (0.84%)	5 (1.39%)
PDB entry	6AJD	5YZN

$R_{sym} = \Sigma|I - \text{'I'}|/\Sigma I$, where I is the observed intensity, 'I' is the statistically weighted average intensity of multiple observations of symmetry-related reflections.
[a] Values in parentheses are for the highest resolution shell.

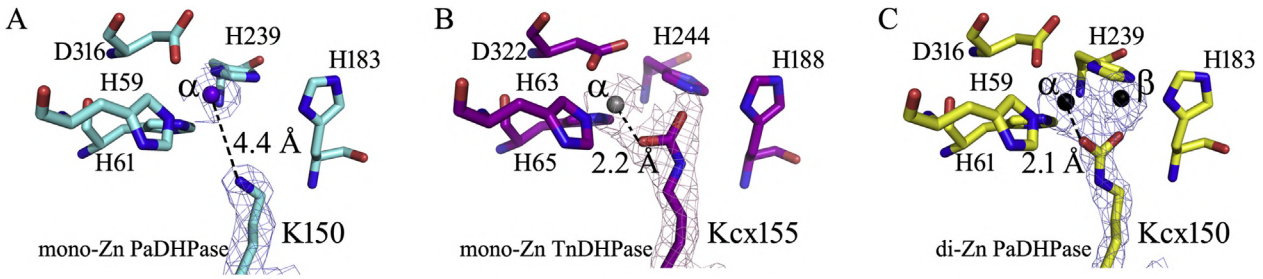

Fig. 1. Structures of the active site. (A) The mono-Zn PaDHPase. Lys150 was not carbamylated in mono-Zn PaDHPase. The composite omit map (at 1.0 σ) showed that the electron density between Znα and Lys150 in mono-Zn PaDHPase was not connected. The distance between the ε-amino group of Lys150 and Znα was 4.4 Å. (B) The mono-Zn TnDHPase. The mono-Zn TnDHPase contains one metal (Znα) and carbamylated Lys155 (Kcx155). The electron density between Znα and Lys155 in mono-Zn TnDHPase is connected. (C) The di-Zn PaDHPase. The di-Zn PaDHPase contains two metals (Znα and Znβ) and carbamylated Lys150 (Kcx150). The Lys in mono-Zn TnDHPase and di-Zn PaDHPase are carbamylated, but not in mono-Zn PaDHPase.

coordination with Znβ of di-Zn PaDHPase, was loosely associated with Znα at a distance of 3.38 Å. Unlike in mono-Zn TnDHPase (Fig. 1B) [3], Lys150 was not carbamylated in mono-Zn PaDHPase (Fig. 1A). The composite omit map showed that the electron density between Znα and Lys150 in mono-Zn PaDHPase was not connected. The distance (4.4 Å) between the ε-amino group of Lys150 and Znα was not reasonable for interaction (Table 2). In addition, crystallographic analyses also indicated that Znβ in di-Zn PaDHPase (Fig. 1C) was easily removed. Thus, structural evidence in this study indicated that the Lys in mono-Zn TnDHPase [3] and di-Zn PaDHPase [30] are carbamylated, but not in mono-Zn PaDHPase (PDB entry 6AJD).

Table 2
Distance between metal and residues.

di-Zn PaDHPase (PDB entry 5E5C)			mono-Zn PaDHPase (PDB entry 6AJD)		
Metal	Residue	Dist. [Å]	Metal	Residue	Dist. [Å]
Znα	H59 [NE2]	2.19	Znα	H59 [NE2]	2.67
Znα	H61 [NE2]	2.30	Znα	H61 [NE2]	2.72
Znα	Kcx150 [OX1]	2.04	Znα	K150 [NZ]	4.39
Znα	D316 [OD1]	2.30	Znα	D316 [OD1]	2.29
Znβ	H183 [ND1]	2.34	Znα	H183 [ND1]	4.61
Znβ	H239 [NE2]	3.13	Znα	H239 [NE2]	3.38
Znβ	K150 [OX2]	1.85			
Znβ	Znα	2.89			

3.3. MS analysis of mono-Zn PaDHPase

The crystal structure of mono-Zn PaDHPase revealed that carbamylation did not occur. To verify whether the Lys was still uncarbamylated in solution, mono-Zn PaDHPase and di-Zn PaDHPase were analyzed via mass spectrometry. MALDI-TOF MS analysis of the mono-Zn PaDHPase (Fig. 2A) and di-Zn PaDHPase (Fig. 2B) gave molecular weights of 52 952.87 and 52 997.34, respectively. The molecular weight of mono-Zn PaDHPase agreed well with the theoretical value for the uncarbamylated PaDHPase. The difference (52 997.34−52 952.87 = 44.47) was reasonable for CO_2. Thus, mono-Zn PaDHPase in both crystalline and solution did not have carbamylated Lys (Figs. 1A and 2A, respectively). Unlike TnDHPase, one metal atom (Znα) bound in the active site of PaDHPase was not sufficient to maintain the carbamylation on Lys150.

3.4. Structural comparison of the di-Zn PaDHPase and mono-Zn PaDHPase

Besides the post-translational carbamylation, the superimposed structures of di-Zn PaDHPase and mono-Zn PaDHPase also revealed conformational changes at the active sites (Fig. 3), especially for His239 and His183. Relative to their positions in mono-Zn PaDHPase (cyan), the side-chain orientations of His239 and His183 in di-Zn PaDHPase (yellow) shifted by angles of 20.09° and 12.95° and distances of 1.14 and 0.58 Å, respectively. The conformation of carbamylated Lys150 in di-Zn PaDHPase and uncarbamylated Lys150 in mono-Zn PaDHPase did not significantly differ in position.

3.5. Post-carbamylated lysine was not required for Znα binding in PaDHPase

The post-translational lysine carbamylation facilitated either one or two metal ions coordination, such as in the following: RuBisCO [35], which binds one Mg^{2+}; and urease [2,6], which binds two Ni^{2+} ions. Intuitively, for the Lys side chain to serve as bridging ligand to the two metals within the binuclear metal center, carbamylation through a reaction with carbon dioxide in di-metal amidohydrolase superfamily needs to occur first [3]. However, the Lys in mono-Zn PaDHPase did not undergo carbamylation (Fig. 1A). The composite omit map clearly showed that the electron density

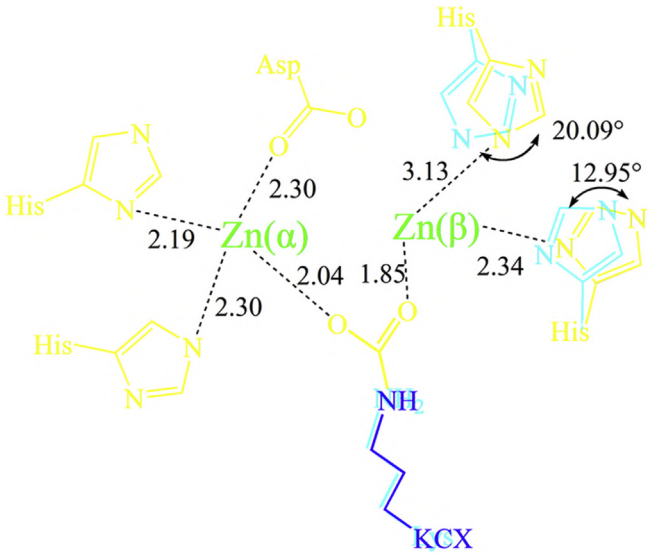

Fig. 3. Structural comparison of the di-Zn PaDHPase and mono-Zn PaDHPase. Besides the post-translational carbamylation, the superimposed structures of di-Zn PaDHPase and mono-Zn PaDHPase also revealed conformational changes at the active sites, especially for His239 and His183. Relative to their positions in mono-Zn PaDHPase (cyan), the side-chain orientations of His239 and His183 in di-Zn PaDHPase (yellow) shifted by angles of 20.09° and 12.95° and distances of 1.14 and 0.58 Å, respectively. (For interpretation of the references to colour in this figure legend, the reader is referred to the Web version of this article.)

between Znα and Lys150 in mono-Zn PaDHPase was not connected. In addition, post-carbamylated Lys was not required for Znα binding in PaDHPase. Based on these structural data, we concluded that the post-carbamylation mechanism on the Lys among these metalloenzymes may differ.

3.6. Crystal structure of huDHOase K1556A mutant

Whether the post-carbamylated Lys is also not required for Znα binding in DHOase remains unclear. We made an attempt to crystallize mono-Zn huDHOase, but we did not get suitable crystals for structure determination. However, we obtained crystals of huDHOase K1556A mutant successfully. Like DHPase, huDHOase is also a member of the cyclic amidohydrolase family [36]. The crystal

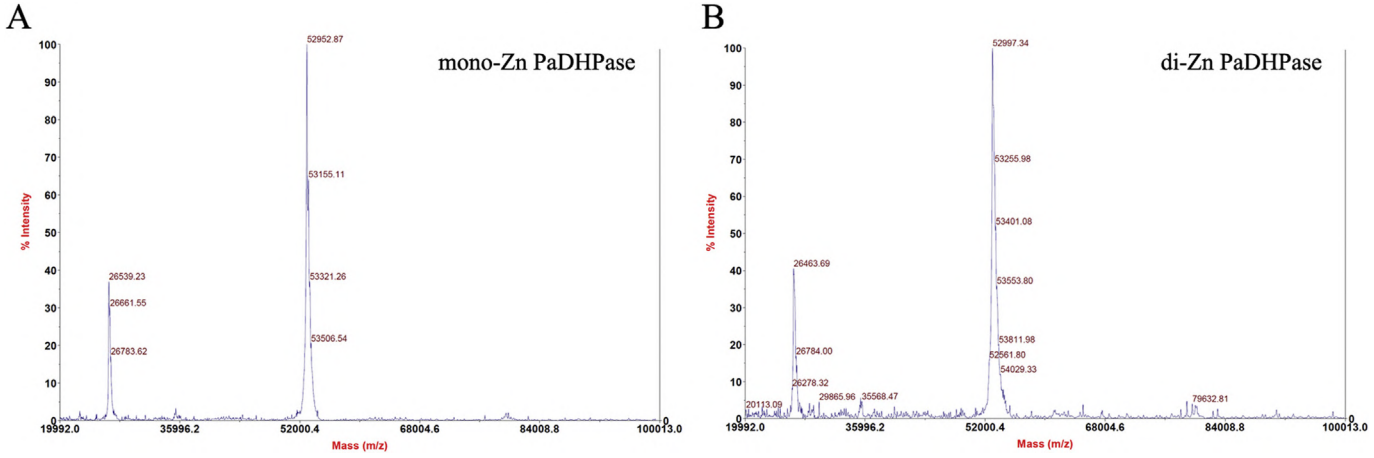

Fig. 2. MS analysis. To verify whether the Lys was uncarbamylated in solution, (A) mono-Zn PaDHPase and (B) di-Zn PaDHPase were analyzed via MALDI-TOF MS. The mono-Zn PaDHPase and di-Zn PaDHPase gave molecular weights of 52 952.87 and 52 997.34, respectively. The difference (44.47) was reasonable for CO_2. Thus, one metal atom bound in the active site of PaDHPase was not sufficient to maintain the carbamylation on Lys150.

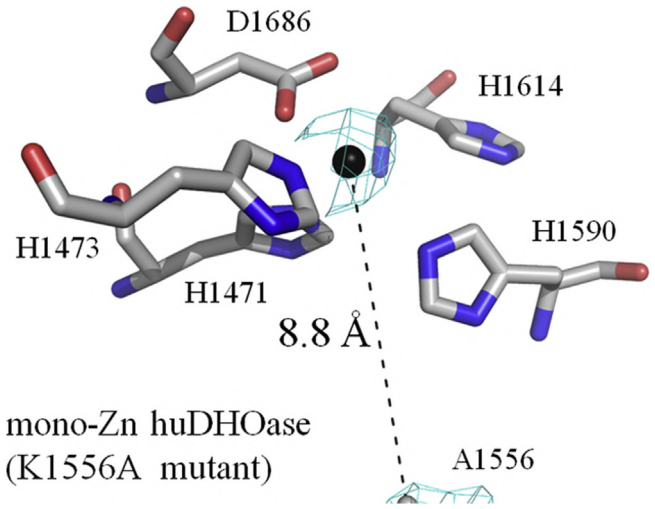

Fig. 4. Crystal structure of huDHOase K1556A mutant. The post-carbamylated Lys in huDHOase is important for di-metal binding. The crystal structure of huDHOase K1556A mutant revealed that the active site contained one metal ion. Thus, oxygen ligands of the carbamylated Lys in huDHOase were not absolutely required for di-metal binding. Like PaDHPase, structural evidence showed that only Znβ in huDHOase was affected by the carbamylation/decarbamylation in huDHOase.

structure of huDHOase K1556A mutant was solved at 2.77 Å (Fig. 4; PDB entry 5YNZ). The crystal structure revealed that when the carbamylated Lys was absent, huDHOase did not lose Zn^{2+} ions completely. Like mono-Zn PaDHPase, huDHOase K1556A mutant still contained one metal ion (Znα). Thus, oxygen ligands of the carbamylated Lys in huDHOase were not absolutely required for di-metal binding. Only Znβ in huDHOase was affected by the carbamylation/decarbamylation.

In conclusion, we prepared and characterized mono-Zn PaDHPase through X-ray crystal structural and MS analyses. Post-translational carbamylated Lys was not required for Znα binding in PaDHPase, both in crystalline state (Fig. 1) and solution (Fig. 2). Post-translational carbamylated Lys was also not required for Znα binding in huDHOase. These cases were different from that of vertebrate DHPase (TnDHPase). Furthermore, one metal ion in PaDHPase was not sufficient to stabilize carbamylation, and mono-Zn PaDHPase was inactive. Hence, the di-Zn metal center in PaDHPase was essential [8].

Disclosure statement

The author has no conflicts of interest.

Acknowledgments

We thank the experimental facility and the technical services provided by the Synchrotron Radiation Protein Crystallography Facility of the National Core Facility Program for Biotechnology, Ministry of Science and Technology and the National Synchrotron Radiation Research Center, a national user facility supported by the Ministry of Science and Technology, Taiwan, ROC. This research was supported by a grant from the Ministry of Science and Technology, Taiwan (MOST 107-2320-B-040-014 to C.Y. Huang).

Appendix A. Supplementary data

Supplementary data to this article can be found online at https://doi.org/10.1016/j.bbrc.2018.09.153.

Transparency document

Transparency document related to this article can be found online at https://doi.org/10.1016/j.bbrc.2018.09.153.

References

[1] J. Murn, Y. Shi, The winding path of protein methylation research: milestones and new frontiers, Nat. Rev. Mol. Cell Biol. 18 (2017) 517–527.
[2] E. Jabri, M.B. Carr, R.P. Hausinger, P.A. Karplus, The crystal structure of urease from *Klebsiella aerogenes*, Science 268 (1995) 998–1004.
[3] Y.C. Hsieh, M.C. Chen, C.C. Hsu, S.I. Chan, Y.S. Yang, C.J. Chen, Crystal structures of vertebrate dihydropyrimidinase and complexes from *Tetraodon nigroviridis* with lysine carbamylation: metal and structural requirements for post-translational modification and function, J. Biol. Chem. 288 (2013) 30645–30658.
[4] Y.Y. Ho, Y.H. Huang, C.Y. Huang, Chemical rescue of the post-translationally carboxylated lysine mutant of allantoinase and dihydroorotase by metal ions and short-chain carboxylic acids, Amino Acids 44 (2013) 1181–1191.
[5] C.Y. Huang, C.C. Hsu, M.C. Chen, Y.S. Yang, Effect of metal binding and post-translational lysine carboxylation on the activity of recombinant hydantoinase, J. Biol. Inorg. Chem. 14 (2009) 111–121.
[6] I.S. Park, R.P. Hausinger, Requirement of carbon dioxide for in vitro assembly of the urease nickel metallocenter, Science 267 (1995) 1156–1158.
[7] C.C. Hsu, L.Y. Lu, Y.S. Yang, From sequence and structure of sulfotransferases and dihydropyrimidinases to an understanding of their mechanisms of action and function, Expet Opin. Drug Metabol. Toxicol. 6 (2010) 591–601.
[8] C.Y. Huang, Inhibition of a putative dihydropyrimidinase from *Pseudomonas aeruginosa* PAO1 by flavonoids and substrates of cyclic amidohydrolases, PLoS One 10 (2015), e0127634.
[9] J. Abendroth, K. Niefind, D. Schomburg, X-ray structure of a dihydropyrimidinase from *Thermus* sp. at 1.3 A resolution, J. Mol. Biol. 320 (2002) 143–156.
[10] J.A. Gerlt, P.C. Babbitt, Divergent evolution of enzymatic function: mechanistically diverse superfamilies and functionally distinct suprafamilies, Annu. Rev. Biochem. 70 (2001) 209–246.
[11] G.J. Kim, H.S. Kim, Identification of the structural similarity in the functionally related amidohydrolases acting on the cyclic amide ring, Biochem. J. 330 (1998) 295–302.
[12] Y.Y. Ho, H.C. Hsieh, C.Y. Huang, Biochemical characterization of allantoinase from *Escherichia coli* BL21, Protein J. 30 (2011) 384–394.
[13] K. Kim, M.I. Kim, J. Chung, J.H. Ahn, S. Rhee, Crystal structure of metal-dependent allantoinase from Escherichia coli, J. Mol. Biol. 387 (2009) 1067–1074.
[14] W.F. Peng, C.Y. Huang, Allantoinase and dihydroorotase binding and inhibition by flavonols and the substrates of cyclic amidohydrolases, Biochimie 101 (2014) 113–122.
[15] M. Barba, N. Glansdorff, B. Labedan, Evolution of cyclic amidohydrolases: a highly diversified superfamily, J. Mol. Evol. 77 (2013) 70–80.
[16] C.C. Wang, H.W. Tsau, W.T. Chen, C.Y. Huang, Identification and characterization of a putative dihydroorotase, KPN01074, from *Klebsiella pneumoniae*, Protein J. 29 (2010) 445–452.
[17] J.B. Thoden, G.N. Phillips Jr., T.M. Neal, F.M. Raushel, H.M. Holden, Molecular structure of dihydroorotase: a paradigm for catalysis through the use of a binuclear metal center, Biochemistry 40 (2001) 6989–6997.
[18] Z. Xu, Y. Liu, Y. Yang, W. Jiang, E. Arnold, J. Ding, Crystal structure of D-Hydantoinase from *Burkholderia pickettii* at a resolution of 2.7 Angstroms: insights into the molecular basis of enzyme thermostability, J. Bacteriol. 185 (2003) 4038–4049.
[19] C.Y. Huang, Y.S. Yang, A novel cold-adapted imidase from fish *Oreochromis niloticus* that catalyzes hydrolysis of maleimide, Biochem. Biophys. Res. Commun. 312 (2003) 467–472.
[20] C.Y. Huang, Y.S. Yang, The role of metal on imide hydrolysis: metal content and pH profiles of metal ion-replaced mammalian imidase, Biochem. Biophys. Res. Commun. 297 (2002) 1027–1032.
[21] Y.S. Yang, S. Ramaswamy, W.B. Jakoby, Rat liver imidase, J. Biol. Chem. 268 (1993) 10870–10875.
[22] Y.H. Huang, C.Y. Huang, SAAV2152 is a single-stranded DNA binding protein: the third SSB in *Staphylococcus aureus*, Oncotarget 9 (2018) 20239–20254.
[23] Y.H. Huang, H.H. Guan, C.J. Chen, C.Y. Huang, *Staphylococcus aureus* single-stranded DNA-binding protein SsbA can bind but cannot stimulate PriA helicase, PLoS One 12 (2017), e0182060.
[24] Y.H. Huang, Y. Lien, C.C. Huang, C.Y. Huang, Characterization of *Staphylococcus aureus* primosomal DnaD protein: highly conserved C-terminal region is crucial for ssDNA and PriA helicase binding but not for DnaA protein-binding and self-tetramerization, PLoS One 11 (2016), e0157593.
[25] C.Y. Huang, C.H. Hsu, Y.J. Sun, H.N. Wu, C.D. Hsiao, Complexed crystal structure of replication restart primosome protein PriB reveals a novel single-stranded DNA-binding mode, Nucleic Acids Res. 34 (2006) 3878–3886.
[26] D.R. Evans, H.I. Guy, Mammalian pyrimidine biosynthesis: fresh insights into an ancient pathway, J. Biol. Chem. 279 (2004) 33035–33038.
[27] Y.H. Huang, C.Y. Huang, Creation of a putative third metal binding site in type II dihydroorotases significantly enhances enzyme activity, Protein Pept. Lett.

22 (2015) 1117–1122.
[28] Z. Otwinowski, W. Minor, Processing of X-ray diffraction data collected in oscillation mode, Methods Enzymol. 276 (1997) 307–326.
[29] A.J. McCoy, R.W. Grosse-Kunstleve, P.D. Adams, M.D. Winn, L.C. Storoni, R.J. Read, Phaser crystallographic software, J. Appl. Crystallogr. 40 (2007) 658–674.
[30] C.T. Tzeng, Y.H. Huang, C.Y. Huang, Crystal structure of dihydropyrimidinase from *Pseudomonas aeruginosa* PAO1: insights into the molecular basis of formation of a dimer, Biochem. Biophys. Res. Commun. 478 (2016) 1449–1455.
[31] A. Grande-Garcia, N. Lallous, C. Diaz-Tejada, S. Ramon-Maiques, Structure, functional characterization, and evolution of the dihydroorotase domain of human CAD, Structure 22 (2014) 185–198.
[32] J.J. Headd, N. Echols, P.V. Afonine, R.W. Grosse-Kunstleve, V.B. Chen, N.W. Moriarty, D.C. Richardson, J.S. Richardson, P.D. Adams, Use of knowledge-based restraints in phenix.refine to improve macromolecular refinement at low resolution, Acta Crystallogr. D Biol. Crystallogr. 68 (2012) 381–390.
[33] P. Emsley, K. Cowtan, Coot: model-building tools for molecular graphics, Acta Crystallogr. D Biol. Crystallogr. 60 (2004) 2126–2132.
[34] C.W. Liu, M.W. Chien, G.F. Chen, S.Y. Chen, C.S. Yu, M.Y. Liao, C.C. Lai, Quantum dot enhancement of peptide detection by matrix-assisted laser desorption/ionization mass spectrometry, Anal. Chem. 83 (2011) 6593–6600.
[35] F.C. Hartman, M.R. Harpel, Structure, function, regulation, and assembly of D-ribulose-1,5-bisphosphate carboxylase/oxygenase, Annu. Rev. Biochem. 63 (1994) 197–234.
[36] Z. Gojkovic, L. Rislund, B. Andersen, M.P. Sandrini, P.F. Cook, K.D. Schnackerz, J. Piskur, Dihydropyrimidine amidohydrolases and dihydroorotases share the same origin and several enzymatic properties, Nucleic Acids Res. 31 (2003) 1683–1692.

Hindawi
Bioinorganic Chemistry and Applications
Volume 2018, Article ID 9564391, 8 pages
https://doi.org/10.1155/2018/9564391

Research Article

Structural Basis for pH-Dependent Oligomerization of Dihydropyrimidinase from *Pseudomonas aeruginosa* PAO1

Jen-Hao Cheng,[1] Chien-Chih Huang,[1] Yen-Hua Huang,[1] and Cheng-Yang Huang [1,2]

[1]*School of Biomedical Sciences, Chung Shan Medical University, No. 110, Sec. 1, Chien-Kuo N. Rd., Taichung, Taiwan*
[2]*Department of Medical Research, Chung Shan Medical University Hospital, No. 110, Sec. 1, Chien-Kuo N. Rd., Taichung, Taiwan*

Correspondence should be addressed to Cheng-Yang Huang; cyhuang@csmu.edu.tw

Received 17 October 2017; Revised 20 November 2017; Accepted 3 December 2017; Published 30 January 2018

Academic Editor: Luigi Casella

Dihydropyrimidinase, a dimetalloenzyme containing a carboxylated lysine within the active site, is a member of the cyclic amidohydrolase family, which also includes allantoinase, dihydroorotase, hydantoinase, and imidase. Unlike all known dihydropyrimidinases, which are tetrameric, pseudomonal dihydropyrimidinase forms a dimer at neutral pH. In this paper, we report the crystal structure of *P. aeruginosa* dihydropyrimidinase at pH 5.9 (PDB entry 5YKD). The crystals of *P. aeruginosa* dihydropyrimidinase belonged to space group $C222_1$ with cell dimensions of $a = 108.9$, $b = 155.7$, and $c = 235.6$ Å. The structure of *P. aeruginosa* dihydropyrimidinase was solved at 2.17 Å resolution. An asymmetric unit of the crystal contained four crystallographically independent *P. aeruginosa* dihydropyrimidinase monomers. Gel filtration chromatographic analysis of purified *P. aeruginosa* dihydropyrimidinase revealed a mixture of dimers and tetramers at pH 5.9. Thus, *P. aeruginosa* dihydropyrimidinase can form a stable tetramer both in the crystalline state and in the solution. Based on sequence analysis and structural comparison of the dimer-dimer interface between *P. aeruginosa* dihydropyrimidinase and *Thermus* sp. dihydropyrimidinase, different oligomerization mechanisms are proposed.

1. Introduction

Dihydropyrimidinase is a key enzyme for pyrimidine catabolism [1, 2]. Dihydropyrimidinase catalyzes the reversible cyclization of dihydrouracil to *N*-carbamoyl-*β*-alanine in the second step of the pyrimidine degradation pathway (Figure 1). Dihydropyrimidinase can also detoxify xenobiotics with an imide functional group, ranging from linear imides to heterocyclic imides [3–9]. Homologous enzymes from microorganisms are known as hydantoinase, used as biocatalyst for hydrolysis of 5-monosubstituted hydantoins in the synthesis of D- and L-amino acids [10, 11]. Optically pure amino acids have been widely used as intermediates for semisynthesis of antibiotics, active peptides, hormones, antifungal agents, pesticides, and sweeteners. Dihydropyrimidinase and hydantoinase generally possess a similar active site, but their overall sequence identity and substrate specificity may differ [3, 12]. For example, hydantoinase purified from *Agrobacterium* species has no 5,6-dihydropyrimidine amidohydrolase activity [13]. Dihydropyrimidinases from the yeast *Saccharomyces kluyveri* and the slime mold *Dictyostelium discoideum* do not hydrolyze hydantoin [14]. Thus, several bacterial hydantoinases are still named and identified as dihydropyrimidinase because of their catalytic activity toward natural substrates, namely, dihydrouracil and dihydrothymine. These bacterial enzymes include *Pseudomonas aeruginosa* and *Thermus* sp. dihydropyrimidinases [15, 16].

Dihydropyrimidinase, hydantoinase, imidase, allantoinase, and dihydroorotase belong to the cyclic amidohydrolase family because of their functional and structural similarities [17]. Members of this enzyme family catalyze the ring-opening hydrolysis of the cyclic amide bond of each substrate in either five- or six-membered rings. Even if these enzymes have similar functions, they have relatively low amino acid sequence identity. In addition, the substrate selectivity and specificity of these enzymes highly differ [18, 19]. Most of the active sites of dihydropyrimidinases, hydantoinases, allantoinases, and dihydroorotases contain four histidines, one aspartate, and one carboxylated lysine residue, which are required for metal binding and catalytic

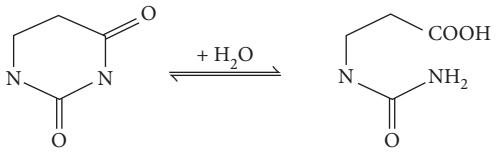

Dihydrouracil *N*-carbamoyl-β-alanine

Figure 1: The physiological reaction of dihydropyrimidinase. Dihydropyrimidinase catalyzes the reversible cyclization of dihydrouracil to *N*-carbamoyl-β-alanine in the second step of the pyrimidine degradation pathway.

activity [8, 15, 18, 20, 21]. The presence of a carboxylated lysine in hydantoinase is also required for the self-assembly of the binuclear metal center [12, 20, 22] and increases the nucleophilicity of the hydroxide for catalysis [23]. The global architecture of the dihydropyrimidinase monomer consists of two domains, namely, a large domain with a classic $(\beta/\alpha)_8$-barrel structure core embedding the catalytic dimetal center and a small β-sandwich domain [16, 22, 24, 25].

All known dihydropyrimidinases are tetramers except pseudomonal enzymes. Hydantoinase from *P. putida* YZ-26 functions as a dimer [26, 27]. Recently, we identified that dihydropyrimidinase from *P. aeruginosa* PAO1 also forms a dimer [28]. In addition, the crystal structure of *P. aeruginosa* PAO1 dihydropyrimidinase indicated that several residues crucial for tetramerization are not found in *P. aeruginosa* dihydropyrimidinase [28]. In this study, we found that the oligomerization of *P. aeruginosa* PAO1 dihydropyrimidinase is a pH-dependent process. At pH 5.9, *P. aeruginosa* PAO1 dihydropyrimidinase mainly formed a tetramer. To confirm this result and determine how this enzyme can also form a tetramer, we also determined the crystal structure of *P. aeruginosa* PAO1 dihydropyrimidinase at 2.17 Å resolution at acidic environment. Structural comparison indicated that although *P. aeruginosa* PAO1 dihydropyrimidinase can also form a tetramer, the residues being crucial for tetramerization are different from those in *Thermus* sp. dihydropyrimidinases.

2. Materials and Methods

2.1. Cloning, Protein Expression, and Purification. Construction of the *P. aeruginosa* dihydropyrimidinase expression plasmid has been reported [15]. Recombinant *P. aeruginosa* dihydropyrimidinase was expressed and purified using the protocol described previously [15]. The protein purified from the soluble supernatant by Ni^{2+}-affinity chromatography (HiTrap HP; GE Healthcare Bio-Sciences, Piscataway, NJ, USA) was eluted with Buffer A (20 mM Tris-HCl, 250 mM imidazole, and 0.5 M NaCl, pH 7.9) and dialyzed against a dialysis buffer (20 mM HEPES and 100 mM NaCl, pH 7.0; Buffer B). Protein purity remained > 97% as determined by SDS-PAGE (Mini-PROTEAN Tetra System; Bio-Rad, CA, USA).

2.2. Gel Filtration Chromatography. Gel filtration chromatography was carried out by the AKTA-FPLC system (GE Healthcare Bio-Sciences, Piscataway, NJ, USA). In brief, purified protein (5 mg/mL) in Buffer C (20 mM MES and 100 mM NaCl, pH 5.9) was applied to a Superdex 200 prep grade column (GE Healthcare Bio-Sciences, Piscataway, NJ, USA) equilibrated with the same buffer [29]. The column was operated at a flow rate of 0.5 mL/min, and the proteins were detected at 280 nm. The column was calibrated with proteins of known molecular weight: thyroglobulin (670 kDa), γ-globulin (158 kDa), ovalbumin (44 kDa), myoglobin (17 kDa), and vitamin B_{12} (1.35 kDa).

Table 1: Data collection and refinement statistics.

Data collection	
Crystal	*P. aeruginosa* dihydropyrimidinase
Wavelength (Å)	0.975
Resolution (Å)	30–2.17
Space group	$C222_1$
Cell dimension (Å)	$a = 108.9$, $\alpha = 90$ $b = 155.7$, $\beta = 90$ $c = 235.6$, $\gamma = 120$
Completeness (%)	99.8 (100)*
$<I/\sigma I>$	15.13 (3.7)
R_{sym} or R_{merge} (%)	0.122 (0.599)
Redundancy	7.1 (7.3)
Refinement	
Resolution (Å)	30–2.17
Number of reflections	100197
R_{work}/R_{free}	0.1759/0.2312
Number of atoms	
Protein	1912
Water	312
RMS deviation	
Bond lengths (Å)	0.0151
Bond angles (°)	1.6495
Ramachandran plot	
In preferred regions	1345 (94.19%)
In allowed regions	68 (4.76%)
Outliers	15 (1.05%)
PDB entry	5YKD

*Values in parentheses are for the highest resolution shell.

2.3. Crystallography. Before crystallization, *P. aeruginosa* dihydropyrimidinase was concentrated to 20 mg/mL in Buffer C. Crystals were grown at room temperature by hanging drop vapor diffusion in 10% PEG 8000, 100 mM HEPES, 200 mM calcium acetate, pH 5.9. Data collection and refinement statistics for the crystal of *P. aeruginosa* dihydropyrimidinase are shown in Table 1. Data were collected using an ADSC Quantum-315r CCD area detector at SPXF beamline BL13C1 at NSRRC (Taiwan, ROC). All data integration and scaling were carried out using HKL-2000 [30]. There were four *P. aeruginosa* dihydropyrimidinase monomers per asymmetric unit. The crystal structure of *P. aeruginosa* dihydropyrimidinase was solved at 2.17 Å resolution with the molecular replacement software AMoRe [31] using the dihydropyrimidinase (PDB entry 5E5C) [28] as

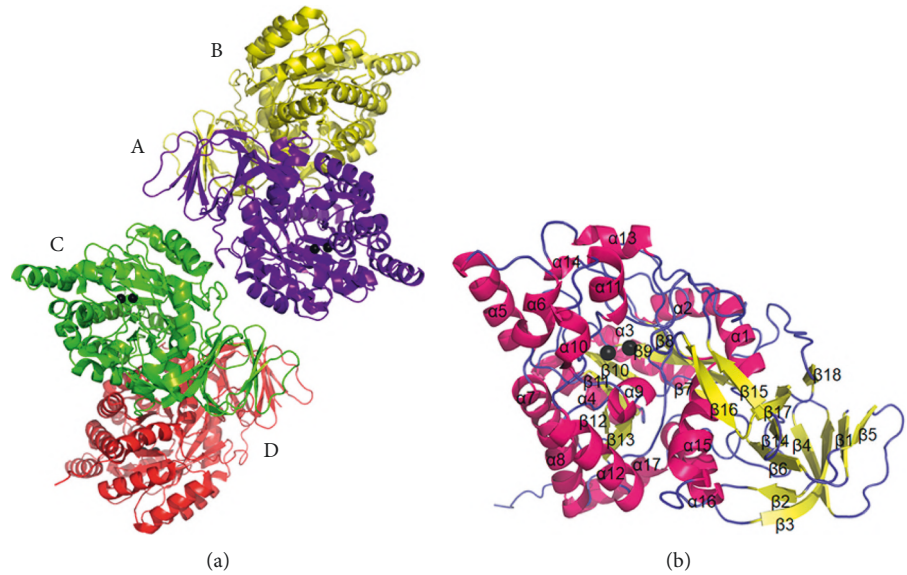

(a) (b)

Figure 2: Crystal structure of *P. aeruginosa* dihydropyrimidinase. (a) Ribbon diagram of a *P. aeruginosa* dihydropyrimidinase tetramer. Each *P. aeruginosa* dihydropyrimidinase monomer is color-coded. Two zinc ions in the active site are presented as black spheres. (b) Ribbon diagram of a *P. aeruginosa* dihydropyrimidinase monomer with the secondary structures labeled.

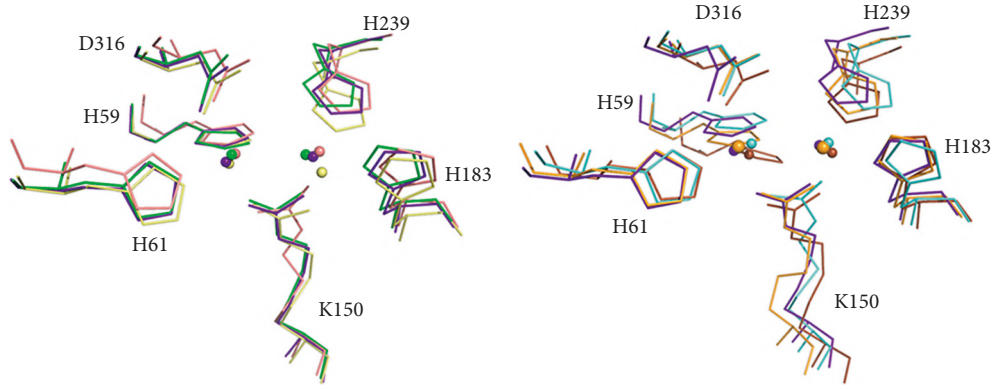

(a) (b)

Figure 3: Structural comparison. (a) Superposition of the active site of dihydropyrimidinases. Their active sites contain four histidines, one aspartate, and one carboxylated lysine residue, which are required for metal binding and catalytic activity. Dihydropyrimidinases from *P. aeruginosa* (PDB entry 5E5C; green), *Thermus* sp. (PDB entry 1GKQ; salmon), *Tetraodon nigroviridis* (PDB entry 4H01; pale yellow), and the structure (PDB entry 5YKD; purple blue) in this study are shown. The architecture of these active sites is similar. (b) Superposition of the active site of members of the amidohydrolase family. Their active sites contain four histidines, one aspartate, and one carboxylated lysine residue, which are required for metal binding and catalytic activity. *P. aeruginosa* dihydropyrimidinase (PDB entry 5YKD; purple blue), *Escherichia coli* allantoinase (PDB entry 3E74; bright orange), *Burkholderia pickettii* hydantoinase (PDB entry 1NFG; aquamarine), and *E. coli* dihydroorotase (PDB entry 1J79; brown) are shown. The architecture of these active sites is similar.

model. After molecular replacement, model building was carried out using XtalView [32]. CNS was used for molecular dynamics refinement [33]. The final structure was refined to an R-factor of 0.1759 and an R_{free} of 0.2312. Atomic coordinates and related structural factors have been deposited in the PDB with accession code 5YKD.

3. Results and Discussion

3.1. Structure of the P. aeruginosa Dihydropyrimidinase Monomer. Crystals of *P. aeruginosa* dihydropyrimidinase were grown at room temperature by hanging drop vapor diffusion in 10% PEG 8000, 100 mM HEPES, 200 mM calcium acetate, pH 5.9. The crystals of *P. aeruginosa* dihydropyrimidinase grown under this condition belonged to space group $C222_1$ with cell dimensions of $a = 108.9$, $b = 155.7$, and $c = 235.6$ Å. The crystal structure of *P. aeruginosa* dihydropyrimidinase was solved at 2.17 Å resolution (Table 1). The unit cell contained eight molecules. An asymmetric unit of the crystal contained four crystallographically independent *P. aeruginosa* dihydropyrimidinase monomers, in which two zinc ions were found in the active site per

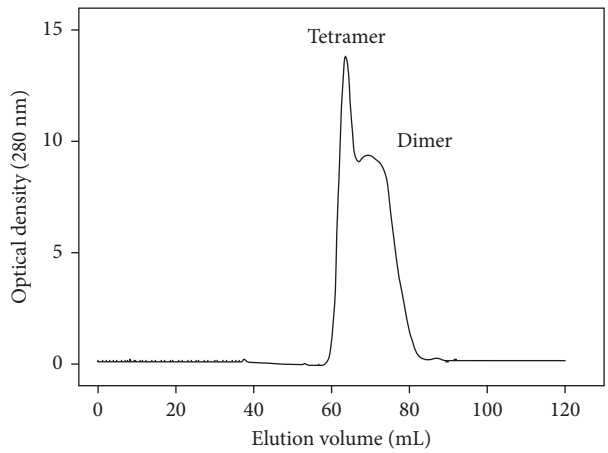

Figure 4: Gel filtration chromatographic analysis. Gel filtration chromatography was carried out by the AKTA-FPLC system in Buffer C (20 mM MES and 100 mM NaCl, pH 5.9). The corresponding peaks show the eluting *P. aeruginosa* dihydropyrimidinase. The column was calibrated with proteins of known molecular weight: thyroglobulin (670 kDa), γ-globulin (158 kDa), ovalbumin (44 kDa), myoglobin (17 kDa), and vitamin B_{12} (1.35 kDa).

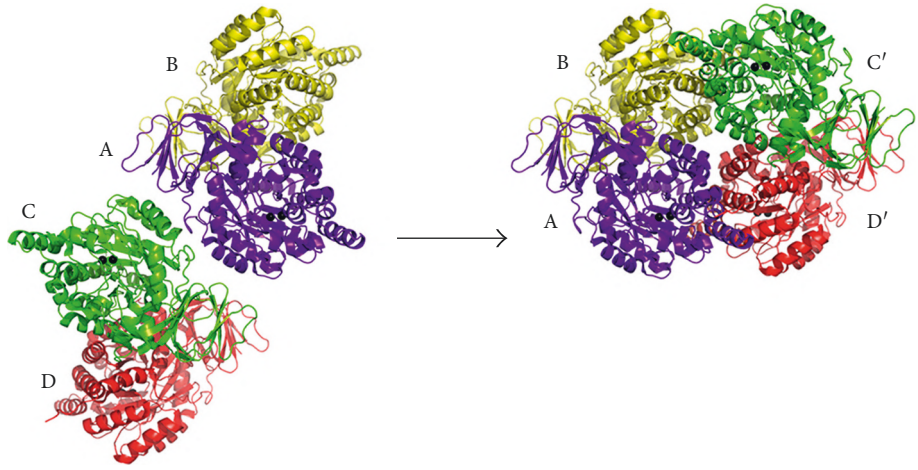

Figure 5: The structure of *P. aeruginosa* dihydropyrimidinase tetramer. An asymmetric unit contains four crystallographically independent *P. aeruginosa* dihydropyrimidinase monomers B-A-C-D. Crystallographically related tetramer B-A-C′-D′ was formed and further stabilized via many hydrogen bonds and salt bridges. This tetramerization structure was similar to that of *Thermus* sp. dihydropyrimidinase (PDB entry 1GKQ).

monomer (Figure 2(a)). The majority of the electron density for *P. aeruginosa* dihydropyrimidinase exhibited good quality, and no discontinuity was observed. Briefly, the overall structure of each *P. aeruginosa* dihydropyrimidinase unit consists of 17 α-helices, 19 β-sheets, and two zinc ions (Figure 2(b)). At pH 5.9, the architecture of the *P. aeruginosa* dihydropyrimidinase monomer consists of two domains, namely, a large domain with a classic $(\beta/\alpha)_8$-barrel structure core embedding the catalytic dimetal center and a small β-sandwich domain.

3.2. Structural Comparison. The overall structure and architecture of the active site of *P. aeruginosa* dihydropyrimidinase are similar to those of other dihydropyrimidinases (Figure 3(a)) and other members of the amidohydrolase family of enzymes, such as hydantoinases, dihydroorotases, and allantoinases (Figure 3(b)). The active sites of these enzymes contain four histidines, one aspartate, and one carboxylated lysine residue, which are required for metal binding and catalytic activity [12, 14, 15, 19, 20, 34, 35].

3.3. pH-Dependent Oligomerization of P. aeruginosa Dihydropyrimidinase. It was noted that the crystals of the dimeric *P. aeruginosa* dihydropyrimidinase belonged to space group $P3_121$ grown at the condition of 28% PEG 6000, 100 mM HEPES, 200 mM lithium acetate, pH 7.5 [28]. Due to the different crystallization condition, we attempted to test whether the oligomerization of *P. aeruginosa* dihydropyrimidinase is pH-dependent. All known dihydropyrimidinases are tetramers. However, pseudomonal dihydropyrimidinase/hydantoinase forms a dimer at neutral pH [26–28]. Given that the structure implies that

Table 2: The formation of hydrogen bonds at the dimer-dimer interface of *P. aeruginosa* dihydropyrimidinase.

Subunit 1	Distance [Å]	Subunit 2
A: K374 [NZ]	3.00	B: E14 [OE1]
A: H13 [NE2]	2.88	B: E14 [OE1]
A: R386 [NH2]	3.86	B: E14 [OE2]
A: R386 [NH1]	2.81	B: E15 [OE2]
A: R386 [NH2]	2.83	B: E15 [OE2]
A: R468 [NH2]	3.61	B: Q306 [OE1]
A: R253 [NH1]	3.27	B: S307 [O]
A: R253 [NH2]	3.13	B: S307 [O]
A: R467 [NH1]	2.92	B: V354 [O]
A: R468 [NE]	2.95	B: G357 [O]
A: R468 [NH2]	3.09	B: G357 [O]
A: R468 [NH2]	3.40	B: R358 [O]
A: R467 [NH1]	3.24	B: L359 [O]
A: E14 [OE1]	3.09	B: K374 [NZ]
A: E14 [OE1]	2.47	B: H13 [NE2]
A: E15 [OE2]	2.70	B: R386 [NH1]
A: S307 [O]	3.30	B: R253 [NH1]
A: S307 [O]	3.55	B: R253 [NH2]
A: V354 [O]	2.91	B: R467 [NH1]
A: G357 [O]	2.94	B: R468 [NH2]
A: G357 [O]	2.94	B: R468 [NE]
A: R358 [O]	3.56	B: R468 [NH2]
A: L359 [O]	3.16	B: R467 [NH1]
C′: H13 [NE2]	2.79	D′: E14 [OE1]
C′: K374 [NZ]	3.25	D′: E14 [OE1]
C′: R386 [NH1]	2.85	D′: E15 [OE1]
C′: R386 [NH2]	2.59	D′: E15 [OE2]
C′: R468 [NH2]	3.26	D′: Q306 [OE1]
C′: R253 [NH1]	3.13	D′: S307 [O]
C′: R253 [NH2]	3.16	D′: S307 [O]
C′: R468 [NE]	2.71	D′: G357 [O]
C′: R468 [NH2]	3.11	D′: R358 [O]
C′: E14 [OE1]	2.88	D′: H13 [NE2]
C′: E14 [OE1]	2.89	D′: K374 [NZ]
C′: E15 [OE2]	2.88	D′: R386 [NH1]
C′: E15 [OE2]	2.73	D′: R386 [NH2]
C′: Q306 [OE1]	3.53	D′: R468 [NH2]
C′: S307 [O]	3.21	D′: R253 [NH1]
C′: S307 [O]	3.59	D′: R253 [NH2]
C′: G357 [O]	2.65	D′: R468 [NE]
C′: R358 [O]	3.33	D′: R468 [NH2]

Table 3: The formation of salt bridges at the dimer-dimer interface of *P. aeruginosa* dihydropyrimidinase.

Subunit 1	Distance [Å]	Subunit 2
A: K374 [NZ]	3.00	B: E14 [OE1]
A: H13 [NE2]	2.88	B: E14 [OE1]
A: R386 [NH2]	3.86	B: E14 [OE2]
A: H13 [NE2]	3.75	B: E14 [OE2]
A: R386 [NH1]	3.55	B: E15 [OE1]
A: R386 [NH1]	2.81	B: E15 [OE2]
A: R386 [NH2]	2.83	B: E15 [OE2]
A: E14 [OE1]	3.09	B: K374 [NZ]
A: E14 [OE1]	2.47	B: H13 [NE2]
A: E14 [OE2]	3.93	B: H13 [NE2]
A: E15 [OE1]	3.69	B: R386 [NH1]
A: E15 [OE2]	3.00	B: R386 [NH2]
A: E15 [OE2]	2.70	B: R386 [NH1]
C′: H13 [NE2]	2.79	D′: E14 [OE1]
C′: K374 [NZ]	3.25	D′: E14 [OE1]
C′: H13 [NE2]	3.86	D′: E14 [OE2]
C′: R386 [NH1]	2.85	D′: E15 [OE1]
C′: R386 [NH2]	3.84	D′: E15 [OE1]
C′: R386 [NH1]	2.96	D′: E15 [OE2]
C′: R386 [NH2]	2.59	D′: E15 [OE2]
C′: E14 [OE1]	2.88	D′: H13 [NE2]
C′: E14 [OE1]	2.89	D′: K374 [NZ]
C′: E14 [OE2]	3.78	D′: H13 [NE2]
C′: E15 [OE1]	3.34	D′: R386 [NH1]
C′: E15 [OE2]	2.88	D′: R386 [NH1]
C′: E15 [OE2]	2.73	D′: R386 [NH2]

P. aeruginosa dihydropyrimidinase may also form a tetramer in the crystalline state at pH 5.9 (Figure 2(a)), we performed biochemical verification to confirm the oligomerization state. To confirm whether or not the oligomerization of *P. aeruginosa* dihydropyrimidinase is pH-dependent, we conducted gel filtration chromatography at pH 5.9. As shown in Figure 4, the results revealed that two species with elution volume of 63.25 and 69. 26 mL did coexist. The molecular mass of a *P. aeruginosa* dihydropyrimidinase monomer, as calculated from the amino acid sequence, is 53 kDa. Assuming that these two forms of *P. aeruginosa* dihydropyrimidinase have a shape and partial specific volume similar to the standard proteins, the native molecular masses of *P. aeruginosa* dihydropyrimidinase were estimated to be 105 and 180 kDa, approximately 1.9 and 3.5 times the molecular mass of a *P. aeruginosa* dihydropyrimidinase monomer, respectively. In comparison at pH 7.5, gel filtration chromatographic analysis of *P. aeruginosa* dihydropyrimidinase revealed a single peak; the native molecular mass was estimated to be 117 kDa [28]. The two forms of this enzyme obtained from the gel filtration chromatography at pH 5.9 had similar specific activity (data not shown). Thus, *P. aeruginosa* dihydropyrimidinase did exist as a mixture of dimers and tetramers at pH 5.9.

3.4. Structural Insights into Dimer of Dimer (Tetramer) Formation of Dihydropyrimidinase. In this study, we have identified that *P. aeruginosa* dihydropyrimidinase did exist as a mixture of dimers and tetramers at pH 5.9. To assess how *P. aeruginosa* dihydropyrimidinase can form a stable tetramer, the dimer-dimer interface was analyzed. In the

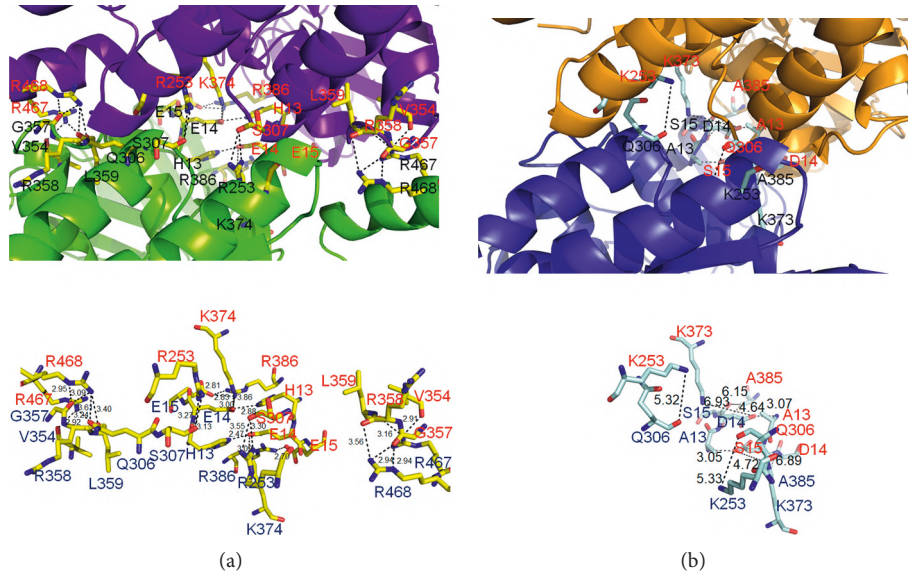

Figure 6: Comparison of the tetrameric structures of *Thermus* sp. dihydropyrimidinase and *P. aeruginosa* dihydropyrimidinase. (a) Structural analysis of the dimer-dimer interface of *P. aeruginosa* dihydropyrimidinase. The distance (Å) of the residues is shown. (b) Many residues crucial for forming hydrogen bonds at the dimer-dimer interface of *P. aeruginosa* dihydropyrimidinase were not found in the dimer-dimer interface of *Thermus* sp. dihydropyrimidinase.

```
MSLLIRGATVVTHEESYRADVLCANGLIQAIGENLETPSGCDVLDGGGQYLMPGGIDPHT  60
MPLLIKNGEIITADSRYKADIYAEGETITRIGQNLEAPPGTEVIDATGKYVFPGFIDPHV  60

HMQLPFMGTVASEDFFSGTAAGLAGGTTSIIDFVIPNPRQSLLEAFHTWRGWAQ-KSAAD 119
HIYLPFMATFAKDTHETGSKAALMGGTTTYIEMCCPSRNDDALEGYQLWKSKAEGNSYCD 120

YGFHVAITWWSDEVAREMGELVAQHGVNSFKHFMAYKNAIMAADDTLVASFERCLELGAV 179
YTFHMAVSKFDEKTEGQLREIVAD-GISSFKIFLSYKNFFGVDDGEMYQTLRLAKELGVI 179

PTVHAENGELVFHLQQKLLAQGLTGPEAHPLSRPPQVEGEAASRAIRIAETLGTPLYLVH 239
VTAHCENAELVGRLQQKLLSEGKTGPEWHEPSRPEAVEAEGTARFATFLETTGATGYVVH 239

ISSREALDEIAYARAKGQPVYGEVLAGHLLLDDSVYRHPDWATAAGYVMSPPFRPVEHQE 299
LSCKPALDAAMAAKARGVPIYIESVIPHFLLDKT-YAERGGVEAMKYIMSPPLRDKRNQK 298

ALWRGLQSGNLHTTATDHCCFCAEQKAMGRDDFSKIPNGTAGIEDRMALLWDAGVNSGRL 359
VLWDALAQGFIDTVGTDHCPFDTEQKLLGKEAFTAIPNGIPAIEDRVNLLYTYGVSRGRL 358

SMHEFVALTSTNTAKIFNLFPRKGAIRVGADADLVLWDPQGSRTLSAATHHQRVDFNIFE 419
DIHRFVDAASTKAAKLFGLFPRKGTIAVGSDADLVVYDPQYRGTISVKTQHVNNDYNGFE 418

GRTVRGIPSHTISQGKLLWAAGDLRAEPGAGRYVER-PAYPSVYEVLGRRAERQRPVAVE 478
GFEIDGRPSVVTVRGKVAVRDGQFVGEKGWGKLLRREPMYF-------------------- 458

R   Pseudomonas aeruginosa PAO1                                   479
-   Thermus sp.
```

Figure 7: Sequence alignment of dihydropyrimidinases from *P. aeruginosa* and *Thermus* sp. The amino acids that are involved in dimer-dimer interface of *P. aeruginosa* and *Thermus* sp. dihydropyrimidinase are boxed, respectively.

crystal of *P. aeruginosa* dihydropyrimidinase, the four molecules formed two pairs of dimers, B-A and C-D, respectively (Figure 5). Since the two dimers of *P. aeruginosa* dihydropyrimidinase associate via few contacts to create the tetramer, it was thought that the tetrameric state may be possibly due to crystal packing forces. We noted that in the crystal, another crystallographically related tetramer B-A-C′-D′ (Figure 5) was formed and further stabilized via many

hydrogen bonds and salt bridges (Tables 2 and 3). This tetramerization structure was similar to that of *Thermus* sp. dihydropyrimidinase (PDB entry 1GKQ).

We also compared the residues important for tetramerization located at the B-A-C′-D′ dimer-dimer interface with those of *Thermus* sp. dihydropyrimidinase (Figure 6). Although their overall structures are similar, the important residues for tetramer (dimer B-C′ with dimer A-D′) formation are quite different. For the tetramer formation of *P. aeruginosa* dihydropyrimidinase, many hydrogen bonds with close distance were found: these bonds (<3 Å) include K374(A)–E14(B), H13(A)–E14(B), R386(A)–E14(B), R386 (A)–E15(B), R467(A)–V354(B), R468(A)–G357(B), E14(A)–H13(B), E15(A)–R386(B), V354(A)–R467(B), G357(A)–R468(B), H13(C′)–E14(D′), R386(C′)–E15(D′), R468(C′)–G357(D′), E14(C′)–H13(D′), E14(C′)–K374(D′), E15(C′)–R386(D′), and G357(C′)–R468(D′); however, these residues were not found for the tetramer formation of *Thermus* sp. dihydropyrimidinase (Figure 6). Only A13–D14 hydrogen bond was found in *Thermus* sp. dihydropyrimidinase (i.e., H13–E14 in *P. aeruginosa* dihydropyrimidinase). Thus, the dimer-dimer interface between *P. aeruginosa* dihydropyrimidinase and *Thermus* sp. dihydropyrimidinase was significantly different (Figure 7). Comparison by superimposition indicated that many Arg residues (R253, R358, R386, R467, and R468) found in *P. aeruginosa* dihydropyrimidinase, but not in *Thermus* sp. dihydropyrimidinase, may play a crucial role for the pH-dependent oligomerization. If consider the pK_a, a much better candidate is His13, which is involved in intermolecular interactions and, dependent on the environment of its side chain, which may easily change protonation state between pH 5.9 and pH 7.5. However, this speculation needs to be confirmed by further biochemical experiments.

3.5. Different Mechanisms for Tetramer Formation of Dihydropyrimidinases. In this study, we identified *P. aeruginosa* dihydropyrimidinase can be a tetramer both in the crystalline state and in solution (Figure 4). The structure of the tetrameric *Thermus* sp. dihydropyrimidinase and *P. aeruginosa* dihydropyrimidinase was compared (Figure 6). Many important residues for *Thermus* sp. dihydropyrimidinase tetramer formation are different from those for *P. aeruginosa* dihydropyrimidinase (Figure 7). On the basis of these results, we concluded that *P. aeruginosa* dihydropyrimidinase could form a tetramer, but its oligomerization mechanism differed from those of other dihydropyrimidinases such as *Thermus* sp. dihydropyrimidinase.

Conflicts of Interest

The authors declare that they have no conflicts of interest regarding the publication of this paper.

Acknowledgments

The authors thank the technical services provided by the Synchrotron Radiation Protein Crystallography Facility of the National Core Facility Program for Biotechnology, Ministry of Science and Technology, and the National Synchrotron Radiation Research Center, a national user facility supported by the Ministry of Science and Technology, Taiwan, ROC. This research was supported by a grant from the Ministry of Science and Technology, Taiwan (MOST 106-2320-B-040-004) to Cheng-Yang Huang.

References

[1] K. D. Schnackerz and D. Dobritzsch, "Amidohydrolases of the reductive pyrimidine catabolic pathway purification, characterization, structure, reaction mechanisms and enzyme deficiency," *Biochimica et Biophysica Acta*, vol. 1784, no. 3, pp. 431–444, 2008.

[2] D. P. Wallach and S. Grisolia, "The purification and properties of hydropyrimidine hydrase," *Journal of Biological Chemistry*, vol. 226, no. 1, pp. 277–288, 1957.

[3] C. C. Hsu, L. Y. Lu, and Y. S. Yang, "From sequence and structure of sulfotransferases and dihydropyrimidinases to an understanding of their mechanisms of action and function," *Expert Opinion on Drug Metabolism & Toxicology*, vol. 6, no. 5, pp. 591–601, 2010.

[4] C. Y. Huang and Y. S. Yang, "Discovery of a novel N-iminylamidase activity: substrate specificity, chemicoselectivity and catalytic mechanism," *Protein Expression and Purification*, vol. 40, no. 1, pp. 203–211, 2005.

[5] C. Y. Huang and Y. S. Yang, "A novel cold-adapted imidase from fish *Oreochromis niloticus* that catalyzes hydrolysis of maleimide," *Biochemical and Biophysical Research Communications*, vol. 312, no. 12, pp. 467–472, 2003.

[6] C. Y. Huang, S. K. Chiang, Y. S. Yang, and Y. J. Sun, "Crystallization and preliminary X-ray diffraction analysis of thermophilic imidase from pig liver," *Acta Crystallographica Section D Biological Crystallography*, vol. 59, no. 5, pp. 943–945, 2003.

[7] C. Y. Huang, Y. P. Chao, and Y. S. Yang, "Purification of industrial hydantoinase in one chromatographic step without affinity tag," *Protein Expression and Purification*, vol. 30, no. 1, pp. 134–139, 2003.

[8] C. Y. Huang and Y. S. Yang, "The role of metal on imide hydrolysis: metal content and pH profiles of metal ion-replaced mammalian imidase," *Biochemical and Biophysical Research Communications*, vol. 297, no. 4, pp. 1027–1032, 2002.

[9] Y. S. Yang, S. Ramaswamy, and W. B. Jakoby, "Rat liver imidase," *Journal of Biological Chemistry*, vol. 268, no. 15, pp. 10870–10875, 1993.

[10] H. E. Schoemaker, D. Mink, and M. G. Wubbolts, "Dispelling the myths–biocatalysis in industrial synthesis," *Science*, vol. 299, no. 5613, pp. 1694–1697, 2003.

[11] J. Altenbuchner, M. Siemann-Herzberg, and C. Syldatk, "Hydantoinases and related enzymes as biocatalysts for the synthesis of unnatural chiral amino acids," *Current Opinion in Biotechnology*, vol. 12, no. 6, pp. 559–563, 2001.

[12] C. Y. Huang, C. C. Hsu, M. C. Chen, and Y. S. Yang, "Effect of metal binding and posttranslational lysine carboxylation on the activity of recombinant hydantoinase," *Journal of Biological Inorganic Chemistry*, vol. 14, no. 1, pp. 111–121, 2009.

[13] S. M. Runser and P. C. Meyer, "Purification and biochemical characterization of the hydantoin hydrolyzing enzyme from Agrobacterium species. A hydantoinase with no 5,6-dihydropyrimidine amidohydrolase activity," *European Journal of Biochemistry*, vol. 213, no. 3, pp. 1315–1324, 1993.

[14] Z. Gojkovic, L. Rislund, B. Andersen et al., "Dihydropyrimidine amidohydrolases and dihydroorotases share the same origin and several enzymatic properties," *Nucleic Acids Research*, vol. 31, no. 6, pp. 1683–1692, 2003.

[15] C. Y. Huang, "Inhibition of a putative dihydropyrimidinase from *Pseudomonas aeruginosa* PAO1 by flavonoids and substrates of cyclic amidohydrolases," *PLoS One*, vol. 10, no. 5, Article ID e0127634, 2015.

[16] J. Abendroth, K. Niefind, and D. Schomburg, "X-ray structure of a dihydropyrimidinase from *Thermus* sp. at 1.3 A resolution," *Journal of Molecular Biology*, vol. 320, no. 1, pp. 143–156, 2002.

[17] L. Holm and C. Sander, "An evolutionary treasure: unification of a broad set of amidohydrolases related to urease," *Proteins: Structure, Function, and Genetics*, vol. 28, no. 1, pp. 72–82, 1997.

[18] W. F. Peng and C. Y. Huang, "Allantoinase and dihydroorotase binding and inhibition by flavonols and the substrates of cyclic amidohydrolases," *Biochimie*, vol. 101, pp. 113–122, 2014.

[19] C. C. Wang, H. W. Tsau, W. T. Chen, and C. Y. Huang, "Identification and characterization of a putative dihydroorotase KPN01074, from *Klebsiella pneumoniae*," *Protein Journal*, vol. 29, no. 6, pp. 445–452, 2010.

[20] Y. Y. Ho, Y. H. Huang, and C. Y. Huang, "Chemical rescue of the post-translationally carboxylated lysine mutant of allantoinase and dihydroorotase by metal ions and short-chain carboxylic acids," *Amino Acids*, vol. 44, no. 4, pp. 1181–1191, 2013.

[21] D. R. Evans and H. I. Guy, "Mammalian pyrimidine biosynthesis: fresh insights into an ancient pathway," *Journal of Biological Chemistry*, vol. 279, no. 32, pp. 33035–33038, 2004.

[22] Y. C. Hsieh, M. C. Chen, C. C. Hsu, S. I. Chan, Y. S. Yang, and C. J. Chen, "Crystal structures of vertebrate dihydropyrimidinase and complexes from *Tetraodon nigroviridis* with lysine carbamylation: metal and structural requirements for post-translational modification and function," *Journal of Biological Chemistry*, vol. 288, no. 42, pp. 30645–30658, 2013.

[23] V. Kumar, N. Saxena, M. Sarma, and K. V. Radha Kishan, "Carboxylated lysine is required for higher activities in hydantoinases," *Protein & Peptide Letters*, vol. 18, no. 7, pp. 663–669, 2011.

[24] S. Martinez-Rodriguez, A. I. Martinez-Gomez, J. M. Clemente-Jimenez et al., "Structure of dihydropyrimidinase from *Sinorhizobium meliloti* CECT4114: new features in an amidohydrolase family member," *Journal of Structural Biology*, vol. 169, pp. 200–208, 2010.

[25] B. Lohkamp, B. Andersen, J. Piskur, and D. Dobritzsch, "The crystal structures of dihydropyrimidinases reaffirm the close relationship between cyclic amidohydrolases and explain their substrate specificity," *Journal of Biological Chemistry*, vol. 281, no. 19, pp. 13762–13776, 2006.

[26] X. Y. Zhang, L. X. Niu, Y. W. Shi, and J. M. Yuan, "The flexibility of the non-conservative region at the C terminus of D-hydantoinase from Pseudomonas putida YZ-26 is extremely limited," *Applied Biochemistry and Biotechnology*, vol. 144, no. 3, pp. 237–247, 2008.

[27] L. Niu, X. Zhang, Y. Shi, and J. Yuan, "Subunit dissociation and stability alteration of D hydantoinase deleted at the terminal amino acid residue," *Biotechnology Letters*, vol. 29, no. 2, pp. 303–308, 2007.

[28] C. T. Tzeng, Y. H. Huang, and C. Y. Huang, "Crystal structure of dihydropyrimidinase from *Pseudomonas aeruginosa* PAO1: insights into the molecular basis of formation of a dimer," *Biochemical and Biophysical Research Communications*, vol. 478, no. 3, pp. 1449–1455, 2016.

[29] Y. H. Huang, Y. Lien, C. C. Huang, and C. Y. Huang, "Characterization of *Staphylococcus aureus* primosomal DnaD protein: highly conserved C-terminal region is crucial for ssDNA and PriA helicase binding but not for DnaA protein-binding and self-tetramerization," *PLoS One*, vol. 11, no. 6, Article ID e0157593, 2016.

[30] Z. Otwinowski and W. Minor, "Processing of X-ray diffraction data collected in oscillation mode," *Methods in Enzymology*, vol. 276, pp. 307–326, 1997.

[31] J. Navaza, "AMoRe: an automated package for molecular replacement," *Acta Crystallographica Section A Foundations of Crystallography*, vol. 50, no. 2, pp. 157–163, 1994.

[32] D. E. McRee, "XtalView/Xfit–A versatile program for manipulating atomic coordinates and electron density," *Journal of Structural Biology*, vol. 125, no. 2-3, pp. 156–165, 1999.

[33] A. T. Brunger, P. D. Adams, G. M. Clore et al., "Crystallography & NMR system: a new software suite for macromolecular structure determination," *Acta Crystallographica Section D Biological Crystallography*, vol. 54, no. 5, pp. 905–921, 1998.

[34] Y. H. Huang and C. Y. Huang, "Creation of a putative third metal binding site in type II dihydroorotases significantly enhances enzyme activity," *Protein & Peptide Letters*, vol. 22, no. 12, pp. 1117–1122, 2015.

[35] Y. Y. Ho, H. C. Hsieh, and C. Y. Huang, "Biochemical characterization of allantoinase from *Escherichia coli* BL21," *Protein Journal*, vol. 30, no. 6, pp. 384–394, 2011.

RSC Advances

PAPER

Cite this: *RSC Adv.*, 2018, **8**, 28367

Characterization of single-stranded DNA-binding protein SsbB from *Staphylococcus aureus*: SsbB cannot stimulate PriA helicase

Kuan-Lin Chen,[a] Jen-Hao Cheng,[a] Chih-Yang Lin,[ab] Yen-Hua Huang[a] and Cheng-Yang Huang *[ac]

Single-stranded DNA-binding proteins (SSBs) are essential to cells as they participate in DNA metabolic processes, such as DNA replication, repair, and recombination. The functions of SSBs have been studied extensively in *Escherichia coli*. Unlike *E. coli*, which contains only one type of SSB (EcSSB), some bacteria have more than one paralogous SSB. In *Staphylococcus aureus*, three SSBs are found, namely, SsbA, SaSsbB, and SsbC. While EcSSB can significantly stimulate EcPriA helicase, SaSsbA does not affect the SaPriA activity. It remains unclear whether SsbBs can participate in the PriA-directed DNA replication restart process. In this study, we characterized the properties of SaSsbBs through structural and functional analyses. Crystal structure of SaSsbB determined at 2.9 Å resolution (PDB entry 5YYU) revealed four OB folds in the N-terminal DNA-binding domain. DNA binding analysis using EMSA showed that SaSsbB binds to ssDNA with greater affinity than SaSsbA does. Gene map analysis demonstrated that *SAAV0835* encoding SaSsbB is flanked by unknown genes encoding hypothetical proteins, namely, putative Sipho_Gp157, ERF, and HNHc_6 gene products. Structure-based mutational analysis indicated that the four aromatic residues (Phe37, Phe48, Phe54, and Tyr82) in SaSsbB are at positions that structurally correspond to the important residues of EcSSB for binding to ssDNA and are also critical for SaSsbB to bind ssDNA. Similar to EcSSB and other SSBs such as SaSsbA and SaSsbC, SaSsbB also exhibited high thermostability. However, unlike EcSSB, which can stimulate EcPriA, SaSsbB did not affect the activity of SaPriA. Based on results in this study and previous works, we therefore established that SsbA and SsbB, as well as SsbC, do not stimulate PriA activity.

Received 23rd May 2018
Accepted 28th July 2018

DOI: 10.1039/c8ra04392b

rsc.li/rsc-advances

Introduction

Single-stranded DNA-binding proteins (SSBs) play crucial roles in DNA metabolic processes, such as DNA replication, repair, and recombination in prokaryotes and eukaryotes.[1,2] During these reactions, SSB is necessary to maintain the transient unwinding of duplex DNA in a single-stranded state.[3] SSB binds to ssDNA with high affinity in a sequence-independent manner. Bacterial SSBs are typically homotetramers, in which four oligonucleotide/oligosaccharide-binding folds (OB fold) form a DNA-binding domain. In additional to ssDNA, SSB also binds to many DNA metabolism proteins that constitute the SSB interactome.[4,5] The C-terminal acidic tail (DDDIPF) and the intrinsically disordered linker (IDL) of SSB are necessary to mediate protein–protein interactions.[4] The entire C-terminal domain of SSB is disordered even in the presence of ssDNA.[6]

The structure, DNA binding properties, and functions of SSB have been studied extensively in *Escherichia coli* (EcSSB).[7,8] EcSSB has three distinct DNA binding modes that are dependent on protein and salt concentrations in a solution.[9] ssDNA unwrapping analysis shows that EcSSB can diffuse along ssDNA in the different binding modes, indicating a highly dynamic complex.[10]

Several bacteria have two paralogous SSBs, namely, SsbA and SsbB.[11] Based on the sequence identity and the DNA binding properties, the third SSB (SsbC) is also identified in *Staphylococcus aureus*.[12] *S. aureus*, a Gram-positive pathogen, causes serious problems to public health worldwide.[13] Some SSB inhibitors as broad-spectrum antibacterial agents targeting *S. aureus* and other pathogens have been discovered.[12,14]

SsbA is referred to as a counterpart of EcSSB. SsbA and SsbB are essential for genome maintenance and transformational recombination, respectively.[15–18] Significant differences for SsbBs are found in their C-terminal sequences and DNA binding properties. In *Bacillus subtilis*, SsbB binds to ssDNA with lesser affinity than BsSsbA does.[17] However, *Streptomyces*

[a]*School of Biomedical Sciences, Chung Shan Medical University, No. 110, Sec. 1, Chien-Kuo N. Rd., Taichung City, Taiwan. E-mail: cyhuang@csmu.edu.tw; Tel: +886-4-24730022 ext. 11472*

[b]*School of Medicine, College of Medicine, Chung Shan Medical University, No. 110, Sec. 1, Chien-Kuo N. Rd., Taichung City, Taiwan*

[c]*Department of Medical Research, Chung Shan Medical University Hospital, No. 110, Sec. 1, Chien-Kuo N. Rd., Taichung City, Taiwan*

coelicolor SsbB (ScSsbB) exhibits greater DNA-binding affinity than ScSsbA does.[18] Unlike *Streptococcus pneumonia* SsbB (SpSsbB), BsSsbB and ScSsbB lack the C-terminal acidic tail of SSB for protein–protein interactions.[16–18] Thus, SsbBs from different organisms exhibit different protein–DNA and protein–protein interaction specificities.

PriA is a DEXH-type helicase used for replication restart in bacteria.[19–22] PriA is a poor helicase and needs some specific loading proteins to reload the replicative DnaB helicase back onto the chromosome. In *E. coli*, accessory proteins PriB and SSB are known to stimulate PriA helicase activity.[23,24] However, SaSsbA, a counterpart of EcSSB, does not trigger SaPriA.[25] Instead, SaDnaD is found to enhance the ATPase activity of SaPriA.[26] The manner by which SaSsbA and SaSsbB participate in SaPriA-directed primosome assembly and in DNA replication restart remains unclear.

SSB has mainly been studied in Gram-negative *E. coli*, and, to a lesser extent, in Gram-positive bacteria. Little is known about the fundamental function of SsbB for the assembly of the replication restart primosome. For instance, nothing is known whether or not SsbB can stimulate PriA helicase. Because of lacking experimental evidences, whether SsbB is thermostable and whether SsbB has the typical C-terminal acidic tail of SSB for protein–protein interactions also remain unclear. Whether PriB, an EcSSB-like ssDNA-binding protein lacking the C-terminal domain of SSB,[27–29] is a counterpart of SsbB still needs to be further elucidated.

In this study, we have cloned, expressed, purified, and biochemically characterized SaSsbB. We also have crystallized SaSsbB and determined its molecular structure. Unlike EcSSB, SsbB could not enhance PriA activity. Thus, we established that these three EcSSB-like proteins in *S. aureus* (SsbA, SsbB, and SsbC) do not stimulate PriA activity.

Experimental

Construction of plasmids for SaSsbA, SaSsbB, SaDnaD, and SaPriA expression

SaSsbA,[25] SaDnaD,[26] and SaPriA[30] expression plasmids have been constructed in other studies. *SAAV0835*, the gene encoding a putative SaSsbB, was amplified through PCR by using the genomic DNA of *S. aureus* subsp. *aureus* ED98 as a template. The primers used for the construction of the pET21-SaSsbB plasmid are summarized in Table 1.

Protein expression and purification

Recombinant SaSsbA,[25] SaDnaD,[26] and SaPriA[30] have been purified in other studies. Recombinant SaSsbB was expressed and purified in accordance with a previously described protocol for PriB.[27,28] In brief, *E. coli* BL21(DE3) cells were transformed with the expression vector, and the overexpression of the plasmids was induced by incubating with 1 mM isopropyl thio-galactopyranoside. The protein was purified from a soluble supernatant through Ni^{2+} affinity chromatography (HiTrap HP; GE Healthcare Bio-Sciences), eluted with Buffer A (20 mM Tris–HCl, 250 mM imidazole, and 0.5 M NaCl, pH 7.9) and dialyzed against a dialysis buffer (20 mM HEPES and 100 mM NaCl, pH 7.0; Buffer B). Protein purity remained at >97% as determined by SDS-PAGE (Mini-PROTEAN Tetra System; Bio-Rad, CA, USA).

Preparation of dsDNA substrate

The double-stranded DNA substrate (dsDNA) PS4/PS3-dT30 for ATPase assay was prepared at a 1 : 1 concentration ratio.[25,26] PS4/PS3-dT30 was formed in 20 mM HEPES (pH 7.0) and 100 mM NaCl by briefly heating at 95 °C for 5 min and by slowly cooling to room temperature overnight.

Electrophoretic mobility shift assay (EMSA)

EMSA for SaSsbB was conducted in accordance with a previously described protocol for SSB.[31] In brief, various lengths of ssDNA oligonucleotides were radiolabeled with [γ^{32}P] ATP (6000 Ci/mmol; PerkinElmer Life Sciences, Waltham, MA) and T4 polynucleotide kinase (Promega, Madison, WI, USA). The protein (0, 0.01, 0.02, 0.039, 0.078, 0.1563, 0.3125, 0.625, 1.25, and 2.5 μM; tetramer) was incubated for 30 min at 25 °C with 1.7 nM DNA substrates in a total volume of 10 μL in 20 mM Tris–HCl (pH 8.0) and 100 mM NaCl. Aliquots (5 μL) were removed from each of the reaction solutions and added to 2 μL of gel-loading solution (0.25% bromophenol blue and 40% sucrose). The resulting samples were resolved on 8% native polyacrylamide gel at 4 °C in TBE buffer (89 mM Tris borate and

Table 1 Primers used for construction of plasmids[a]

Oligonucleotide	Primer
SaSsbB-NdeI-N	GGGCATATGTTAAACAGAGTAGTTTTAGTA
SaSsbB-XhoI-C	GGGCTCGAGGAACGGGAGGTCTGAAAAATC
SaSsbB(F37A)-N	ACATTAGCAGTAAACAGAACAGCCACGAATGCTCAA
SaSsbB(F37A)-C	CTCGCCTTGAGCATTCGTGGCTGTTCTGTTTACTGC
SaSsbB(F48A)-N	GGCGAGCGTGAAGCAGAGCTTATAAACGTAGTAGTGTTC
SaSsbB(F48A)-C	GAACACTACTACGTTTATAAGCTCTGCTTCACGCTCGCC
SaSsbB(F54A)-N	TTTATAAACGTAGTAGTGGCCAAAAAACAAGCTGAAAAC
SaSsbB(F54A)-C	TTCAGCTTGTTTTTTGGCCACTACTACGTTTATAAAATC
SaSsbB(Y82A)-N	CGACTACAAACACGTAACGCCGAAAACAAAGACGGGCAA
SaSsbB(Y82A)-C	TTGCCCGTCTTTGTTTTCGGCGTTACGTGTTTGTAGTCG

[a] These plasmids were verified by DNA sequencing. Underlined nucleotides indicate the designated site for the restriction site or the mutation site.

1 mM EDTA) for 1 h at 100 V and visualized through phosphorimaging. A phosphor storage plate was scanned, and data regarding complex and free DNA bands were digitized for quantitative analysis. The ssDNA binding ability of the protein was estimated through linear interpolation from the concentration of the protein that bound 50% of the input DNA.

ATPase assay

SaPriA ATPase assay[25,26] was performed with 0.4 mM [γ-^{32}P] ATP and 0.12 μM SaPriA in a reaction buffer containing 40 mM Tris (pH 8.0), 10 mM NaCl, 2 mM DTT, 2.5 mM $MgCl_2$, and 0.1 μM PS4/PS3-dT30 DNA substrate. Aliquots (5 μL) were taken and spotted onto a polyethyleneimine cellulose thin-layer chromatography plate, which was subsequently developed in 0.5 M formic acid and 0.25 M LiCl for 30 min. Reaction products were visualized by autoradiography and quantified with a phosphorimager.

Site-directed mutagenesis

SaSsbB mutants were generated with a QuikChange Site-Directed Mutagenesis kit in accordance with the manufacturer's protocol (Stratagene, LaJolla, CA, USA) by using the primers (Table 1) and the wild-type plasmid pET21b-SaSsbB as the template. The presence of mutation was verified through DNA sequencing.

Bioinformatics

The amino acid sequences of 150 sequenced SSB homologs were aligned using ConSurf,[32] and the structures were visualized by using PyMol.

Crystallography

Before crystallization was performed, SaSsbB was concentrated to 15 mg mL^{-1} in Buffer B. Crystals were grown at room temperature through hanging drop vapor diffusion in 30% PEG 4000, 100 mM Tris, and 200 mM sodium acetate at pH 8.5. Data were collected with an ADSC Quantum-315r CCD area detector at SPXF beamline BL13C1 at NSRRC (Taiwan, ROC). Data were integrated and scaled with HKL-2000.[33] Four SaSsbB monomers per asymmetric unit were present. The crystal structure of SaSsbB was determined at 2.98 Å resolution with the molecular replacement software Phaser-MR[34] by using SaSsbA as a model (PDB entry 5XGT).[25] A model was built and refined with PHENIX[35] and Coot.[36] The final structure was refined to *R*-factor of 0.2139 and R_{free} of 0.2995. The atomic coordinates and related structure factors have been deposited in the PDB with the accession code 5YYU.

Results and discussion

Sequence analysis of SaSsbB

SAAV0835, which encodes SaSsbB of 141 aa, was found on the basis of the nucleotide sequence similar to BsSsbB and EcSSB. The amino acid sequence of SaSsbB shared 36% identity to that of SaSsbA. The ConSurf analysis reveals that the C-terminal region of SaSsbB was variable (Fig. 1). Like EcSSB, SaSsbB also had a long flexible region, but its flexible region was composed of few proline and glycine residues. SaSsbB (109–141 aa) had one Gly residue and two Pro residues (Fig. 1), which are significantly less than those of EcSSB (116–178 aa; 15 Gly residues and 10 Pro residues). In addition, SaSsbB did not have a C-terminal acidic peptide tail. The C-terminal acidic tail DDDIPF in EcSSB involved in protein–protein interactions was FSDLPF in SaSsbB.

Analysis of *ssb* (*SAAV0835*)

Fig. 2 shows the gene map of *S. aureus* chromosomal region with the *ssb* gene *SAAV0835*, which is flanked by unknown genes encoding hypothetical proteins with similarity to Sipho_Gp157, ERF, and HNHc_6. Unlike *E. coli*, which contains one type of SSB, *S. aureus* have three paralogous SSBs (SsbA, SsbB, and SsbC).[12] The gene map analyses of *ssb* show significant differences.[12,25] Unlike EcSSB located adjacent to *uvrA*, SaSsbA is flanked by *rpsF* and *rpsR*,[25] which encode the ribosomal proteins S6 and S18, respectively. SaSsbC is flanked by the putative *SceD*, the putative *YwpF*, and *fabZ* genes, which code for a transglycosylase, a hypothetical protein, and a β-hydroxyacyl-ACP dehydratase, respectively.[12] The gene regulation for SaSsbB is still unknown. Given that SsbB is essential for transformational recombination, these function-undetermined genes (Fig. 2) in *S. aureus* may be regulated with SaSsbB in a single signaling control and may be also involved in transformational recombination. However, this hypothesized relationship must be further confirmed by a detailed transcription analysis.

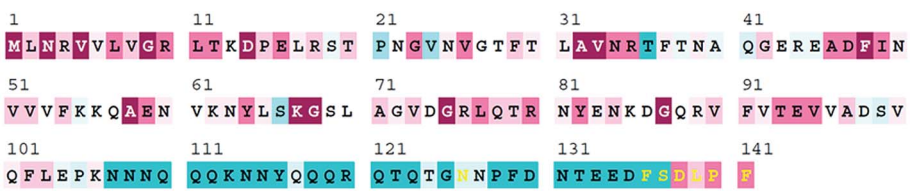

Fig. 1 Sequence analysis of SaSsbB. An alignment consensus of 150 sequenced SSB homologs by ConSurf reveals the degree of variability at each position along the primary sequence. Highly variable amino acid residues are colored teal, whereas highly conserved amino acid residues are burgundy. A consensus sequence was established by determining the most commonly found amino acid residue at each position relative to the primary sequence of SaSsbB.

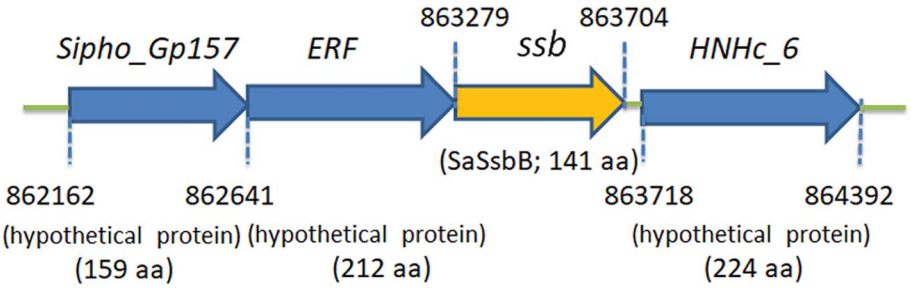

Fig. 2 Gene map of *S. aureus* chromosomal region with the *ssb* gene *SAAV0835*. The gene *SAAV0835* coding for SaSsbB maps from the 863279 to 863704 nt of the *S. aureus* genome. This *ssb* gene is flanked by unknown genes encoding hypothetical proteins, namely, the putative gene products similar to Sipho_Gp157, ERF, and HNHc_6.

SaSsbB bound to ssDNA

We studied the binding of purified SaSsbB (Fig. 3) to ssDNA (dT15-40) at various protein concentrations by using EMSA. To compare the DNA-binding abilities of SaSsbB, we quantified $[\text{Protein}]_{50}$ through linear interpolation from the protein concentration (Fig. 4 and Table 2). The binding ability of SaSsbB to dT40 in the presence of 0.4 M NaCl was also analyzed (Fig. 4). $[\text{SaSsbB}]_{50}$ of dT40 binding was 90 ± 4 nM, which was about fourfold lower than that in the presence of 0.4 M NaCl (382 ± 16 nM). Thus, the binding ability of SaSsbB to ssDNA is salt-dependent. Under the condition, only one band shift was found for dT20-60 (Fig. 5).

Stimulation of the ATPase activity of SaPriA by SaSsbB

To date, it remains unclear whether SsbB can stimulate the activity of the primosomal protein PriA. To investigate the possible effect of SaSsbB, we performed an ATPase assay for SaPriA. SaDnaD,[26] which stimulates the SaPriA activity, was used as a positive control. In contrast to SaDnaD,[26] we found that the ATPase activity of SaPriA in the presence of SaSsbB was not changed (Fig. 6). Given that the C-terminal domain of SsbB did not contain the acidic tail (Fig. 1), SsbB may not bind to PriA. Thus, no stimulation occurred (Fig. 6).

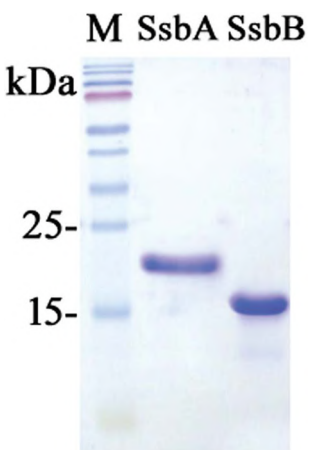

Fig. 3 Coomassie Blue-stained SDS-PAGE (15%) of the purified SaSsbA, SaSsbB, and molecular mass standards. The sizes of the standard proteins, from the top down, are as follows: 170, 130, 100, 70, 55, 40, 35, 25, and 15 kDa.

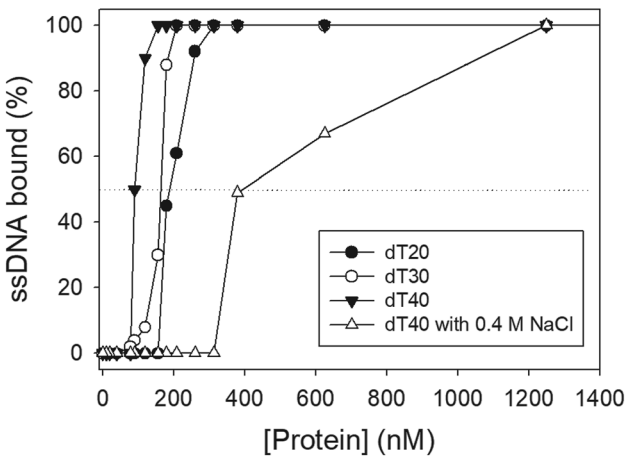

Fig. 4 ssDNA binding of SaSsbB. Protein was incubated at 25 °C for 30 min with ssDNA in a total volume of 10 μL in 20 mM Tris–HCl (pH 8.0) and 100 mM NaCl. The $[\text{Protein}]_{50}$ values of SaSsbB as a function of the length of the ssDNA were determined using EMSA.

Crystal structure of SaSsbB

In this study, we have shown that unlike EcSSB, SaSsbB did not contain the C-terminal acidic peptide and could not stimulate SaPriA helicase. To deeply understand the structure–function relationship of SaSsbB, we crystallized SaSsbB through hanging

Table 2 The $[\text{Protein}]_{50}$ values of SaSsbB as analyzed by EMSA[a]

DNA	$[\text{Protein}]_{50}$ (nM)
dT15	>2000
dT20	190 ± 8
dT30	164 ± 7
dT40	90 ± 4
dT40 (with 0.4 M NaCl)	382 ± 16

[a] $[\text{Protein}]_{50}$ was calculated from the titration curves of EMSA by determining the concentration of the protein needed to achieve the midpoint value for input DNA binding. Errors are standard deviations determined by three independent titration experiments.

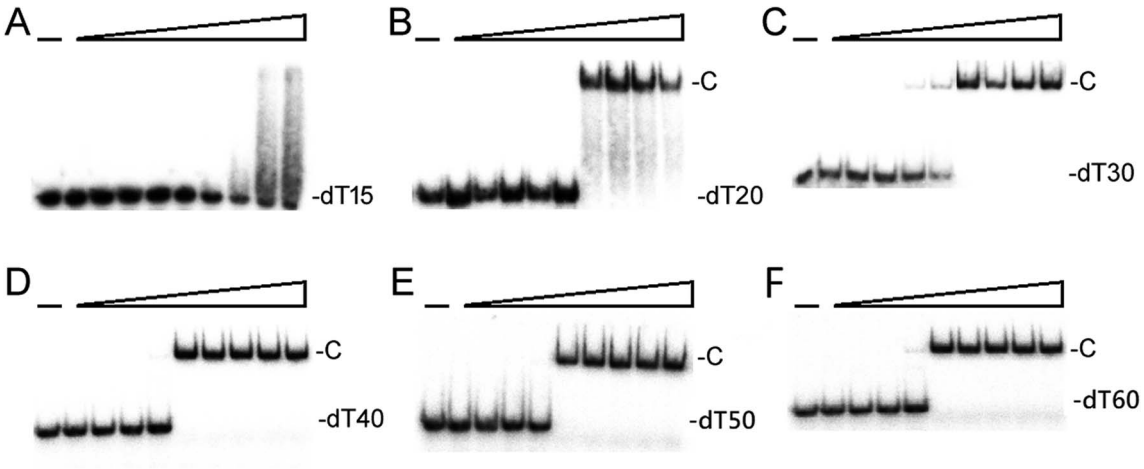

Fig. 5 EMSA of SaSsbB. Protein (0, 0.01, 0.02, 0.039, 0.078, 0.1563, 0.3125, 0.625, 1.25, and 2.5 μM; tetramer) was incubated at 25 °C for 30 min with 1.7 nM of (A) dT15, (B) dT20, (C) dT30, (D) dT40, (E) dT50, or (F) dT60 in a total volume of 10 μL in 20 mM Tris–HCl (pH 8.0) and 100 mM NaCl. Only one band shift was found for these ssDNAs.

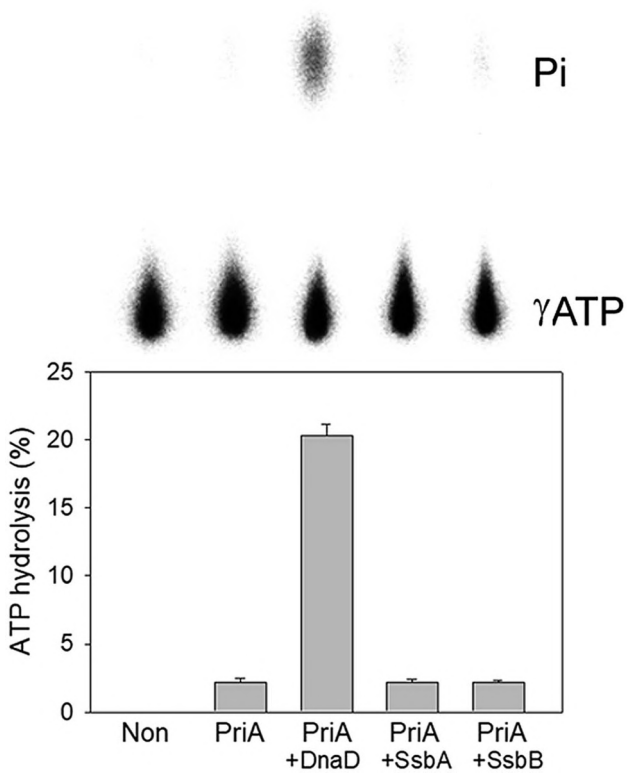

Fig. 6 The ATPase activity of SaPriA did not change when acting with SaSsbB. SaPriA ATPase assay was performed with 0.4 mM [γ-^{32}P] ATP, 0.12 μM of SaPriA, and 0.1 μM PS4/PS3-dT30 DNA substrate for 1 h. To study the effect, SaSsbA (10 μM), SaSsbB (10 μM), or SaDnaD (4 μM) was added into the assay solution. Reaction products were visualized by autoradiography and quantified with a phosphorimager.

Table 3 Data collection and refinement statistics

Data collection	
Crystal	SaSsbB
Wavelength (Å)	0.975
Resolution (Å)	30–2.98
Space group	$P2_12_12_1$
Cell dimension (Å)	$a = 63.99$, $\alpha = 90$ $b = 84.74$, $\beta = 90$ $c = 84.86$, $\gamma = 90$
Completeness (%)	99.8 (99.8)[a]
$\langle I/\sigma I \rangle$	13 (2.5)
R_{sym} or R_{merge} (%)[b]	0.125 (0.541)
Redundancy	3.8 (4.0)
Refinement	
Resolution (Å)	30–2.98
No. reflections	9334
R_{work}/R_{free}	0.2139/0.2995
No. atoms	
Protein	399
Water	16
R.m.s deviation	
Bond lengths (Å)	0.011
Bond angles (°)	1.385
Ramachandran plot	
In preferred regions	359 (93.25%)
In allowed regions	20 (5.19%)
Outliers	6 (1.56%)
PDB entry	5YYU

[a] Values in parentheses are for the highest resolution shell. [b] $R_{sym} = \Sigma|I - 'I'|/\Sigma I$, where I is the observed intensity, 'I' is the statistically weighted average intensity of multiple observations of symmetry-related reflections.

drop vapor diffusion and determined its structure at a resolution of 2.98 Å (Table 3). The secondary structural element of SaSsbB is similar to that of SaSsbA (Fig. 7A). The amino acids 107–141 in SaSsbB ternary structure were not observed. Consistent with the result from gel filtration analysis (data not shown), four monomers of SaSsbB per asymmetric unit were present (Fig. 7B). The SaSsbB monomer has an OB-fold domain similar to EcSSB, and the core of the OB-fold domain possesses a β-barrel capped with an α-helix. Unlike ScSSB, which contains

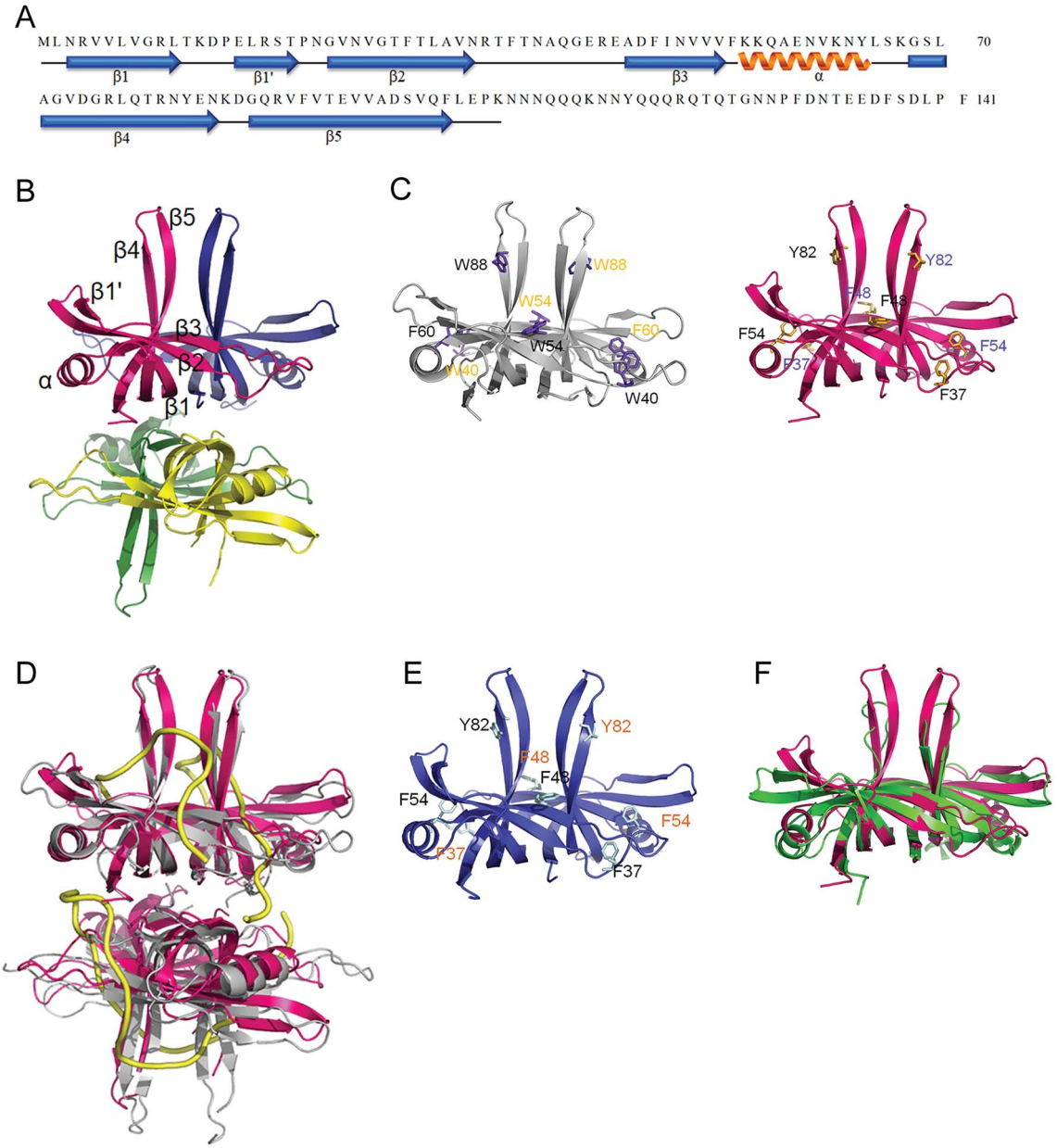

Fig. 7 Crystal structure of SaSsbB. (A) The secondary structural element of SaSsbB. The secondary structural element of SaSsbB is shown above its sequence. (B) Crystal structure of SaSsbB. Four monomers of SaSsbB per asymmetric unit were present. The entire C-terminal domain was disordered. (C) ssDNA-binding mode of SaSsbB. In the EcSSB–ssDNA complex (PDB entry 1EYG), Trp40, Trp54, Phe60, and Trp88 participated in ssDNA binding *via* stacking interactions. The corresponding residues in SaSsbB, namely, Phe37, Phe48, Phe54, and Tyr82, might play roles in ssDNA binding similar to those of EcSSB. For clarity, only a dimer of EcSSB and SaSsbB is shown. (D) Superposition of SaSsbB and EcSSB. The N-terminal domains of SaSsbB and EcSSB (gray) are similar. (E) Crystal structure of SaSsbA. The residues proposed for binding DNA in SaSsbB are also identical to those in SaSsbA. (F) Superposition of SaSsbB and KpPriB. The N-terminal domain of SaSsbB and KpPriB (PDB entry 4APV; green) are similar, in which the only significant difference is in the lengths of the β4 and β5 sheets.

an additional strand (β6),[18] SaSsbB does not contain β6. Additional β6 strands clamp two neighboring subunits together in a tetrameric SSB.[18] Thus, SsbBs from different organisms may exhibit different protein–DNA and protein–protein interaction specificities.

Trp40, Trp54, Phe60, and Trp88 in EcSSB participate in ssDNA binding *via* stacking interactions (Fig. 7C). Correspondingly, Phe37, Phe48, Phe54, and Tyr82 in SaSsbB might play roles in ssDNA binding (Fig. 7D). These residues proposed for binding DNA in SaSsbB were also identical to those in SaSsbA (Fig. 7E). SaSsbB structurally resembles PriB,[27,28] but significant differences in the lengths of β4- and β5-sheets were found (Fig. 7F).

Mutational analysis

According to crystal structure of SaSsbB, we speculated that Phe37, Phe48, Phe54, and Tyr82 in SaSsbB allow nucleic acids to

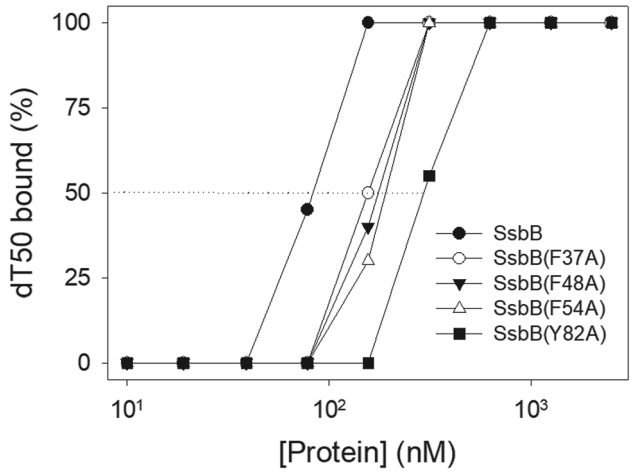

Fig. 8 Mutational analysis of SaSsbB for ssDNA binding. Binding of SaSsbB mutant protein (F37A, F48A, F54A, and Y82A) to dT50. The mutant protein was incubated with dT50. The phosphor storage plate was scanned, and the data for complex and free DNA bands were digitized for quantitative analysis.

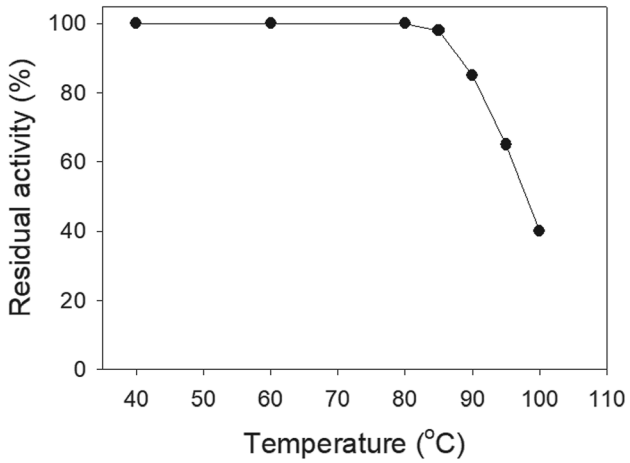

Fig. 9 The thermostability of SaSsbB. Protein (1 μM) was incubated at temperatures ranging from 40 °C to 100 °C for 30 min. The resultant protein solution was incubated at 25 °C for 30 min with dT30. The phosphor storage plate was scanned, and the data for complex and free DNA bands were digitized for quantitative analysis.

wrap around the whole SaSsbB. We constructed and analyzed alanine substitution mutants (*i.e.*, F37A, F48A, F54A, and Y82A) through EMSA (Fig. 8). Table 4 summarizes $[Protein]_{50}$ of the binding of these SaSsbB variants to dT50. These SaSsbB mutants have $[Protein]_{50}$ higher than that of the wild-type SaSsbB. The mutational effect on the ssDNA binding activity of SaSsbB followed the order Y82A > F54A > F48A > F37A. Structure-based mutational analysis indicated that SaSsbB might bind to ssDNA in a manner similar to that of EcSSB (Table 4).

Thermostability

SSB proteins have high thermostability.[37] SsbA and SsbC are highly thermostable.[12] It is still unknown whether SsbB has high thermostability. We performed indirect thermostability experiments (Fig. 9). The activity of SaSsbB incubated at 100 °C, 95 °C, 90 °C, and 85 °C for 30 min decreased by 60%, 35%, 15%, and 2%, respectively. Given that the activity of EcSSB decreased by 50% after 30 min incubation at 95 °C,[37] we determined that the thermostability of these SSBs followed the order SaSsbA = SaSsbB > SaSsbC > EcSSB (Table 5). Thus, SaSsbB also exhibited high thermostability.

SsbB is not a counterpart of PriB

PriB is a dimeric ssDNA-binding protein with two OB folds,[27–29] only found in some Gram-negative bacteria.[21,22] Our crystal structure reveals that the N-terminal DNA-binding domain of SaSsbB structurally resembles PriB, although they significantly differ in the lengths of β4- and β5-sheets (Fig. 7F). Like SaSsbB, PriB also lacks the acidic tail. Because *E. coli* has only one SSB, it may raise a question whether PriB is the second SSB in *E. coli* and plays a functional role that is similar to SsbB in *S. aureus*. Sequence comparisons and operon organization analyses also show that PriB evolves from the duplication of the SSB gene.[38] However, PriA activity can be significantly stimulated by PriB but not by SsbB (Fig. 6). Thus, SaSsbB and EcPriB have different functions, and PriB is not a counterpart of SsbB. Considering that the mechanisms of action of primosomes involved in DNA replication restart differ between *E. coli*[21,22] and Gram-positive

Table 4 The $[Protein]_{50}$ values of SaSsbB mutants as analyzed by EMSA[a]

dT50	$[Protein]_{50}$ (nM)
SaSsbB	83 ± 7
SaSsbB(F37A)	155 ± 12
SaSsbB(F48A)	176 ± 10
SaSsbB(F54A)	191 ± 16
SaSsbB(Y82A)	296 ± 18

[a] $[Protein]_{50}$ was calculated from the titration curves of EMSA by determining the concentration of the protein (tetramers) needed to achieve the midpoint value for input DNA binding. Errors are standard deviations determined by three independent titration experiments.

Table 5 Thermostability of SaSsbB[a]

	The decreased activity (%)			
Temperature	SaSsbA	SaSsbB	SaSsbC	EcSSB
85 °C	2	2	2	
90 °C	15	15	20	
95 °C	35	35	40	50
100 °C	60	60	70	

[a] Protein (1 μM) was incubated at temperatures ranging from 40 °C to 100 °C for 30 min. The resultant protein solution was incubated at 25 °C for 30 min with dT30. The phosphor storage plate was scanned, and the data for complex and free DNA bands were digitized for quantitative analysis. Results of SaSsbA,[12] SaSsbC,[12] and EcSSB[37] are adapted from previous works for comparison.

bacteria,[39] we should elucidate the process by which PriA can cooperate with various loading factors to reactivate the same stalled forks.

Recently, we have identified and characterized the third SSB (SsbC) in *S. aureus*.[12] The structure and ssDNA-binding mode of SaSsbA,[25] SaSsbB (this study), and SaSsbC[12] are similar. Further studies are still needed to understand why SSB in *S. aureus* is necessary to evolve three similar but different SSBs.

Conflicts of interest

There are no conflicts of interest to declare.

Acknowledgements

We thank the experimental facility and the technical services provided by the Synchrotron Radiation Protein Crystallography Facility of the National Core Facility Program for Biotechnology, Ministry of Science and Technology and the National Synchrotron Radiation Research Center, a national user facility supported by the Ministry of Science and Technology, Taiwan, ROC. This research was supported by a grant from the Ministry of Science and Technology, Taiwan (MOST 107-2320-B-040-014 to C. Y. Huang).

References

1 D. J. Richard, E. Bolderson and K. K. Khanna, *Crit. Rev. Biochem. Mol. Biol.*, 2009, **44**, 98–116.
2 E. Antony and T. M. Lohman, *Semin. Cell Dev. Biol.*, 2018, DOI: 10.1016/j.semcdb.2018.03.017.
3 R. R. Meyer and P. S. Laine, *Microbiol. Rev.*, 1990, **54**, 342–380.
4 P. R. Bianco, *Prog. Biophys. Mol. Biol.*, 2017, **127**, 111–118.
5 A. Costes, F. Lecointe, S. McGovern, S. Quevillon-Cheruel and P. Polard, *PLoS Genet.*, 2010, **6**, e1001238.
6 S. N. Savvides, S. Raghunathan, K. Futterer, A. G. Kozlov, T. M. Lohman and G. Waksman, *Protein Sci.*, 2004, **13**, 1942–1947.
7 T. H. Dickey, S. E. Altschuler and D. S. Wuttke, *Structure*, 2013, **21**, 1074–1084.
8 S. Raghunathan, A. G. Kozlov, T. M. Lohman and G. Waksman, *Nat. Struct. Biol.*, 2000, **7**, 648–652.
9 T. M. Lohman and M. E. Ferrari, *Annu. Rev. Biochem.*, 1994, **63**, 527–570.
10 S. Suksombat, R. Khafizov, A. G. Kozlov, T. M. Lohman and Y. R. Chemla, *eLife*, 2015, **4**, e08193.
11 C. Lindner, R. Nijland, M. van Hartskamp, S. Bron, L. W. Hamoen and O. P. Kuipers, *J. Bacteriol.*, 2004, **186**, 1097–1105.
12 Y. H. Huang and C. Y. Huang, *Oncotarget*, 2018, **9**, 20239–20254.
13 N. Koyama, J. Inokoshi and H. Tomoda, *Molecules*, 2012, **18**, 204–224.
14 J. G. Glanzer, J. L. Endres, B. M. Byrne, S. Liu, K. W. Bayles and G. G. Oakley, *J. Antimicrob. Chemother.*, 2016, **71**, 3432–3440.
15 S. Ayora, B. Carrasco, P. P. Cardenas, C. E. Cesar, C. Canas, T. Yadav, C. Marchisone and J. C. Alonso, *FEMS Microbiol. Rev.*, 2011, **35**, 1055–1081.
16 L. Attaiech, A. Olivier, I. Mortier-Barriere, A. L. Soulet, C. Granadel, B. Martin, P. Polard and J. P. Claverys, *PLoS Genet.*, 2011, **7**, e1002156.
17 T. Yadav, B. Carrasco, A. R. Myers, N. P. George, J. L. Keck and J. C. Alonso, *Nucleic Acids Res.*, 2012, **40**, 5546–5559.
18 T. Paradzik, N. Ivic, Z. Filic, B. A. Manjasetty, P. Herron, M. Luic and D. Vujaklija, *Nucleic Acids Res.*, 20, **41**, 3659–3672.
19 G. C. Allen Jr, N. E. Dixon and A. Kornberg, *Cell*, 1993, **74**, 713–722.
20 C. A. Ouzounis and B. J. Blencowe, *Nucleic Acids Res.*, 1991, **19**, 6953.
21 Y. H. Huang and C. Y. Huang, *BioMed Res. Int.*, 2014, **2014**, 195162.
22 T. A. Windgassen, S. R. Wessel, B. Bhattacharyya and J. L. Keck, *Nucleic Acids Res.*, 2018, **46**, 504–519.
23 C. J. Cadman, M. Lopper, P. B. Moon, J. L. Keck and P. McGlynn, *J. Biol. Chem.*, 2005, **280**, 39693–39700.
24 C. J. Cadman and P. McGlynn, *Nucleic Acids Res.*, 2004, **32**, 6378–6387.
25 Y. H. Huang, H. H. Guan, C. J. Chen and C. Y. Huang, *PLoS One*, 2017, **12**, e0182060.
26 Y. H. Huang, Y. Lien, C. C. Huang and C. Y. Huang, *PLoS One*, 2016, **11**, e0157593.
27 Y. H. Huang, Y. H. Lo, W. Huang and C. Y. Huang, *Genes Cells*, 2012, **17**, 837–849.
28 C. Y. Huang, C. H. Hsu, Y. J. Sun, H. N. Wu and C. D. Hsiao, *Nucleic Acids Res.*, 2006, **34**, 3878–3886.
29 J. H. Liu, T. W. Chang, C. Y. Huang, S. U. Chen, H. N. Wu, M. C. Chang and C. D. Hsiao, *J. Biol. Chem.*, 2004, **279**, 50465–50471.
30 Y. H. Huang, C. C. Huang, C. C. Chen, K. J. Yang and C. Y. Huang, *Protein J.*, 2015, **34**, 169–172.
31 C. Y. Huang, Determination of the binding site-size of the protein-DNA complex by use of the electrophoretic mobility shift assay, in *Stoichiometry and Research: The Importance of Quantity in Biomedicine*, ed. Innocenti A, InTech Press, Rijeka, Croatia, 2012, pp. 235–242.
32 M. Landau, I. Mayrose, Y. Rosenberg, F. Glaser, E. Martz, T. Pupko and N. Ben-Tal, *Nucleic Acids Res.*, 2005, **33**, W299–W302.
33 Z. Otwinowski and W. Minor, *Methods Enzymol.*, 1997, **276**, 307–326.
34 A. J. McCoy, R. W. Grosse-Kunstleve, P. D. Adams, M. D. Winn, L. C. Storoni and R. J. Read, *J. Appl. Crystallogr.*, 2007, **40**, 658–674.
35 J. J. Headd, N. Echols, P. V. Afonine, R. W. Grosse-Kunstleve, V. B. Chen, N. W. Moriarty, D. C. Richardson, J. S. Richardson and P. D. Adams, *Acta Crystallogr., Sect. D: Biol. Crystallogr.*, 2012, **68**, 381–390.
36 P. Emsley and K. Cowtan, *Acta Crystallogr., Sect. D: Biol. Crystallogr.*, 2004, **60**, 2126–2132.
37 M. Nowak, M. Olszewski, M. Spibida and J. Kur, *BMC Microbiol.*, 2014, **14**, 91.

38 V. A. Ponomarev, K. S. Makarova, L. Aravind and E. V. Koonin, *J. Mol. Microbiol. Biotechnol.*, 2003, **5**, 225–229.

39 M. Velten, S. McGovern, S. Marsin, S. D. Ehrlich, P. Noirot and P. Polard, *Mol. Cell*, 2003, **11**, 1009–1020.